Aus dem

Institut für Kardiovaskuläre Physiologie und Pathophysiologie im Walter-Brendel-Zentrum für Experimentelle Medizin

Ludwig-Maximilians-Universität München

Blood cell function during fetal development

Dissertation
zum Erwerb des Doctor of Philosophy (Ph.D.)
an der Medizinischen Fakultät der
Ludwig-Maximilians-Universität München

vorgelegt von
Lou Martha Wackerbarth

aus
Geismar/Deutschland

Jahr
2024

Mit Genehmigung der Medizinischen Fakultät der
Ludwig-Maximilians-Universität München

Erstes Gutachten:	Prof. Dr. Markus Sperandio
Zweites Gutachten:	Prof. Dr. Christian Schulz
Drittes Gutachten:	Priv.Doz. Dr. Stefanie Steiger
Viertes Gutachten:	Prof. Dr. Bernhard Heindl

Dekan: Prof. Dr. med. Thomas Gudermann

Tag der mündlichen Prüfung: 01.02.2024

Affidavit

LMU LUDWIG-MAXIMILIANS-UNIVERSITÄT MÜNCHEN | Promotionsbüro Medizinische Fakultät | MMRS

Affidavit

Wackerbarth, Lou Martha

Surname, first name

Großhaderner Str. 9

Street

82152 Planegg-Martinsried, Germany

Zip code, town, country

I hereby declare, that the submitted thesis entitled:

“Blood cell function during fetal development”

is my own work. I have only used the sources indicated and have not made unauthorised use of services of a third party. Where the work of others has been quoted or reproduced, the source is always given.

I further declare that the dissertation presented here has not been submitted in the same or similar form to any other institution for the purpose of obtaining an academic degree.

Munich, 08.02.2024

place, date

Lou Martha Wackerbarth

Signature doctoral candidate

Confirmation of congruency

LMU LUDWIG-MAXIMILIANS-UNIVERSITÄT MÜNCHEN

Promotionsbüro Medizinische Fakultät

MMRS

Confirmation of congruency between printed and electronic version of the doctoral thesis

Wackerbarth, Lou Martha

Surname, first name

Großhaderner Str. 9

Street

82152 Planegg-Martinsried, Germany

Zip code, town, country

I hereby declare, that the submitted thesis entitled:

“Blood cell function during fetal development”

is congruent with the printed version both in content and format.

Munich, 30.10.2023

place, date

Lou Martha Wackerbarth

Signature doctoral candidate

Table of content

List of abbreviations

Btk	Bruton's tyrosine kinase
DAMP	Damage associated molecular pattern
E	Embryonic day
ESCRT	Endosomal sorting complexes required for transport
ELISA	Enzyme-linked immunosorbent assay
GBD	Global Burden of Disease
GSDMD	Gasdermin D
G-CSFR	GCSF-receptor
G-CSF	Granulocyte-colony stimulating factor
h	Hour
IKK	IkB kinase
IL-1β	Interleukin-1β
JAK2	Janus kinase 2
LPS	Lipopolysaccharide
LT-α	Lymphotoxin α
MST1	Mammalian sterile 20-like kinase 1
MRP	Myeloid-related protein
NIK	NF-κB-inducing kinase
NF-κB	Nuclear factor κB
STAT3	Signal transducer and activator of transcription 3
SNP	Single nucleotide polymorphism
TNFRII	TNF receptor type II
TLR	Toll-like receptor
TNF	Tumor necrosis factor
TNFAIP3	Tumor necrosis factor-alpha-induced protein 3
WT	Wild-type

List of publications

1.1 List of publications utilized for the current cumulative thesis

Paper I:

Rohwedder I, **Wackerbarth LM**, Heinig K, Ballweg A, Altstätter J, Ripphahn M, Nussbaum C, Salvermoser M, Bierschenk S, Straub T, Gunzer M, Schmidt-Supprian M, Kolben T, Schulz C, Ma A, Walzog B, Heinig M, Sperandio M. A20 and the noncanonical NF-κB pathway are key regulators of neutrophil recruitment during fetal ontogeny. JCI Insight. 2023 Feb 22;8(4):e155968. doi: 10.1172/jci.insight.155968.

Paper II:

Pruenster M, Immler R, Roth J, Kuchler T, Bromberger T, Napoli M, Nussbaumer K, Rohwedder I, **Wackerbarth LM**, Piantoni C, Hennis K, Fink D, Kallabis S, Schroll T, Masgrau-Alsina S, Budke A, Liu W, Vestweber D, Wahl-Schott C, Roth J, Meissner F, Moser M, Vogl T, Hornung V, Broz P and Sperandio M. E-selectin-mediated rapid NLRP3 inflammasome activation regulates S100A8/S100A9 release from neutrophils via transient gasdermin D pore formation. Nat Immunol (2023). doi: 10.1038/s41590-023-01656-1.

Paper III:

Masgrau-Alsina S, **Wackerbarth LM**, Lim DS, Sperandio M. MST1 controls murine neutrophil homeostasis via the G-CSFR/STAT3 axis. Front Immunol. 2022 Dec 23;13:1038936. doi: 10.3389/fimmu.2022.1038936.

1.2 Complete list of publications

Becker IC, Scheller I, **Wackerbarth LM**, Beck S, Heib T, Aurbach K, Manukjan G, Gross C, Spindler M, Nagy Z, Witke W, Lappalainen P, Bender M, Schulze H, Pleines I, Nieswandt B. Actin/microtubule crosstalk during platelet biogenesis in mice is critically regulated by Twinfilin1 and Cofilin1. Blood Adv. 2020 May 26;4(10):2124-2134. doi: 10.1182/bloodadvances.2019001303.

Heib T, Hermanns HM, Manukjan G, Englert M, Kusch C, Becker IC, Gerber A, **Wackerbarth LM**, Burkard P, Dandekar T, Balkenhol J, Jahn D, Beck S, Meub M, Dütting S, Stigloher C, Sauer M, Cherpokova D, Schulze H, Brakebusch C, Nieswandt B, Nagy Z, Pleines I. RhoA/Cdc42 signaling drives cytoplasmic maturation but not endomitosis in megakaryocytes. Cell Rep. 2021 May 11;35(6):109102. doi: 10.1016/j.celrep.2021.109102.

Englert M, Aurbach K, Becker IC, Gerber A, Heib T, **Wackerbarth LM**, Kusch C, Mott K, Araujo GHM, Baig AA, Dütting S, Knaus UG, Stigloher C, Schulze H, Nieswandt B, Pleines I, Nagy Z. Impaired microtubule dynamics contribute to microthrombocytopenia in RhoB-deficient mice. Blood Adv. 2022 Sep 13;6(17):5184-5197. doi: 10.1182/bloodadvances.2021006545.

2. Contribution to the publications

2.1 Contribution to paper I

As a shared first author of the publication “A20 and the noncanonical NF-κB pathway are key regulators of neutrophil recruitment during fetal ontogeny”, I was involved in designing and conducting experiments, analyzing data as well as writing the manuscript, which I will outline in detail in the following paragraphs.

At the beginning of my time as a doctoral candidate in July 2020, I started to conduct essential *in vivo* experiments for the project. I performed intravital microscopy on TNF-α–stimulated mouse cremaster muscle venules, resulting in Figure 5 of the publication as well as Supplemental Figure 3. In addition, I performed important immunoblots as well as flow cytometry, resulting in Figure 2 E as well as Figure 3 A, D and E and Supplemental Figure 2 A and B. Finalizing these experiments took until spring 2021 and in the following months, Ina Rohwedder and I co-wrote the manuscript.

After receiving reviewer comments from JCI Insight, I started working fulltime on the publication again in November 2021. In the first months of the revision, Ina Rohwedder and I planned, designed and conducted all necessary experiments together.

In detail, we performed imaging flow cytometry, resulting in revised Figure 2 B and C, as well as new Supplemental Figure 1 C and D. Figure 3 was complemented with new experiments, resulting in Figure 3 B, F, G, H, J, K. I mainly conducted flow cytometry for Figure 3 B, H and K as well as new Supplemental Data Figure 2 B and D. In addition, I performed flow chamber experiments for Figure 3 G as well as all the *in vivo* experiments for intravital microscopy of the yolk sac vessels for Figure 3 J. Furthermore, I performed immunoblots for new Figure 3 F as well as new Supplemental Data Figure 2 C. Additionally, I performed cytospin experiments for new Supplemental Figure 2 B.

From September 2022 until the final publication of the manuscript in January 2023, I exclusively took care of the finalization of experiments, re-writing and revising of the manuscript and the final submission, since Ina Rohwedder had ended her PostDoc at the Sperandio lab and had left the institute at this point.

Taken together, Ina Rohwedder and I have both provided equal first-author-level contributions to the published work, which was an intense multi-year collaborative effort. Contributing to the publication by acquiring and analyzing data, but most importantly taking the lead in the revision and being the main responsible person for the final resubmission, thus explains my shared first authorship.

2.2 Contribution to paper II

As an author of the publication “E-selectin-mediated rapid NLRP3 inflammasome activation regulates S100A8/A9 release from neutrophils via transient gasdermin D pore formation”, I was involved in conducting experiments as well as analyzing data.

Contributing to this publication started with establishing the FAM-FLICA assay for analysis of capsase1 activity in human neutrophils in our laboratory. I conducted experiments and acquired the respective confocal images, seen in Figure 2 C and was further responsible for the image analysis, resulting in Figure 2 D and E.

Additionally, I performed the experiments for analyzing ASC speck formation in murine neutrophils. I acquired confocal images of ASC speck formation and took care of the following image analysis, resulting in Figure 4 E and G.

2.3 Contribution to paper III (Appendix A)

As an author of the publication “MST1 controls murine neutrophil homeostasis via the G-CSFR/STAT3 axis”, I was involved in the revision phase, conducting experiments as well as analyzing data.

During the revision phase, I established the Annexin V staining protocol for apoptotic murine neutrophils in our laboratory, conducted necessary experiments and analyzed flow cytometry data, resulting in Figure 2 G. Furthermore, I helped in revising and submitting the manuscript.

3. Introductory summary

Neutrophils are the most abundant circulating leukocytes in humans and also the first immune cells arriving at sites of tissue damage or pathogen invasion during the inflammatory response (1). Dissecting the molecular details of neutrophil recruitment starting in the intravascular compartment until they reach their target tissues has been the leading topic of my time as a doctoral candidate, with a particular focus on this scenario during fetal life, studying the ontogeny and maturation of fetal neutrophils.

3.1 Novel insights on maturation and function of neutrophils in early life

Newborn infants, particularly when born prematurely, are at high risk of infections and severe sepsis is still a leading cause of death among neonates worldwide, especially in low-income countries. Neonatal sepsis describes a systemic infection with very high morbidity and mortality, occurring in the first four weeks of a newborn's life (2, 3). Estimated numbers provided by the Global Burden of Disease (GBD) study in 2016–2017, reach over 1 million annual incident cases of neonatal sepsis worldwide and approximately 200.000 deaths which are attributed to sepsis (4). The mechanism of neonatal susceptibility to infections has been extensively studied in the past decades and immaturity of neonatal immunity has been discovered as a major reason for the higher neonatal infection rate (5), especially affecting preterm infants, who exhibited more immature immune responses compared to term infants (6).

The early life immune system is characterized by high plasticity in order to adapt most sufficiently to the rapidly changing environments of the protected mother's womb to the extrauterine world with its pathogenic challenges (7, 8). Tight regulation of inflammatory responses is crucial, since severe inflammation can also prompt detrimental health consequences in still developing fetuses. Especially during organ development, tissue damage and oxidative stress following overshooting immune responses can lead to harmful conditions for the fetus itself (9, 10).

Innate immunity is particularly relevant for neonates, as they largely depend on the innate immune system to protect against sepsis. In contrast, the adaptive immune system plays only a minor role in this period of life (11). Investigating the innate immune system, neutrophils are major players in host defense (12), as they are the first line of defense during inflammatory responses and comprise the largest fraction of circulating white blood cells in humans (13). Following inflammatory stimuli, neutrophils are recruited by a well-de-

fined process that ultimately culminates in their extravasation from circulation into inflamed tissues. This multistep adhesion process depends on a complex interplay between various adhesion molecules with their corresponding ligands located on the neutrophil membrane and on endothelial cells (14). Initially, circulating neutrophils start rolling along the vessel wall by binding of endothelial selectins (such as P- or E-selectin) to their respective neutrophil expressed selectin-ligands, e.g. PSGL-1, which brings them in close proximity to chemokines presented on the inflamed endothelium (15). Binding to specific chemokine receptors on the neutrophil surface induces a conformational change and is followed by activation of β2 integrins (inside-out signaling). This culminates in neutrophil arrest and subsequent transmigration into the inflamed tissue (14). Studies on human and murine neutrophils identified that this recruitment cascade is severely impaired in function when comparing early stages of fetal development with adults (16, 17), resulting in diminished rolling and adhesion of neutrophils *in vivo* as well as *in vitro*. The finding that the exposure to the extrauterine environment does not stimulate the maturation of neutrophils in prematurely born infants led to the hypothesis that neutrophil maturation might be controlled by an intrinsic molecular program (16).

The publication “A20 and the noncanonical NF-κB pathway are key regulators of neutrophil recruitment during fetal ontogeny” aimed to dissect these molecular mechanisms and to elucidate maturation of neutrophils during fetal development.

Conducting a transcriptome analysis of human fetal neutrophils (derived from cord-blood, either from premature (<37 weeks of gestation) and mature (≥ 37 weeks of gestation) born infants) and comparing their gene expression profile to neutrophils from adult donors, we discovered significant differences. The transcriptomic screen revealed 124 genes to be regulated differently and further analysis pointed out that several of these differentially regulated genes are connected with the nuclear factor κB (NF-κB) signaling pathway.

This pathway comprises a family of transcription factors, namely the proteins p50 and its precursor p105, RelA, c-Rel, RelB and p52 as well as its precursor p100, which are ubiquitously expressed and act as central mediators of inflammatory and innate immune signaling pathways. There are two major pathways for activation of these transcription factors, namely the canonical and the noncanonical NF-κB pathway (18). The activation of canonical signaling occurs in a rapid but transient manner, resulting in a prolonged inflammatory response, while activation of the noncanonical side leads to a rather steady activation of gene transcription and is associated with differentiation and maturation of immune cells as well as secondary lymphoid organogenesis (19). Activation of the canonical pathway is initiated by activation of inflammatory surface receptors on immune cells , for example Toll-like receptors (TLRs) and the tumor necrosis factor–α (TNF-α)

receptor and culminates in the translocation of the transcription factor p65 to the nucleus and subsequent gene transcription of proinflammatory cytokines. The noncanonical side responds to a specific and rather small group of receptors, namely lymphotoxin α receptor/lymphotoxin α1β2 (LTβR/LT-α1β2) or TNF receptor type II/LT-α (TNFRII/LT-α) and mediates translocation of the heterodimer p52/RelB to the nucleus (20).

Out of the 124 differentially regulated genes, we found 56 genes to be upregulated and 68 to be downregulated in fetal compared to adult neutrophils and interestingly, 40 of 56 (71%) genes upregulated in fetal neutrophils were associated with the RelB pathway. RelB, as the major effector protein of the noncanonical cascade, is stabilized in the cytoplasm by p100 in the unstimulated state. After stimulation and subsequent activation of the NF-κB-inducing kinase (NIK) and the IKKα/IKKα complex, phosphorylation-induced ubiquitination of p100 leads to its further processing into the mature p52 subunit. This ultimately causes the formation of the RelB/p52 heterodimer which can translocate to the nucleus and further enables gene transcription (20).

Since the transcriptomic screen revealed this specific RelB-related signature of gene expression in fetal human neutrophils, a first set of experiments was performed to test a potential baseline activity of the noncanonical NF-κB pathway in fetal neutrophils. Analyzing the subcellular location of RelB in unstimulated fetal and adult neutrophils revealed a significant colocalization of RelB to the nucleus of cord blood neutrophils from premature and mature infants, whereas this colocalization was significantly less in adult neutrophils. Performing the same experiments for the subcellular localization of p65, the major transcription factor of the canonical signaling side, colocalization to the nucleus was not different between adult and fetal neutrophils, pointing towards an explicit activation of the noncanonical NF-κB signaling pathway in human fetal neutrophils, already under baseline conditions. This finding was further supported by Western Blot analysis of the cleaved p52 subunit, whose expression was significantly higher in fetal premature and mature neutrophils compared to adult counterparts.

Since these results promoted the hypothesis of a different baseline scenario in fetal neutrophils, characterized by a shift of NF-κB signaling towards the noncanonical side, potential upstream factors inducing this side were analyzed next. Among the receptors known to initiate noncanonical signaling, TNFRII was significantly higher expressed on human mature fetal neutrophils in comparison to adult ones and same tendencies, although not significant, could be detected when analyzing murine neutrophils. One of the most prominent ligands for this receptor is Lymphotoxin-α (LT-α), a close homolog to TNF-α, required for development of secondary lymphoid organs (21). Abundancy of LT-α in serum of cord blood obtained from premature and mature infants as well as in adult serum was quantitatively analyzed by ELISA and revealed significant higher levels of the

ligand in serum from infants compared to adults. These findings further suggested that the LT-α/TNFRII pathway acts as initiator of the noncanonical NF-κB signaling contributing to the observed elevated baseline activation of the latter in fetal neutrophils.

Noncanonical and canonical NF-κB pathways display extensive interplays at different levels and the immune-modulatory capacities of the noncanonical side can exert distinct effects on the canonical NF-κB pathway (20). For that reason, the capability of fetal neutrophils to respond to the initiation of the canonical NF-κB pathway following inflammation was assessed next.

Under unstimulated conditions, inhibitory proteins like IkBα and other IkB family members sequester components of the NF-κB pathway in the cytoplasm. Responding to inflammatory stimuli, the IkB kinase (IKK) complex phosphorylates IkBα, resulting in its ubiquitination and degradation via the proteasom, subsequently leading to the translocation of NF-kB dimers to the nucleus and activation of gene expression (22).

To further investigate this, fetal and adult neutrophils were stimulated with TNF-α, well-known to induce the canonical NF-κB signaling pathway via the TNF receptor, and following phosphorylation of IkBα was analyzed by Western Blot. The stimulation caused pronounced phosphorylation of IkBα in adult but not in fetal neutrophils, supporting the hypothesis that fetal neutrophils can less effectively activate the canonical NF-κB signaling side. The diminished responsiveness of fetal neutrophils to classical inflammatory stimuli like TNF-α was further shown in a decreased upregulation of surface levels of the β2-integrin Mac-1, compared to adult counterparts.

The significantly higher abundancy of LT-α in serum of fetal cord blood compared to adult donors gave rise to the idea that serum factors in general could be responsible for keeping the cells in a less activatable state. To investigate the potential dampening function of fetal serum on neutrophils in regard to inflammatory stimuli in further detail, adult neutrophils were stimulated with either fetal or adult serum and subsequently several effector functions were analyzed. Firstly, fetal serum incubation of neutrophils resulted in less phosphorylated IκBα in comparison to stimulation with serum taken from adult donors. In contrast, when neutrophils were stimulated with serum obtained from fetuses, protein levels of p52 were higher compared to controls. This findings point out that fetal serum could induce a switch in NF-κB signaling towards the noncanonical side in adult neutrophils, which makes them less responsive towards inflammatory stimuli. On the other hand, fetal neutrophils could be switched into a more responsive state after incubation with adult serum as indicated by a significant upregulation of phosphorylated IkBα, which was lacking when cells were incubated with fetal serum. To explore the contribution of LT-α to these findings in more detail, adult neutrophils were incubated with recombinant

human LT-α prior to stimulation with TNF-α, which lead to significantly reduced levels of phosphorylated IκBα, confirming the factor's capacity on dampening the inflammatory response.

To assess the effect of fetal serum on other prominent neutrophil effector functions, adhesion capacity of adult neutrophils after stimulation with fetal and adult serum was then tested in a flow chamber system. Adhesion of neutrophils, which were previously incubated with fetal serum, was significantly reduced compared to their counterparts incubated with adult serum. Similar results were obtained when analyzing phagocytosis of adult neutrophils, as cells after incubation with fetal serum also showed significantly diminished capacity to take up zymosan particles, confirming the hypothesis that several neutrophil effector functions are changed following incubation with fetal serum. To elucidate the role of the TNFRII receptor in more detail, an anti-TNFRII antibody was used to block the receptor on adult neutrophils. This successfully abolished the inhibitory capacity of fetal serum, as phagocytosis of adult neutrophils after stimulation with fetal serum was significantly enhanced when the TNFRII receptor was blocked before. Taken together, these experiments corroborated the critical involvement of the LT-α/TNFRII pathway in the described altered behavior of fetal neutrophils.

Since the reduced responsiveness of fetal neutrophils to inflammatory stimuli and the concomitant shift of the NF-κB pathway to the noncanonical side were so far only investigated in the human scenario, the following experiments aimed to confirm these findings in murine models. Initiation of the canonical NF-κB pathway via LPS-TLR4 binding leads to activation of not only neutrophils but also endothelial cells, ultimately culminating in adhesion of neutrophils to the inflamed vasculature (23, 24). To analyze the latter *in vivo*, we conducted intravital microscopy experiments on neutrophil adhesion in inflamed murine yolk sac vessels following intrauterine LPS stimulation (25). Leukocyte interaction with the inflamed endothelium was low in embryonic day (E) 14.5 yolk sac vessels but significantly increased when analyzing E17.5 vessels, where pronounced neutrophil recruitment could be imaged. Additionally, TNF-α-stimulation of isolated murine neutrophils failed to equally upregulate surface levels of the β2-integrin Mac-1 in fetal compared to adult murine neutrophils, matching the data obtained with human neutrophils.

The initial transcriptomic screen revealed several RelB target genes such as A20 to be upregulated in human fetal neutrophils. A20 (gene name: tumor necrosis factor-alpha-induced protein 3, *TNFAIP3*) is an ubiquitin-modifying enzyme and known as a major negative regulator of innate immune responses. In fact, NF-κB signaling is tightly controlled by ubiquitylation, which generates various post-translational modifications, determining specific biological fates of proteins (26). A20 is described to be a crucial regulator of ubiquitin-dependent signals. It has three functions, cleaving ubiquitin chains, acting as

an ubiquitin E3 ligase and binding to linear ubiquitin chains. Its expression is controlled by transcriptional and post-transcriptional mechanisms and once induced, it negatively regulates canonical NF-κB signaling. Hence, expression of A20 is initiated by signals depending on the NF-κB signaling pathway and consecutively regulates the length and potency of signaling as critical part of a negative feedback loop via interacting with various molecules being part of the NF-κB pathway itself (27). Due to its importance for the NF-κB pathway, A20 was a promising candidate participating in the discovered shift in NF-κB signaling in fetal neutrophils. Indeed, A20 was significantly upregulated on transcriptional and on protein level when comparing murine and human fetal neutrophils with adult ones. In murine neutrophils, A20 mRNA expression progressively decreases at later embryonic stages (E14.5 compared to E17.5), fitting to previous data obtained by intravital microscopy of yolk sac vessels, where the capability of neutrophil recruitment increased with gestational age (E17.5 versus E14.5) (17). This led to the hypothesis that downregulation of A20 expression towards the end of fetal development inversely correlates with increased neutrophil adhesiveness and responsiveness.

Since murine fetal neutrophils are sparse in number, A20-overexpressing Hoxb8 cells have been used as a model system for fetal neutrophils to further investigate the consequences of A20 overexpression on neutrophil function. To analyze their adhesive capacities, differentiated Hoxb8 cells were investigated in a flow chamber system, representing the inflamed endothelium. Our results revealed significantly impaired adhesion of A20-overexpressing cells compared to control cells, again supporting the hypothesis of A20 being a negative regulator of neutrophil function.

Many studies report that a reduction in A20 expression in humans, because of truncated gene variants or single nucleotide polymorphisms (SNPs), can lead to auto-inflammatory pathologies as in systemic lupus erythematosus, rheumatoid arthritis, psoriasis and others (28, 29). Similar observations were made in murine studies, when using mice with either a global A20 deletion (30) or with a conditional knock-out only in the hematopoietic system (31).

In a final set of *in vivo* sterile inflammation experiments, we therefore aimed to investigate the involvement of A20 on the neutrophil recruitment cascade using mice with A20-deficient neutrophils. When performing intravital microscopy in the mouse cremaster muscle following TNF-α–stimulation (32), we observed a significant increase in leukocyte adhesion in mice with neutrophils lacking A20 compared to controls. In addition, stronger extravasation of neutrophils into the inflamed tissue was detected. In conclusion, lack of A20 in neutrophils causes hyperinflammation leading to overshooting neutrophil recruitment to the inflamed tissue. This is in strong contrast to the situation in the fetus, where a significant overexpression of A20 impairs immune responses as illustrated in Figure 1.

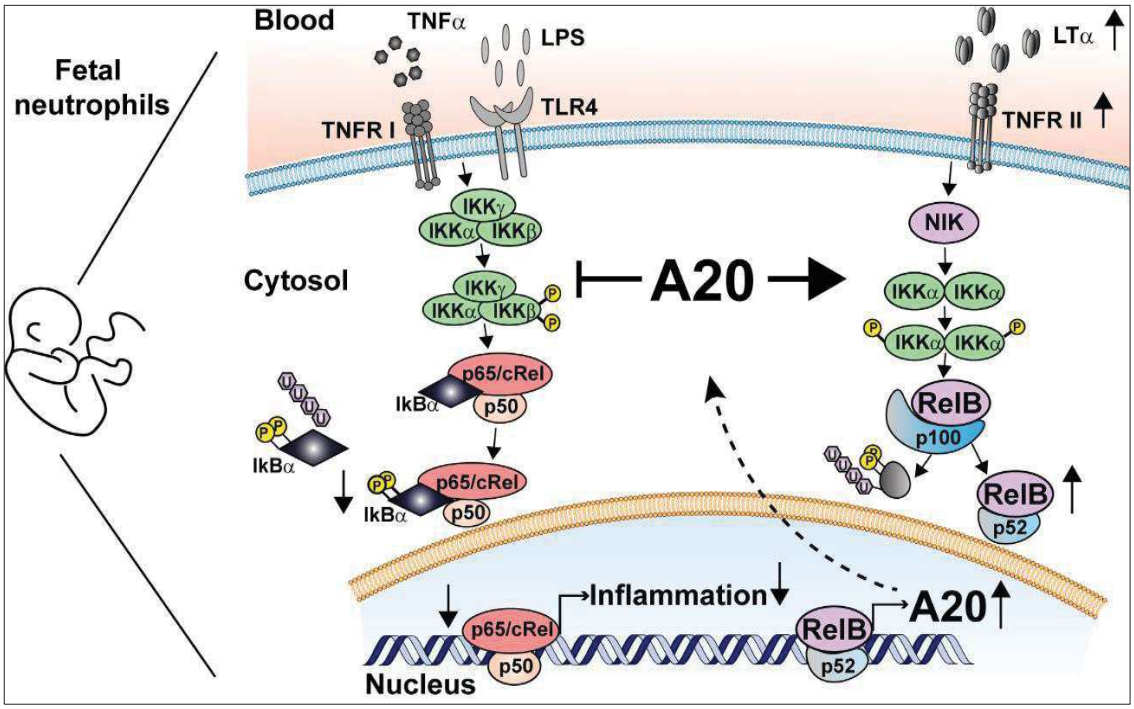

Figure 1: The non-canonical side of the NF-κB signaling pathway and the ubiquitin modifying enzyme A20 are critical components regulating immune responses during fetal ontogeny. Maintaining fetal neutrophils in this A20- and non-canonical NF-κB-dependent non-responsive condition, ultimately leads to downregulated inflammatory responses. Taken from Rohwedder and Wackerbarth et al. (33).

In conclusion, we gained new functional insights into the ontogenetic regulation of fetal neutrophils and unraveled a switch in NF-κB signaling towards the anti-inflammatory noncanonical side of the pathway. This shift in signaling results in the transcriptional upregulation of A20, a potent negative regulator of the classical inflammatory response. For that reason, fetal neutrophils reacted in a restricted and hampered manner following inflammatory stimuli, which ultimately leads to diminished neutrophil recruitment during the inflammatory response. This dampened inflammatory response appears to be strikingly advantageous for the fetus still being in the environment of the mother´s womb, but poses a high risk to those infants born premature, whose immune defense is not able yet for the transition from intrauterine to postnatal life with all its challenges and threats.

3.2 E-selectin mediated NLRP3 inflammasome activation in neutrophils

Another important effector function of neutrophils upon inflammation, next to their ability to leave the blood stream and enter inflamed tissues, is the secretion of factors like damage associated molecular pattern molecules (DAMPs) into the extracellular microenvironment. In the following section, I will outline novel insights on one of these molecules,

namely S100A8/A9, as well described as calprotectin or Myeloid-related protein (MRP) 8/14, which is able to modulate immune responses after its release from the cytosol of neutrophils into the extracellular environment (34).

Human neutrophils are reported to be the major source of S100A8/A9, since it represents about 40% of their total protein content in the cytosol (35). Recent studies from our group identified that during recruitment, rolling neutrophils rapidly secrete S100A8/A9 via an E-selectin-dependent mechanism (36, 37), resulting in high S100A8/A9 abundancy in the blood stream. This is associated with disease progression in various acute and chronic inflammatory pathologies, thus making S100A8/A9 a useful clinical biomarker (34). Passive release of S100A8/A9 into the extracellular space as a consequence of cellular stress or events like NETosis were described before (38, 39) whereas insights on the precise mechanism of its release from neutrophils are still missing.

The publication “E-selectin-mediated rapid NLRP3 inflammasome activation regulates S100A8/A9 release from neutrophils via transient gasdermin D pore formation” aimed to dissect the details of S100A8/A9 release during inflammation and its further consequences. The alarmin S100A8/A9 is deficient in a signal peptide which is needed to be secreted via the conventional pathway of secretion (34). This distinct feature also applies to interleukin-1β (IL-1β), which is known to be released via gasdermin D (GSDMD) pore formation, a process dependent on upstream inflammasome activation and subsequent activation of the effector caspase-1 and GSDMD cleavage (40). Unlike IL-1β, S100A8/A9 is already stored in the cytosol of neutrophils and released in a rapid manner, happening shortly after stimulation. As seen in Figure 2, we were able to unravel E-selectin as a rapid NLRP3 inflammasome activator, leading to caspase-1 cleavage and subsequent GSDMD pore formation, clarifying the exit mechanism for S100A8/A9 to leave neutrophils. Signaling events downstream of E-selectin activation involve the Tec family kinase Bruton tyrosine kinase (Btk), mediating tyrosine phosphorylation of NLRP3 as well as K^+-efflux via the potassium voltage-gated channel $K_V1.3$. Remarkably, this process did not culminate in pyroptotic cell death, but rather consists in a transient process, ensuring subsequent and successful neutrophil recruitment to the site of injury. The endosomal sorting complexes required for transport (ESCRT) machinery was described to play a critical role in this time-limited and reversible process, removing GSDMD pores from the neutrophil plasma membrane in order to circumvent pyroptosis.

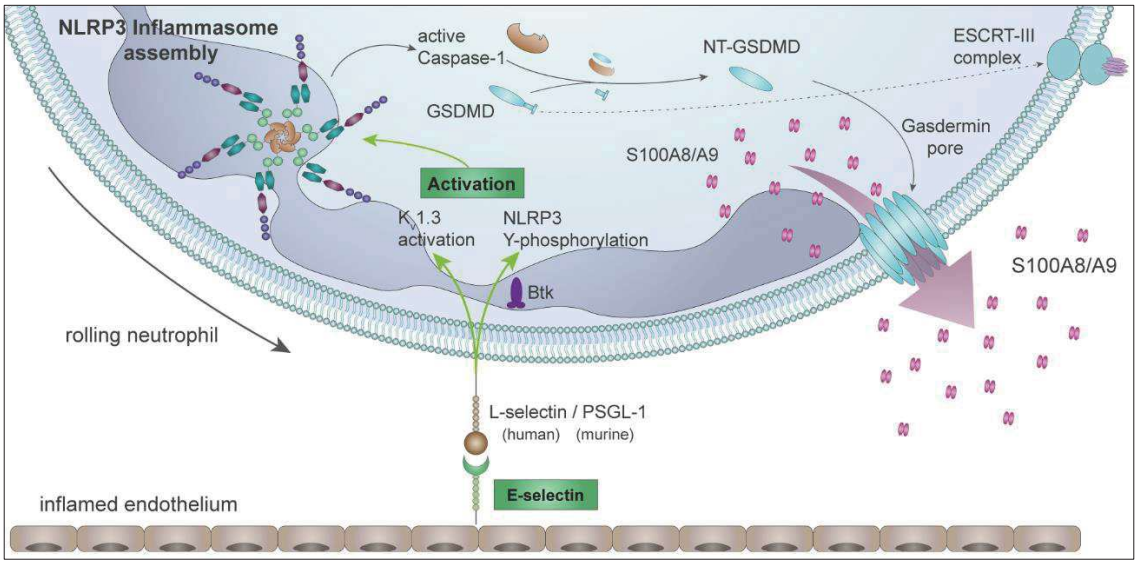

Figure 2: Engagement of E-selectin triggers rapid Btk dependent NLRP3 Y-phosphorylation and Kv1.3 activation. Downstream signaling involves inflammasome assembly, caspase-1 cleavage and ensues GSDMD pore formation by which S100A8/A9 exits the cells. This process does not lead to cell death, but is of self-limiting nature involving rapid activation of the endosomal sorting complexes required for transport (ESCRT) machinery.

This finding is in contrast to the so far described mechanisms of NLRP3 inflammasome activation in cells like macrophages and monocytes, which usually require a first priming step with consecutive de-novo protein synthesis before cells are able to secrete high amounts of cytokines and other pro-inflammatory mediators and eventually undergo pyroptosis (41). Taken together, this publication shed light on the importance of inflammasome activation in neutrophils during the inflammatory response and identifies an E-selectin-induced mechanism leading to a fast, but steady GSDMD pore formation accompanied by S100A8/A9 release during inflammation. This complements our understanding of neutrophils as key players of defense against invasion of microorganisms, for which they need to be fast reacting as well as already equipped with the necessary effector molecules.

3.3 The role of MST1 in neutrophil homeostasis

To complement previously outlined findings on neutrophil function, another crucial factor for the protection of the organism from invasion of pathogens is the process of releasing neutrophils from the bone marrow into the blood stream.

Circulation neutrophils have a short life span of approximately 10-12h (42) before they either fulfill their function as effector cells during inflammation or get removed from the blood stream by organs like spleen, lung or the bone marrow. Therefore mechanisms

which tightly regulate neutrophil availability in the systemic circulation are crucial (43). Granulopoiesis, describing the bone marrow-located process of generation of neutrophils, followed by their mobilization into the circulating blood are particularly important processes in the case of inflammation and found to be regulated by the so called granulocyte-colony stimulating factor (G-CSF) (44). Under baseline conditions, the abundance of this factor is low in human serum but becomes rapidly upregulated in case of an inflammatory event (45). The GCSF-receptor (G-CSFR) homodimerizes upon binding of its ligand, which activates a signaling transduction cascade in neutrophil precursor cells in the bone marrow, where the Janus kinase 2 (JAK2)/signal transducer and activator of transcription 3 (STAT3) axis is critically involved (46). After being released into the bloodstream, neutrophils get recruited to inflamed tissues and finally enter the latter by penetrating the vascular basement membrane. Earlier work from our group revealed that the last step of the cascade requires sequential action of distinct molecules being important for adhesion (47) including Mammalian sterile 20-like kinase 1 (MST1). One additional finding of this initial study was a hypercellular bone marrow indicating either enhanced hematopoiesis/granulopoiesis or defective release. As an important kinase of the Hippo pathway in mammals, the serine/threonine kinase MST1 was initially described to regulate organ size during development (48), but a recent study from our group also reported its involvement in the process of leukocyte transmigration by regulating the mobilization of vesicles containing VLA-3, VLA-6, and neutrophil elastase to the surface of neutrophils (49).

The publication “MST1 controls murine neutrophil homeostasis via the G-CSFR/STAT3 axis” wanted to address this question by investigating the contribution of MST1 to granulopoiesis and neutrophil homeostasis. Accordingly, signaling events resulting from G-CSF interacting with G-CSFR were studied in mice with global MST1 deficiency (*Mst1*$^{-/-}$ mice). In a first set of experiments, we revealed that neutrophil proliferation in the bone marrow and, consequently, the overall number of neutrophils in the bone marrow was increased in *Mst1*$^{-/-}$ mice. Additionally, G-CSF serum levels under resting or stimulated conditions were elevated in these mice in comparison to wild-type (WT) controls. Performing intravital multiphoton laser scanning microscopy and using a mouse skull bone marrow window model, we discovered that mobilization of neutrophils from the bone marrow into the bloodstream was less efficient in *Mst1*$^{-/-}$ mice. Further experiments on the molecular mechanisms behind the impaired mobilization response in the absence of MST1 unraveled a diminished activation of the transcription factor STAT3.

As further described in the scheme seen in Figure 3, G-CSF receptor signaling is required to activate STAT3 and this process was reported to be crucial to release neutrophils from the bone marrow into the vasculature (50). This was in line with the obtained

in vivo data and further supported the hypothesis that MST1 is a key modulator of G-CSFR/STAT3 signaling and therefore an important regulator of neutrophil trafficking from the bone marrow into the periphery and ultimately overall neutrophil homeostasis.

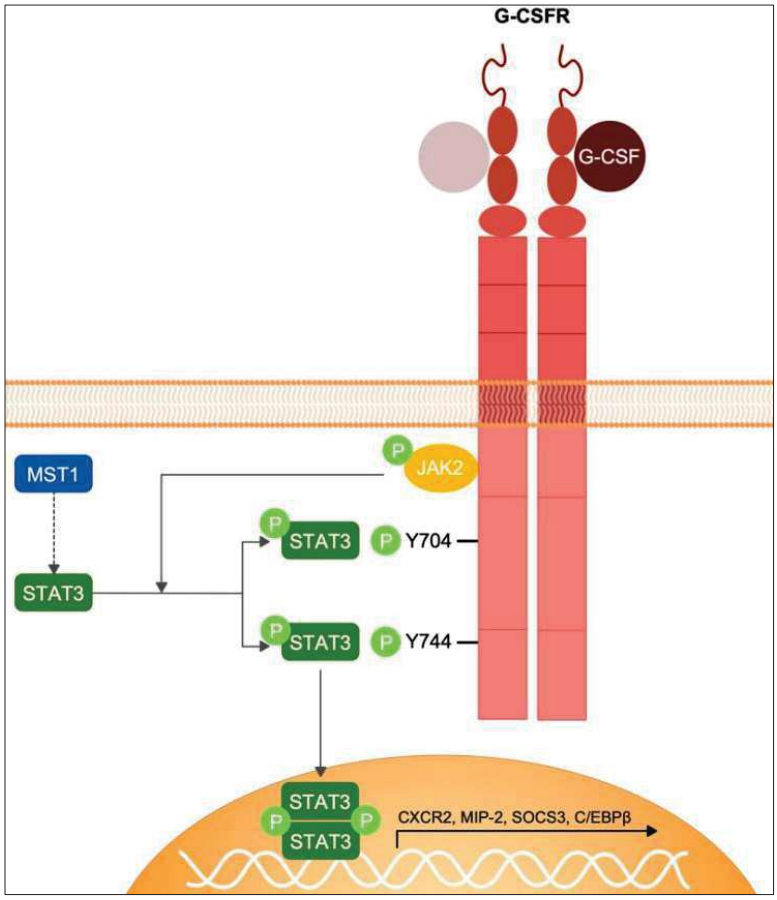

Figure 3: G-CSF interacting with its receptor G-CSFR induces homo-dimerization of the latter. This event is followed by conformational changes of the intracellular domain and JAK2 activation, which subsequently phosphorylates G-CSFR and STAT3. This process is modulated by MST1 underlining the substantial role for this kinase in G-CSF/JAK2-STAT3 signaling. Taken from Masgrau-Alsina et al. (51).

4. Paper I

JCI insight

A20 and the noncanonical NF-κB pathway are key regulators of neutrophil recruitment during fetal ontogeny

Ina Rohwedder, … , Matthias Heinig, Markus Sperandio

JCI Insight. 2023;8(4):e155968. https://doi.org/10.1172/jci.insight.155968.

Research Article | Inflammation

Graphical abstract

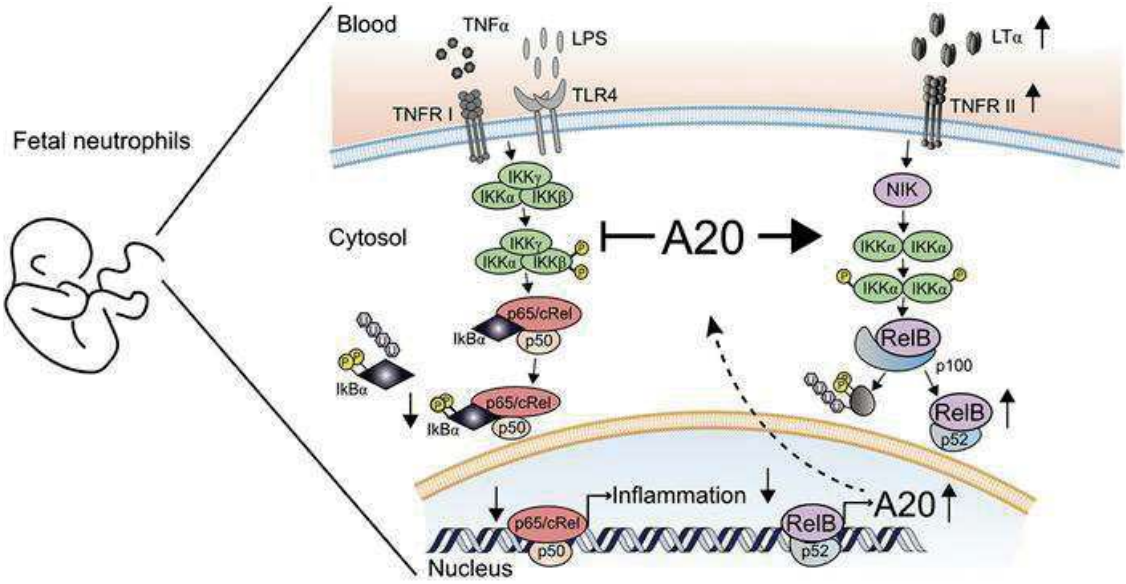

Find the latest version:

https://jci.me/155968/pdf

JCI insight

RESEARCH ARTICLE

A20 and the noncanonical NF-κB pathway are key regulators of neutrophil recruitment during fetal ontogeny

Ina Rohwedder,[1] Lou Martha Wackerbarth,[1] Kristina Heinig,[1] Annamaria Ballweg,[1] Johannes Altstätter,[1] Myriam Ripphahn,[1] Claudia Nussbaum,[2] Melanie Salvermoser,[1] Susanne Bierschenk,[1] Tobias Straub,[3] Matthias Gunzer,[4,5] Marc Schmidt-Supprian,[6] Thomas Kolben,[7] Christian Schulz,[8] Averil Ma,[9] Barbara Walzog,[1] Matthias Heinig,[10,11] and Markus Sperandio[1]

[1]Institute of Cardiovascular Physiology and Pathophysiology, Walter-Brendel-Center of Experimental Medicine, Biomedical Center Munich, LMU Munich, Planegg-Martinsried, Germany. [2]Division of Neonatology, Department of Pediatrics, Dr. von Hauner Children's Hospital, LMU Munich, Munich, Germany. [3]Core Facility Bioinformatics, Biomedical Center Munich, Faculty of Medicine, LMU Munich, Planegg-Martinsried, Germany. [4]Institute for Experimental Immunology and Imaging, University of Duisburg-Essen, Essen, Germany. [5]Leibniz-Institut für Analytische Wissenschaften - ISAS - e.V., Dortmund, Germany. [6]Department of Hematology and Medical Oncology, TU Munich, Munich, Germany. [7]Department of Gynecology and Obstetrics and [8]Medical Clinic I, University Hospital, LMU Munich, Munich, Germany. [9]Department of Medicine, University of California, San Francisco, San Francisco, California, USA. [10]Institute of Computational Biology, Helmholtz Munich, Munich, Germany. [11]Department of Informatics, TU Munich, Munich, Germany.

Newborns are at high risk of developing neonatal sepsis, particularly if born prematurely. This has been linked to divergent requirements the immune system has to fulfill during intrauterine compared with extrauterine life. By transcriptomic analysis of fetal and adult neutrophils, we shed new light on the molecular mechanisms of neutrophil maturation and functional adaption during fetal ontogeny. We identified an accumulation of differentially regulated genes within the noncanonical NF-κB signaling pathway accompanied by constitutive nuclear localization of RelB and increased surface expression of TNF receptor type II in fetal neutrophils, as well as elevated levels of lymphotoxin α in fetal serum. Furthermore, we found strong upregulation of the negative inflammatory regulator A20 (*Tnfaip3*) in fetal neutrophils, which was accompanied by pronounced downregulation of the canonical NF-κB pathway. Functionally, overexpressing A20 in Hoxb8 cells led to reduced adhesion of these neutrophil-like cells in a flow chamber system. Conversely, mice with a neutrophil-specific A20 deletion displayed increased inflammation in vivo. Taken together, we have uncovered constitutive activation of the noncanonical NF-κB pathway with concomitant upregulation of A20 in fetal neutrophils. This offers perfect adaption of neutrophil function during intrauterine fetal life but also restricts appropriate immune responses particularly in prematurely born infants.

Authorship note: IR and LMW contributed equally to this work.

Conflict of interest: The authors have declared that no conflict of interest exists.

Submitted: October 19, 2021
Accepted: January 11, 2023
Published: January 12, 2023

Reference information: *JCI Insight*. 2023;8(4):e155968. https://doi.org/10.1172/jci.insight.155968.

Introduction

Prematurely born infants are highly susceptible to bacterial, fungal, and viral infections and have increased morbidity and mortality from neonatal sepsis compared with term babies (1, 2). This clinical observation reflects the contrasting requirements the immune system has to fulfill to guarantee normal growth and development during intrauterine life on one hand and, on the other hand, to cope with the challenges and threats infants are exposed to in the outside world after birth (3, 4). For the innate immune system, key players in host defense are neutrophils, which, upon an inflammatory stimulus, are attracted to the site of inflammation by a well-orchestrated recruitment process that finally leads to their extravasation from the bloodstream into inflamed tissue (5, 6). This recruitment process is severely restricted during early stages of fetal development when compared with adults (7, 8). As a functional consequence, murine and human fetal neutrophils display a limited capacity to roll and adhere in vitro and in vivo. Interestingly, exposure to the extrauterine environment as in prematurely born infants does not stimulate neutrophil function, but

instead, neutrophil maturation seems to be regulated by an intrinsic molecular program (7). Recently, using various systems biology approaches, several studies have investigated immune system development during the neonatal period (9–11). Besides an increase in type I IFN–related functions, an ontogenetic control of neutrophil signaling was suggested targeting Toll-like receptor– and IL-1–dependent signaling, both of which affect the NF-κB signaling pathways (9).

The NF-κB family of transcription factors is ubiquitously expressed and regulates numerous targets particularly in immune cells (12). Two major signaling pathways exist: the canonical and the noncanonical. The canonical signaling pathway is activated downstream of inflammatory surface receptors on immune cells including Toll-like receptors (TLRs) or the tumor necrosis factor–α (TNF-α) receptor and leads to nuclear translocation of the NF-κB subunit p65. It initiates the rapid but transient activation of gene transcription of proinflammatory cytokines and therefore induces and prolongs the inflammatory response. In contrast, RelB, known as the primary effector of the noncanonical NF-κB signaling pathway, initiated by a diverse range of ligands and receptors, like lymphotoxin α receptor/lymphotoxin α1β2 (LTβR/LT-α1β2) or TNF receptor type II/LT-α (TNFRII/LT-α), elicits a slow and persistent activation of gene transcription (13). While the noncanonical NF-κB signaling pathway is well known for its importance in lymph node development during fetal ontogeny (14), it also functions as a fine-tuning mechanism for inflammatory responses. This was shown by chromatin immunoprecipitation (ChIP) sequencing that revealed numerous RelB downstream targets, among them important immune modulators such as interleukin 1 receptor associated kinase 3 (IRAK-3) and the ubiquitin modifying enzyme A20 (gene name: tumor necrosis factor-alpha-induced protein 3, *TNFAIP3*) (15). A20 is a key negative feedback inhibitor of the canonical NF-κB signaling pathway exerting its immunomodulatory function through its ubiquitin modifying properties (16–18). Accordingly, A20 deficiency in mice results in multiorgan inflammation and premature death (19). Further studies using conditional knockout mice focused on the role of A20 in innate immune cells. Mice with an A20 deficiency (*Tnfaip3*$^{-/-}$ mice) in the myeloid compartment develop spontaneous polyarthritis with sustained proinflammatory cytokine production (20).

Using a whole-transcriptome analysis approach, we aimed to investigate the molecular mechanisms regulating neutrophil maturation during fetal development and found a robust upregulation of RelB target genes in fetal neutrophils, including A20. Furthermore, we could observe nuclear accumulation of RelB in fetal neutrophils, suggesting constitutively active noncanonical NF-κB signaling and A20 as a key modifier of neutrophil function during fetal ontogeny.

Results

Differential gene expression signatures in human fetal and adult neutrophils. Fetal neutrophils from early embryonic stages display a reduced capacity to react to inflammatory stimuli, thus leaving the organism highly vulnerable to invading pathogens or sterile inflammation. This study aimed to investigate the underlying molecular mechanisms regulating fetal neutrophil function during ontogeny. We therefore performed whole-transcriptome analysis of human fetal cord blood–derived neutrophils from premature (<37 weeks of gestation) and mature (>37 weeks of gestation) infants and compared their gene expression profiles with neutrophils from healthy adult donors (Figure 1A). Flow cytometric analysis and cytospin were used to ensure that comparable cell populations of human adult and mature fetal neutrophils were included in the analysis (Supplemental Figure 1, A and B; supplemental material available online with this article; https://doi.org/10.1172/jci.insight.155968DS1). We identified 124 differentially regulated genes (FDR < 5%, Figure 1A); 56 were upregulated and 68 were downregulated in fetal versus adult neutrophils. To understand the biological significance underlying these differentially regulated genes and provide a rough overview, we applied WEB-based Gene SeT AnaLysis Toolkit (WebGestalt), which allowed us to group our candidate genes according to their function and association with biological processes (Figure 1B and Supplemental Table 1). Strikingly, the analysis revealed that most prominent changes in identified gene sets occurred for those sets of genes with negative regulatory functions in cellular defense and activation as well as protein trafficking.

The noncanonical NF-κB subunit RelB determines a specific gene expression signature in fetal human neutrophils. Next, we analyzed the differentially regulated genes found in our transcriptomic screen in more detail. We could associate several of the differentially regulated genes (including *TNFAIP3*, *IRAK3*, *RELB*) to the NF-κB signaling pathway. This prompted us to systematically assess whether binding sites of NF-κB subunits in GM12878 human lymphoblastoid B cells (15) were overrepresented at promoters of genes that were upregulated or downregulated in fetal neutrophils in comparison with adult neutrophils. RelB was

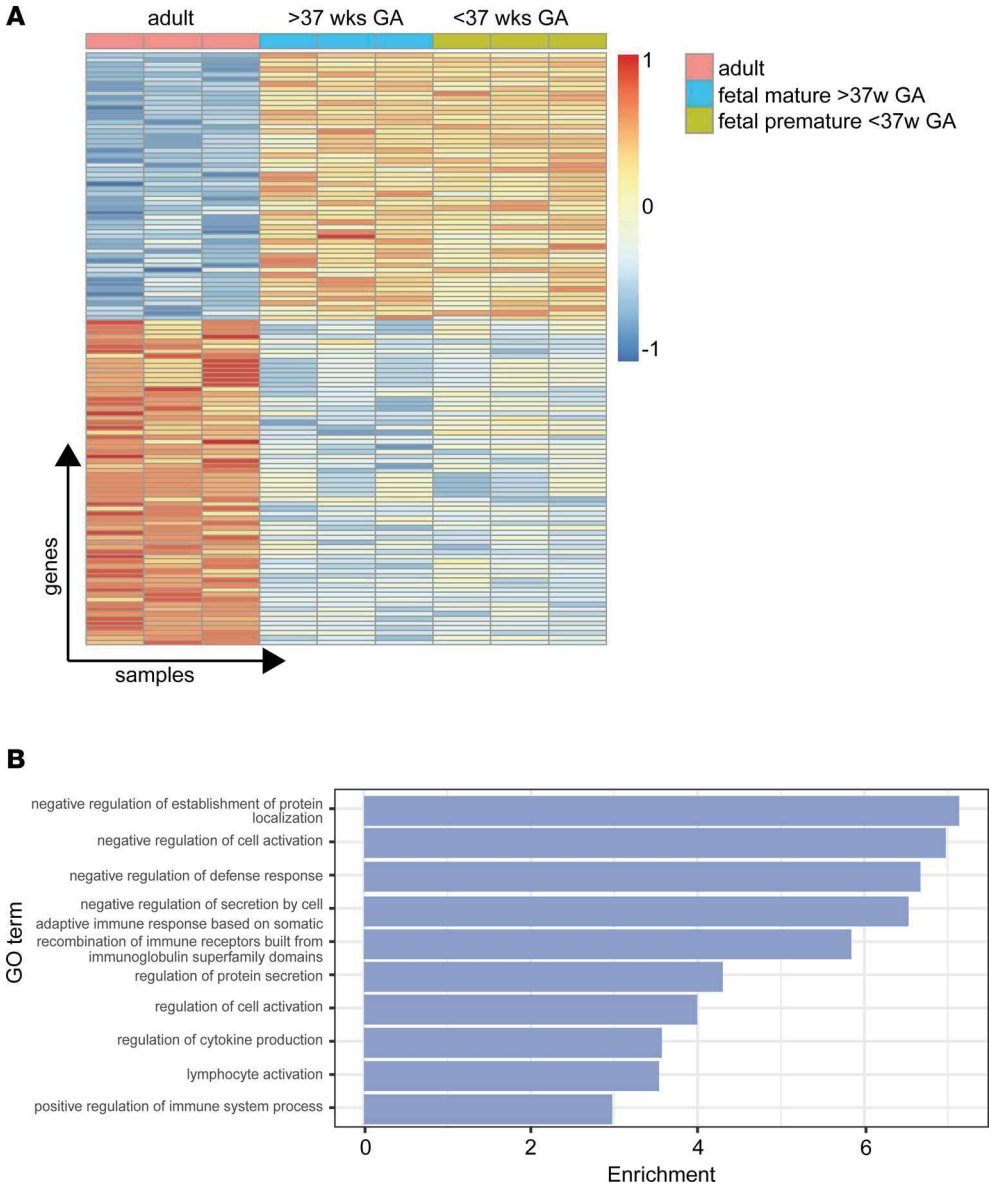

Figure 1. Differential gene expression signatures in human fetal and adult neutrophils. (**A**) Neutrophils were isolated from peripheral blood of adult healthy donors and umbilical cord blood samples from mature fetuses (gestational age > 37 weeks) or premature fetuses (gestational age < 37 weeks) (n = 3 per group). Differentially regulated genes between the samples are shown, each column representing 1 sample and each line 1 gene. Upregulated genes are depicted in red, whereas downregulated genes are depicted in blue. (**B**) Differentially expressed genes were used for gene set enrichment analysis. The bar plot shows the fold enrichment (x axis) of the fraction of members of the gene set within all differentially expressed genes divided by the fraction of members of the gene set in the genome-wide background set for each of the gene sets (y axis), which are among the top 10 of all gene sets with FDR < 5%. GO, Gene Ontology.

the subunit with strongest overrepresentation in promoters of upregulated genes ($P = 5.19 \times 10^{-7}$ Fisher's exact test, OR = 4.0, Supplemental Table 2). Using this approach, we were able to identify 40 RelB target genes that were upregulated in fetal neutrophils compared with their adult counterparts and an additional 24 RelB target genes displaying the opposite signature with lower expression in fetal neutrophils (Figure 2A and Supplemental Table 3). This means that 71% of all fetal upregulated genes and 35% of all fetal downregulated genes are associated with the RelB pathway.

Upon activation of the noncanonical NF-κB signaling pathway, the transcription factor RelB is translocated from the cytoplasm into the nucleus to induce gene transcription. In order to test for baseline activation of the noncanonical pathway, we analyzed RelB localization in fetal and adult human neutrophils using imaging flow cytometry (Amnis). This allows us to assess the subcellular localization of RelB on a

large cell population. We were able to detect colocalization of RelB to the DAPI-stained nucleus of premature and mature fetal neutrophils, while this was significantly reduced in adult neutrophils (Figure 2, B and C). In addition, we could see the same increased colocalization of RelB to the DAPI-stained nucleus in murine fetal neutrophils compared to adult cells (Supplemental Figure 1C). Furthermore, the canonical NF-κB subunit p65 was not differentially colocalizing to the nucleus in fetal or adult neutrophils, suggesting an exclusive baseline activation of the noncanonical NF-κB signaling pathway in human fetal neutrophils (Supplemental Figure 1D). We then quantified total RelB protein in our samples and could observe no significant alterations in overall RelB expression in fetal versus adult neutrophils, although a tendency toward increased RelB amount was detected in samples from premature infants (Supplemental Figure 1E). In resting cells, RelB activation and translocation is inhibited by its binding to p100. Upon activation of the noncanonical NF-κB signaling pathway, p100 is in part proteasomally degraded into p52, and subsequently, as a dimer with RelB, translocated into the nucleus. In accordance with our previous results, we detected significantly higher baseline levels of cleaved p52 in fetal neutrophils compared with adult neutrophils by Western blot analysis, with the highest values in early premature samples under 37 weeks of gestational age (Figure 2D). As these results indicate that in fetal neutrophils NF-κB signaling is shifted toward the noncanonical pathway, we were interested in upstream factors inducing this pathway. While TLR4 and the TNF receptor are well-known inducers of the canonical NF-κB signaling pathway, there are also a variety of receptors that differentially induce the noncanonical pathway, including CD40, Ox40, RANK, LTβR, and TNFRII being expressed on neutrophils. Using flow cytometry analysis, we could detect expression of TNFRII (Figure 2E) and LTβR (Supplemental Figure 2A) on fetal and adult human as well as murine neutrophils. Interestingly, TNFRII displayed significantly higher surface expression levels in human samples obtained at a gestational age under 37 weeks compared with adult, with a similar tendency, although not significant, in murine samples (Figure 2E). One of the ligands for TNFRII is LT-α, well known for its role in the development of secondary lymphatic tissue (21). We analyzed serum levels of LT-α in cord blood serum of human premature and mature infants as well as in adult serum using quantitative ELISA. We detected significantly higher LT-α serum levels in cord blood of premature and mature infants than in samples from adults (Figure 2F), suggesting that the LT-α/TNFRII axis might play a critical role in the observed elevated baseline activation of the immunomodulatory noncanonical NF-κB signaling pathway in fetal neutrophils.

Downregulation of the canonical NF-κB signaling pathway in fetal neutrophils. Because of the described immune-modulatory function of the noncanonical NF-κB signaling pathway and its antagonizing effects on canonical NF-κB signaling, we wanted to test whether fetal neutrophils also display reduced inflammation-driven activation of the canonical NF-κB pathway. To address this, we stimulated fetal and adult human neutrophils for 20 minutes with 10 ng/mL TNF-α, which induces canonical signaling via the TNF receptor. Upon activation of the TNF receptor, a series of kinases is activated, resulting in the phosphorylation of IκBα, IκBβ, and IκBγ, leading to their proteasomal degradation and release of p65 and p50 heterodimers. While TNF-α stimulation resulted in a robust phosphorylation of IκBα in adult neutrophils (Figure 3A), we were unable to observe a similar increase in phosphorylation in fetal samples, indicating that fetal neutrophils are less capable of activating the canonical signaling cascade upon stimulation. This observation was not due to a differential expression of the TNF1 receptor (TNFRI) on the neutrophil surface (Supplemental Figure 2B), suggesting an intracellular regulatory mechanism. Additionally, stimulation with TNF-α was unable to induce upregulation of Mac-1 ($\alpha_M\beta_2$, CD11b/CD18) surface levels in human fetal neutrophils to the same extent as in adult neutrophils (Figure 3B). Surface expressed Mac-1 has been demonstrated to be critical for neutrophil recruitment into inflamed tissue (22). Hypothesizing that factors in fetal serum like LT-α keep fetal neutrophils in a less activatable state, we stimulated adult neutrophils with fetal or adult serum and analyzed the levels of phosphorylated IκBα and p52 as well as neutrophil effector functions (Figure 3C). Incubating neutrophils with fetal serum showed diminished phosphorylation of IκBα compared with stimulation with adult serum. When being stimulated with fetal serum, p52 protein levels increased compared with controls (Figure 3, D and E), indicating that fetal serum induces a shift in adult neutrophils toward the noncanonical signaling pathway, keeping neutrophils in a rather unresponsive state toward inflammatory stimuli. We performed the same experiment as described before on fetal human neutrophils and could see that adult human serum was able to switch fetal neutrophils to a proinflammatory state with upregulated phosphorylated IκB levels (Supplemental Figure 2C). This again reinforces our hypothesis that factors like LT-α in the fetal serum are able to dampen the inflammatory

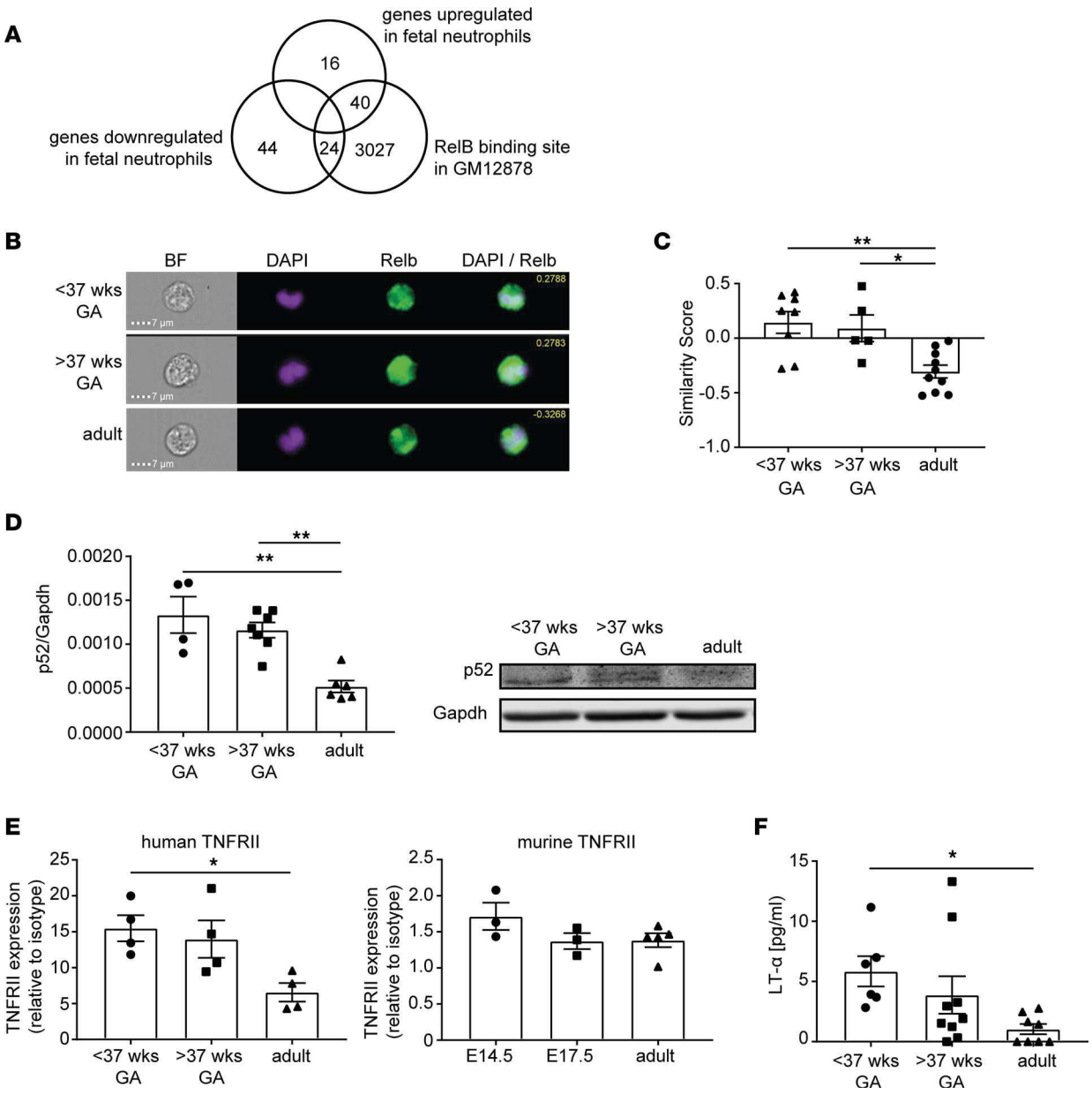

Figure 2. The noncanonical NF-κB subunit RelB determines a specific gene expression signature in fetal human neutrophils. (**A**) Venn diagram representing RelB-regulated genes within all genes up- and downregulated in adult compared with fetal neutrophils. Data were correlated with GM12878 human lymphoblastoid B cells (published data set) (15). (**B**) Imaging flow cytometry was performed on cord blood neutrophils from premature (gestational age < 37 weeks) and mature (gestational age > 37 weeks) fetal samples and peripheral blood from adult healthy donors. Representative pictures of fetal and adult neutrophils are shown as bright-field image, DAPI, NF-κB subunit RelB, and a DAPI/RelB overlay. Respective similarity scores are displayed. Scale bar: 7 μm. (**C**) Quantification of nuclear RelB. Similarity score defines overlap of nuclear DAPI signal and the respective NF-κB subunit. All data are presented as mean ± SEM. (*P < 0.05, **P < 0.005, n = 5–10.) Ordinary 1-way ANOVA with Tukey's multiple comparisons test. (**D**) Western blot and respective quantitative analysis of p52 in isolated neutrophils from premature (gestational age < 37 weeks), mature (gestational age > 37 weeks), and adult samples. Band intensity was normalized to Gapdh. All data are presented as mean ± SEM (**P < 0.005, n = 4–7). Ordinary 1-way ANOVA with Dunnett's multiple comparisons test. (**E**) Flow cytometry analysis of TNFRII expression on human and murine neutrophils out of whole blood from indicated gestational ages. Median fluorescence intensity normalized to isotype control is displayed. All data are presented as mean ± SEM (*P < 0.05, n = 3–5). Ordinary 1-way ANOVA with Dunnett's multiple comparisons test. (**F**) LT-α protein levels in cord blood serum from premature (gestational age < 37 weeks) and mature infants (gestational age >37 weeks) and from whole blood of adult healthy donors by quantitative ELISA. Values are displayed in pg/mL. All data are presented as mean ± SEM. (*P < 0.05, n = 6–9.) Ordinary 1-way ANOVA with Dunnett's multiple comparisons test.

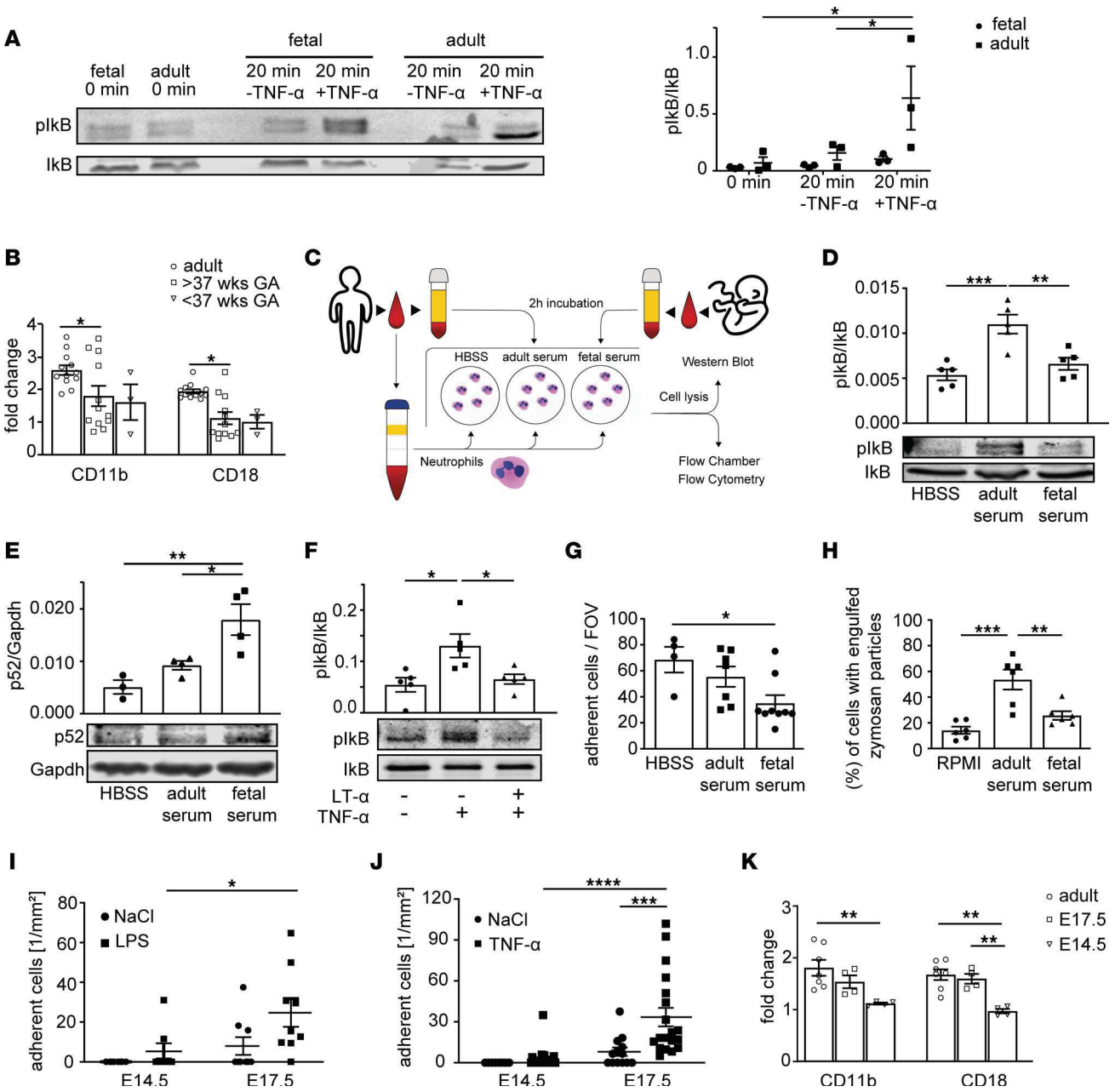

Figure 3. Downregulation of the canonical NF-κB signaling pathway in fetal neutrophils. (**A**) Western blot of IκB phosphorylation after TNF-α stimulation in fetal (gestational age > 37 weeks) and adult human neutrophils. Normalization to IκB. (*P < 0.05, n = 3.) Two-way ANOVA with Tukey's multiple comparisons. (**B**) Quantitative analysis of Mac-1 levels after 2-hour TNF-α stimulation in human adult, mature, and premature fetal neutrophils by flow cytometry. Fold-change: normalization to control. (*P < 0.05, n = 3–12.) Two-way ANOVA with Tukey's multiple comparisons. (**C**) Workflow: adult blood neutrophils after 2-hour stimulation with HBSS or RPMI, fetal or adult serum. (**D**) Western blot analysis of phospho-IκB in adult neutrophils after stimulation with adult or fetal serum or HBSS. Normalization to IκB. (**P < 0.005, ***P < 0.001; n = 3–5.) Ordinary 1-way ANOVA with Tukey's multiple comparisons. (**E**) Western blot analysis of p52 in adult neutrophils after stimulation with adult or fetal serum. Normalization to Gapdh. (*P < 0.05, **P < 0.005, n = 3–4.) Ordinary 1-way ANOVA with Tukey's multiple comparisons. (**F**) Western blot analysis of IκB phosphorylation after incubation of human adult neutrophils with LT-α, followed by TNF-α stimulation. Normalized to IκB. (*P < 0.05; n = 5.) Ordinary 1-way ANOVA with Tukey's multiple comparisons. (**G**) Adherent cells per FOV in flow chambers coated with rhE selectin, rhICAM-1, and rhIL-8 after stimulation of human adult neutrophils with adult or fetal serum. (*P < 0.05; n = 4-9.) Ordinary 1-way ANOVA with Tukey's multiple comparisons. (**H**) Quantitative analysis of phagocytosis by human neutrophils measuring engulfed Zymosan particles by flow cytometry after stimulation with adult or fetal serum. (**P < 0.005, ***P < 0.001; n = 6.) Ordinary 1-way ANOVA with Tukey's multiple comparisons. (**I** and **J**) Quantified adherent cells in yolk sac vessels after LPS (**I**) or TNF-α (**J**) stimulation, compared with control. (*P < 0.05, ***P < 0.001, ****P < 0.0001, n = 3–8 mice.) Two-way ANOVA with Šídák's (**I**) or Tukey's (**J**) multiple comparisons. (**K**) Quantitative analysis of Mac-1 surface levels after 2-hour TNF-α stimulation in murine adult and E14.5 and E17.5 fetal neutrophils by flow cytometry. Fold-change: normalization to control. (**P < 0.005; n = 3–12.) Two-way ANOVA with Tukey's multiple comparisons. All data are presented as mean ± SEM (**A**, **B**, and **D**–**K**).

NF-κB–induced response. Interestingly, incubation of human adult neutrophils with recombinant human LT-α for 2 hours was also able to prevent canonical NF-κB signaling via TNF-α (Figure 3F), as shown by strongly reduced phosphorylation levels of IκBα.

Next, we investigated if incubation of human adult neutrophils with fetal serum is also affecting other neutrophil functions and tested neutrophil adhesion using flow chambers coated with recombinant human intercellular adhesion molecule 1 (rhICAM-1)/rhE selectin and rhCXCL8 as a substrate for adhesion. These experiments showed that adult neutrophils incubated with fetal serum displayed reduced adhesion in the flow chamber compared with cells incubated with adult serum, indicating that fetal serum has the capacity to reduce neutrophil adhesion under flow (Figure 3G).

Using the Zymosan uptake assay, we then analyzed phagocytosis of human adult neutrophils after incubation with fetal serum. Again, fetal serum incubation was able to reduce phagocytosis of Zymosan by adult neutrophils (Figure 3H), providing evidence that various neutrophil functions are altered in the presence of fetal serum. Blocking TNFRII on human adult neutrophils using an anti–human TNFRII antibody was able to prevent the inhibitory activity of fetal serum, since phagocytic activity of adult neutrophils stimulated with fetal serum was significantly increased after blocking of TNFRII beforehand. Adult neutrophils in the presence of adult serum after blocking the TNFRII receptor did not show increased phagocytic activity, verifying an important role of the LT-α/TNFRII axis in modulating fetal neutrophil function (Supplemental Figure 2D). Next, we applied an in vivo model of fetal inflammation and performed intravital imaging experiments on neutrophil adhesion in inflamed mouse yolk sac vessels 2 hours after intrauterine LPS (100 μg) stimulation. These experiments were conducted with *Lyz2*^{GFP} mice (23), where neutrophils harbor a bright GFP signal. LPS via binding to TLR4 is one of the main activators of the canonical NF-κB signaling pathway, inducing a proinflammatory MyD88-dependent transcriptional program that consequently results in the activation of neutrophils and endothelial cells, inducing neutrophil adhesion to the inflamed endothelium. While in E14.5 yolk sac vessels only very few leukocytes interacted with the vessel wall after LPS stimulation (Supplemental Video 1 and Figure 3I), we were able to detect significantly higher numbers of adherent cells at yolk sac vessels of E17.5 fetuses compared with control stimulation using normal saline (Supplemental Video 2). We also applied TNF-α in E14.5 and E17.5 fetuses and obtained similar numbers of adherent cells as in LPS-stimulated fetuses (Figure 3J). To exclude differences in the expression of TLR4 on the neutrophil surface of E14.5 versus E17.5 fetuses, we performed flow cytometry analysis, which revealed similar expression of TLR4 on neutrophils from E14.5 and E17.5 fetuses compared to neutrophils from adult mice (Supplemental Figure 2E).

Adhesion to inflamed vessels critically depends on the interaction between endothelial ICAM-1 and LFA1 (integrin $\alpha_L\beta_2$), expressed on neutrophils. Thus, we analyzed the capacity of E14.5, E17.5, and adult neutrophils to bind soluble recombinant murine ICAM-1 (rmICAM-1 hFC chimera) in vitro. As expected, stimulation of neutrophils with the chemokine CXCL1 or using PMA induced an increase in ICAM-1 binding due to LFA1 activation in adult neutrophils, but this effect was severely reduced in neutrophils from E14.5 or E17.5 fetuses (Supplemental Figure 2F). Finally, stimulation of isolated murine neutrophils with TNF-α was unable to induce upregulation of Mac-1 ($\alpha_M\beta_2$, CD11b/CD18) surface levels in fetal neutrophils (E14.5 and E17.5) to the same extent as in adult neutrophils (Figure 3K).

A20 upregulation in fetal neutrophils results in diminished adhesion. So far, our results revealed that fetal neutrophils exhibit a pronounced baseline activation of the noncanonical NF-κB signaling pathway. Several of the RelB target genes identified in the transcriptomic analysis have immunomodulatory functions and are able to suppress the inflammatory canonical NF-κB signaling pathway. One of those upregulated RelB target genes in fetal neutrophils and detected in the transcriptomic analysis was the ubiquitin-modifying enzyme A20, which has been reported as key negative regulator of innate immune responses. A20 might therefore be an interesting candidate in downmodulating innate immune responses during fetal life. To test this, we first validated A20 upregulation in fetal human neutrophils by real-time PCR (RT-PCR) (Figure 4A) and additionally on the protein level in comparison with adult neutrophils (Figure 4B). We found a significant upregulation of A20 on the transcriptional and on the protein level in fetal neutrophils. Next, we investigated A20 levels in the mouse and validated our findings in human neutrophils, with increased levels of A20 mRNA in fetal versus adult mouse neutrophils (Figure 4C). Interestingly, A20 levels gradually started to decrease at late embryonic stages (E14.5 versus E17.5), which is in line with our in vivo findings of increased adhesion after LPS or TNF-α stimulation at E17.5 versus E14.5. Thus, we conclude that through downregulating A20

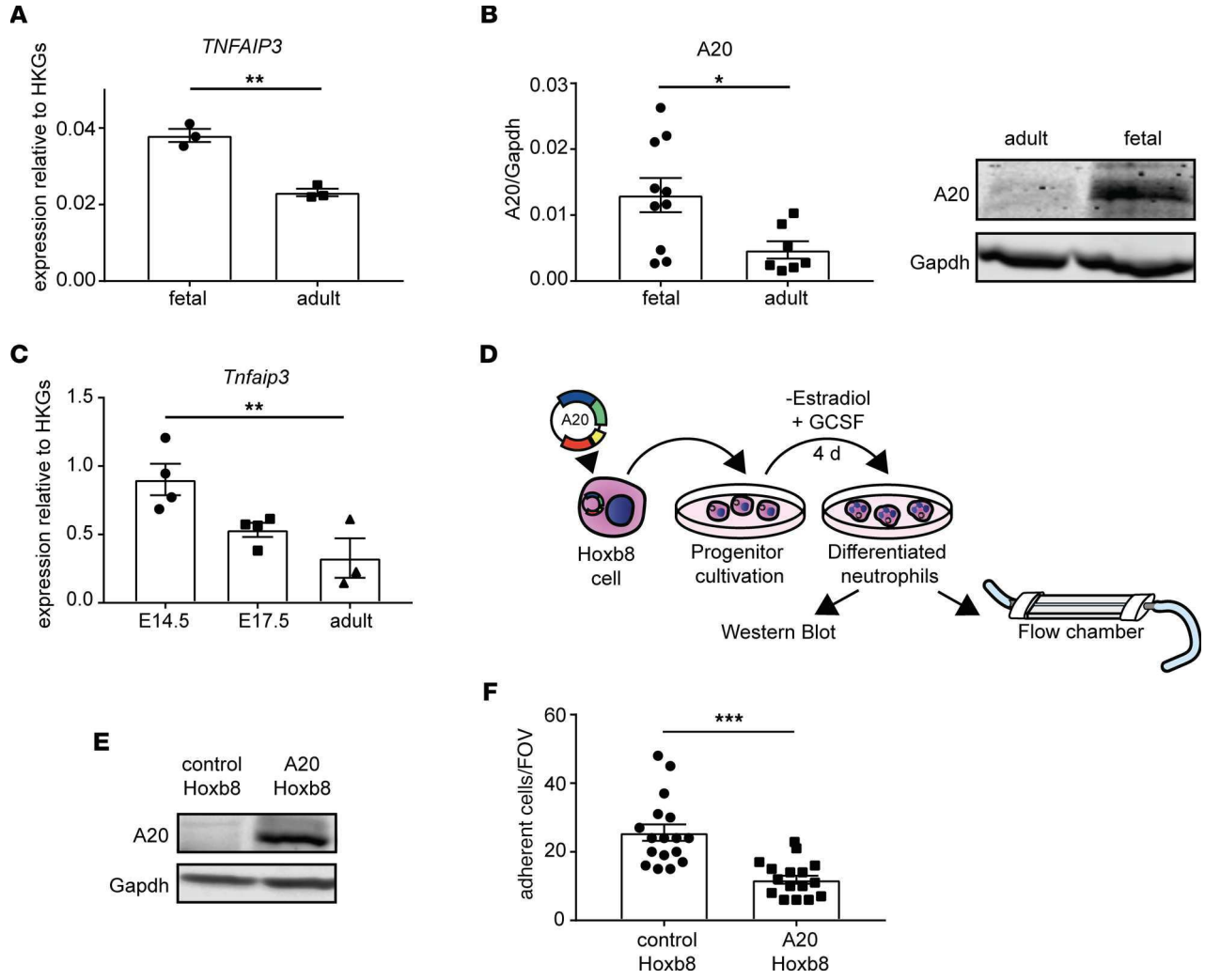

Figure 4. A20 upregulation in fetal neutrophils results in diminished adhesion. (**A**) mRNA expression of *TNFAIP3* in fetal human neutrophils was compared to neutrophils isolated from peripheral blood of adult healthy donors by quantitative RT-PCR. Expression is shown relative to the housekeeping gene (HKG) *GAPDH*. (**$P < 0.005$; $n = 3$.) Unpaired Student's *t* test. (**B**) Western blot and respective quantitative analysis of A20 expression in neutrophils isolated from human fetal cord blood samples and neutrophils from adult peripheral blood. Band intensity was normalized to Gapdh protein. All data are presented as mean ± SEM. (*$P < 0.05$, $n = 8$–10.) Unpaired Student's *t* test. (**C**) Expression of *Tnfaip3* mRNA relative to the HKGs *B2m* and *Gyk* in murine neutrophils was investigated by quantitative RT-PCR in isolated neutrophils of E14.5 and E17.5 embryos and from the peripheral blood of adult mice. (**$P < 0.005$; $n = 3$–4.) Ordinary 1-way ANOVA with Dunnett's multiple comparisons test. (**D**) Workflow of Hoxb8 experiments. Hoxb8 precursor cells overexpressing A20 and Hoxb8 control cells were differentiated into Hoxb8 neutrophils, and subsequently flow chamber experiments were performed in addition to Western blot verification of A20 overexpression. (**E**) Representative Western blot image of A20 expression in control and A20-overexpressing Hoxb8 cells. Gapdh expression is displayed to ensure equal loading. (**F**) Flow chamber analysis of differentiated Hoxb8 control and A20-overexpressing cell adhesion in microflow chambers coated with rmE selectin/rmICAM-1 and rmCXCL1. One representative field was recorded for 10 minutes using an Olympus BX51WI microscope with a CCD camera (model CF8/1, Kappa) and a water immersion objective (×40/0.8 NA, Olympus). All data are presented as mean ± SEM. (***$P < 0.001$; $n = 3$.) Unpaired Student's *t* test.

expression later during fetal ontogeny, neutrophil adhesiveness increases at the same time. To strengthen this hypothesis, we generated A20-overexpressing Hoxb8 cells and analyzed the adhesive behavior of these cells in a flow chamber system (Figure 4D). Vector-transfected cells without the A20 coding region served as controls. Differentiated Hoxb8 cells have been used as an in vitro and in vivo model system to investigate neutrophil function in mice (24). Western blot analysis of A20-overexpressing differentiated Hoxb8 cells clearly showed a strong upregulation of A20 protein compared with control cells (Figure 4E). To test whether overexpression of A20 influences the adhesive behavior of differentiated Hoxb8 cells, we coated microflow chambers with rmE selectin, rmICAM-1, and rmCXCL1 to mimic the inflamed endothelium and introduced differentiated A20-overexpressing or differentiated control Hoxb8 cells into the chambers at a defined shear rate (1 dyne/cm^2). Analysis of the number of

adherent cells/field of view (FOV) revealed a significant decrease in adhesion of A20-overexpressing cells (Figure 4F), suggesting that A20 is a negative regulator of neutrophil adhesion.

Increased neutrophil recruitment in Tnfaip3$^{fl/fl}$ Ly6g-Cre mice in vivo. In the next set of experiments, we investigated A20-depleted neutrophils in an in vivo setting of sterile inflammation. Previous observations on A20-depleted immune cells described hyperinflammation in different endpoint mouse models, but so far, the impact of A20 deficiency on the leukocyte adhesion cascade itself is not known. As the A20 constitutive knockout is prematurely lethal (19), we bred *Tnfaip3$^{fl/fl}$* mice to *Ly6g-tdTomato-Cre* mice (*Tnfaip3$^{fl/fl}$ Ly6g-Cre*), to obtain mice with a highly specific deletion of A20 in mature neutrophils. We first verified A20 depletion in our model and observed a strong decrease in A20 mRNA in neutrophils derived from *Tnfaip3$^{fl/fl}$ Ly6g-Cre* mice, although a complete knockout was not achieved (Supplemental Figure 3A). Using intravital microscopy of TNF-α–stimulated cremaster muscle, we found no differences in the numbers of rolling neutrophils in *Tnfaip3$^{fl/fl}$ Ly6g-Cre* mice after normalization to the white blood cell count (WBC) compared to *Ly6g-Cre* mice (Figure 5A and Supplemental Video 3). Interestingly, neutrophil rolling velocity was not altered between the groups (Supplemental Figure 3B). Next, we analyzed neutrophil adhesion and found a significant increase in absolute numbers of adherent neutrophils/mm^2 in *Tnfaip3$^{fl/fl}$ Ly6g-Cre* mice compared with the control group (Figure 5B), suggesting that loss of A20 in neutrophils leads to a hyperreactive phenotype with increased adhesion to inflamed microvessels. Finally, we stained the exteriorized and fixed cremaster muscle tissue with Giemsa to visualize extravasated neutrophils. Again, we detected a 30% increase of extravasated neutrophils in *Tnfaip3$^{fl/fl}$ Ly6g-Cre* mice compared with *Ly6g-Cre* mice (Figure 5, C and D). The hemodynamic parameters of both groups did not differ (Table 1). In a second set of in vivo experiments using the cremaster muscle model, experiments were performed within 45 minutes after surgical preparation of the cremaster muscle without additional stimulation. In this mild inflammation model, neutrophil-endothelium interactions are mostly limited to P selectin–dependent rolling, with a few adherent neutrophils (25). Again, hemodynamic parameters were equal in *Tnfaip3$^{fl/fl}$ Ly6g-Cre* mice compared to *Ly6g-Cre* mice (Table 2). Interestingly, we observed decreased rolling velocities along with increased adhesion of A20-deficient neutrophils compared to *Ly6g-Cre* controls (Supplemental Figure 3, C and D), suggesting a neutrophil-intrinsic hyperreactive phenotype in the absence of A20, which is the contrary effect of what we observed in fetal neutrophils with high A20 expression.

Discussion

In this study, we aimed to decipher the molecular mechanisms behind the ontogenetic regulation of neutrophil function during fetal development. In a whole transcriptomic survey, we identified over 120 differentially regulated genes in fetal versus adult human neutrophils. Many of those genes upregulated in fetal samples are RelB target genes that together with elevated nuclear RelB localization and higher p52 values suggest a constitutively active noncanonical NF-κB signaling pathway in fetal neutrophils. In contrast, we observed reduced canonical NF-κB signaling in fetal neutrophils upon stimulation and diminished activation of neutrophil adhesion in an intravital microscopy model of the mouse yolk sac of E14.5 fetuses upon intrauterine LPS or TNF-α stimulation. Interestingly, among upregulated genes in fetal neutrophils, we found the ubiquitin-modifying enzyme A20 that is a well-established and potent negative regulator of the inflammatory canonical NF-κB pathway. Indeed, we generated Hoxb8 cells and showed that overexpressing A20 mimics fetal neutrophils and their inability to properly interact with immobilized adhesion molecules in a flow chamber system. On the contrary, murine neutrophils lacking A20 showed a hyperinflammatory phenotype with increased adhesion to inflamed microvessels and extravasation into inflamed cremaster muscle tissue.

Neutrophils are among the body's first line of defense against invading pathogens. Thus, proper function of neutrophils is critical to reestablish homeostasis without harming the body. Prematurely born infants, especially those born under 33 weeks of gestation, harbor a great risk of infections or sepsis (26). This enhanced susceptibility has been linked to lacking maternal antibodies (27) but also to immature innate immune system compared with term infants (28). It has been shown that, under artificial shear stress, neutrophils from mature born infants demonstrate reduced adhesion compared with adult neutrophils (29), an effect that is even more pronounced in premature neutrophils (7), suggesting an ontogenetic regulation of neutrophil function. Also on the level of direct host defense, neonatal neutrophils lack functionality, as shown by reduced neutrophil extracellular trap formation capability in neonates (30, 31). Interestingly, the molecular mechanisms regulating this ontogenetic maturation are still incompletely understood (28). Using a systems biology approach, a recent study by the Kollmann group investigated peripheral blood samples of newborn infants during the first

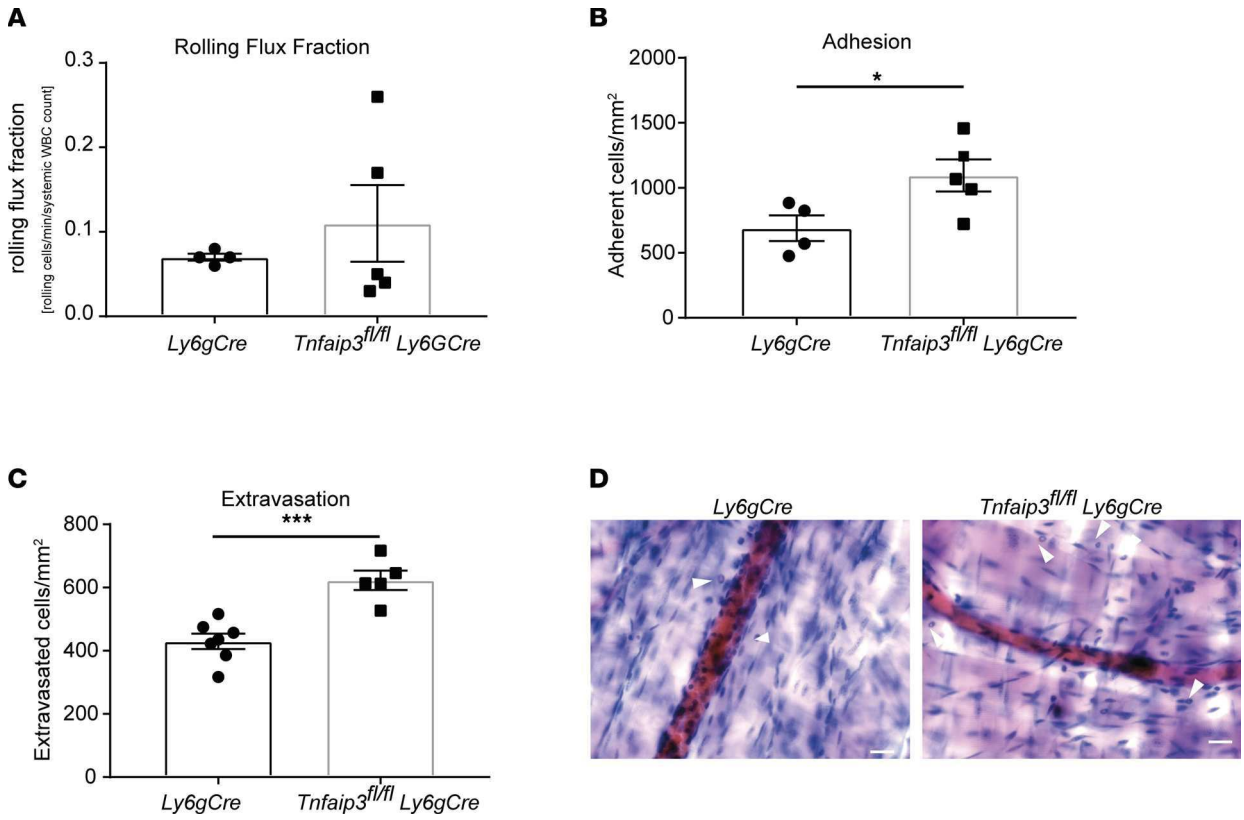

Figure 5. Increased neutrophil recruitment in *Tnfaip3*$^{fl/fl}$ *Ly6g-Cre* mice in vivo. In vivo leukocyte rolling, adhesion, and extravasation were analyzed in 2-hour TNF-α–stimulated venules of mouse cremaster muscles in *Ly6g-Cre* and *Tnfaip3*$^{fl/fl}$ *Ly6g-Cre* mice. (**A**) Rolling flux fraction (rolling cells/min divided by the total leukocyte flux), (**B**) adherent cells/mm^2, and (**C**) leukocyte extravasation in the perivascular region of Giemsa-stained cremaster muscle whole mounts. A total of 4 *Ly6g-Cre* (17 vessels) and 5 *Tnfaip3*$^{fl/fl}$ *Ly6g-Cre* (17 vessels) mice were analyzed. Values are given as mean ± SEM. (*$P < 0.05$, ***$P < 0.001$.) Unpaired Student's *t* test. (**D**) Representative images of Giemsa-stained whole mounts of cremaster muscles of *Ly6g-Cre* and *Tnfaip3*$^{fl/fl}$ *Ly6g-Cre* mice. Arrows point to extravasated neutrophils. Scale bar: 30 μm.

week of life (9). They performed transcriptomic, proteomic, and metabolomic analyses and revealed a dynamic developmental trajectory affecting the interferon and complement pathway. In addition, the analysis also found changes in neutrophil-associated signaling processes affecting TLR-2 and -9 as well as IL-1–dependent signaling (9). In another recent study, Olin and colleagues investigated immune cell populations and selected plasma proteins during the first 3 months of life in preterm and term infants using mass cytometry (10). The authors identified a rather stereotypic postnatal development of the immune system along one shared trajectory. Interestingly, the authors found a complete segregation of 267 investigated plasma proteins and detected significantly lower neutrophil numbers at birth between preterm and term infants (10). Furthermore, they uncovered upregulation of IFN-γ and CXCL8 production with increasing maturation. Of note, cord blood measurements of the immune system did not correlate well to the immune system status postnatally, which the authors traced back to multifactorial perinatal changes.

To shed new light on the regulation of neutrophils' function particularly during human fetal ontogeny, we performed a whole-transcriptome approach. To do this, we analyzed neutrophils derived from cord blood of premature and mature infants and compared it to blood-isolated neutrophils from adults, in search for genes that might explain the observed functional difference between fetal and adult neutrophils. Out of 124 differentially regulated genes, we found a prominent cluster of 64 genes that are associated with the NF-κB/RelB pathway (15). Furthermore, our results show higher nuclear RelB levels in fetal samples as well as higher p52 values, indicating an upregulation of the noncanonical NF-κB pathway. Unlike the canonical, inflammatory NF-κB pathway, noncanonical signaling is more diverse, ranging from secondary lymphatic tissue development to circadian rhythm, but also acts as a modulator of immune response (13). While the role of RelB in the myeloid compartment is less known, studies on RelB single- and RelB/p50 double-knockout mice revealed that RelB also represses excessive neutrophil recruitment (32, 33). Those findings suggest

Table 1. Vessel parameters of *Ly6g-Cre* and *Tnfaip3*$^{fl/fl}$ *Ly6g-Cre* mice after TNF-α injection

	Diameter (μm)	Length (μm)	Centerline velocity (μm/s)	Shear rate (1/s)	Systemic WBC (K/μL)	Systemic neutrophil count (K/μL)
Ly6g-Cre	32.24 ± 1.41	260.95 ± 1.95	1,826.09 ± 172.77	1,441.65 ± 155.56	2.81 ± 0.2	0.64 ± 0.03
Tnfaip3$^{fl/fl}$ *Ly6g-Cre*	30.77 ± 0.98	258.51 ± 1.84	2,142.14 ± 145.57	1,717.18 ± 133.03	3.35 ± 0.4	0.79 ± 0.08

that an upregulation of RelB target genes in neonatal neutrophils could act as immune suppressors of the canonical NF-κB pathway. Our results further lead to the assumption that elevated factors in fetal serum like LT-α and an accompanying stronger surface expression of the TNFRII receptor could initiate this increased signaling. Monocytes from preterm infants were shown to display diminished TLR4 expression and MyD88 signaling, along with decreased cytokine production (34, 35). Similar observations were made for neutrophils derived from premature infants (36). Also in our experiments, TNF-α signaling via TNFR led to decreased IκB phosphorylation that would be required to initiate p65 nuclear translocation. This corroborates our hypothesis of a reduced canonical NF-κB signaling in fetal neutrophils as a consequence of immunosuppressive factors transcribed by the RelB pathway. We additionally show that stimulating adult neutrophils with fetal serum for 2 hours markedly inhibited IκB phosphorylation and, at the same time, elevated p52 levels, as an indicator of increased noncanonical signaling. This silencing of myeloid cells observed in our study is supported by a recent report demonstrating that under baseline conditions, TLR4-induced IL-1β production as well as the biological relevant secretion of cleaved IL-1β is diminished in neonatal monocytes due to impaired formation of the NLRP3 inflammasome protein complex (37). Considering the fact that pathologically high levels of cord blood IL-1β are linked to organ damage in the fetus/newborn (38), tuning down innate immune cell function appears to be beneficial for normal fetal development in its physiological environment. We further verified this by intravital imaging of neutrophil recruitment in yolk sac vessels, where we demonstrated an ontogenetic regulation of neutrophil adhesiveness local LPS or TNF-α stimulation.

Among our RelB target genes that were ontogenetically upregulated in fetal neutrophils, we found the ubiquitin-modifying enzyme A20, a complex regulator of NF-κB signaling. Due to its structure, A20 is able to cleave ubiquitin chains, while at the same time acting as a ubiquitin E3 ligase and binding ubiquitin chains. Therefore, A20 interferes with and modifies ubiquitylated proteins and by this mechanism regulates NF-κB signaling in multiple ways. Originally, A20 was described to be activated by the canonical pathway itself (39) and is now well accepted as a negative feedback regulator that silences the initiated inflammatory response (40, 41) and at the same time activates noncanonical NF-κB signaling (42). In A20-overexpressing HEK293 cells, TNF-induced NF-κB activation is abolished (40) in the same fashion as we observed in fetal samples that harbor high A20 expression. To show the functional consequences of high A20 protein levels on immune cell function, we generated A20-overexpressing Hoxb8 cells and observed a decreased adhesion in a flow chamber system. This further strengthens the suggested role of A20 as a key factor that switches fetal neutrophils toward the noncanonical NF-κB pathway and keeps the canonical NF-κB pathway constitutively silent. On the other hand, loss of A20 function due to truncated gene variants or SNPs is associated with auto-inflammatory disorders like Crohn's disease, psoriasis, rheumatoid arthritis, and many more (16, 43–46). This can also be observed in mice, either with constitutive A20 depletion (19) or with conditional deletion in the hematopoietic compartment (20, 47–50). Interestingly, those mice also display increased IL-1 secretion and increased basal and LPS-induced expression levels of the inflammasome adapter NLRP3 (47, 51). Those previous findings of hyperinflammation in various disease models led us to investigate the neutrophil recruitment cascade itself in the absence of A20, anticipating here an overactive inflammatory phenotype. As expected, we observed more adhesion and transmigration of A20-depleted neutrophils compared with control animals.

Taken together, we provide mechanistic insights into the ontogenetic regulation of neutrophils during fetal life and uncover a shift in NF-κB signaling toward the antiinflammatory noncanonical NF-κB pathway that is accompanied by transcriptional upregulation of A20, a powerful negative regulator of the inflammatory response. In consequence, fetal neutrophils are restricted in their reactivity toward inflammatory signals that would finally lead to neutrophil adhesion and transmigration into inflamed tissue. While this seems to be highly beneficial for the fetus within its protected intrauterine environment, it leads

Table 2. Vessel parameters of *Ly6g-Cre* and *Tnfaip3*$^{fl/fl}$ *Ly6g-Cre* mice (trauma)

	Diameter (μm)	Length (μm)	Centerline velocity (μm/s)	Shear rate (1/s)	Systemic WBC (K/μL)	Systemic neutrophil count (K/μL)
Ly6g-Cre	33.72 ± 1.47	260.01 ± 2.99	2,554.55 ± 189.64	1,924.61 ± 160.29	5.2 ± 0.4	1.6 ± 0.2
Tnfaip3$^{fl/fl}$ *Ly6g-Cre*	32.94 ± 0.92	259.12 ± 1.77	2,005.13 ± 139.45	1,511.13 ± 107.39	6.0 ± 0.7	1.0 ± 0.1

to a substantial increase in morbidity and mortality in prematurely born infants facing the outside world with all its challenges and threats.

Methods

Sample collection and study population. All cord blood samples used in the study were obtained from neonates delivered by Cesarean section at Dr. von Hauner Children's Hospital or University Hospital Grosshadern, LMU Munich. Immediately after delivery, blood was taken in citrate buffer–containing collection tubes or serum-collecting tubes (S-Monovette, Sarstedt). Exclusion criteria included congenital malformations, known infections of the mother, and familial immune diseases. Blood from adult healthy donors was taken by venipuncture. Blood sampling from adults took place at the Biomedical Center Munich, LMU Munich.

Microarray and data processing. Human fetal and adult neutrophils were purified, and RNA was isolated as described below. RNA was loaded on an Hgu133plus (Affymetrix). The R Bioconductor package oligo (52) was used to create expression sets, perform the background correction and quantile normalization per sample, as well as log-transform the data. The microarray data have been deposited in the National Center for Biotechnology Information's public database Gene Expression Omnibus (accession number: GSE222156). See Table 3 for gestational ages and corresponding cell numbers. We tested all genes on the array for differential expression between the fetal and the adult samples using a Student's 2-tailed *t* test for each gene separately and then applied the Benjamini-Hochberg procedure to adjust for multiple-hypothesis testing. Probe sets were annotated to Ensembl gene IDs, and summaries are given on the level of Ensembl gene IDs. Differentially expressed genes were defined as all genes with FDR < 5%.

Gene set enrichment analysis. Gene set enrichment analysis was performed using WebGestalt (53, 54). All differentially expressed genes (FDR < 5%) were used as input. All genes on the Hgu133plus array were used as background. The minimal gene set size was set to 2. Analyses were run separately for gene sets from the "biological process" and "molecular function" ontologies from GO. The hypergeometric test was used to assess the significance of the overlap of the differentially expressed genes with each of the gene sets. The Benjamini-Hochberg procedure was applied to adjust for multiple-hypothesis testing. Significant gene sets were defined as gene sets with FDR < 5%. None of the gene sets of the "molecular function" ontology was significant.

Identification of RelB target genes. We obtained ChIP-Seq peak calls of canonical and noncanonical subunits of Nκ-KB (p65, p50, RelB, and p52) measured in the lymphoblastoid cell line GM12878 (15). For each subunit we defined genes as bound if a binding site of the subunit localized within 1 kb of the gene. Using Fisher's exact test, we assessed whether binding sites for each subunit were overrepresented or depleted separately in the set of up- and downregulated genes identified by the microarray analysis. Genes that were both differentially expressed and bound by a subunit were defined as target genes of the subunit.

Mice. C57BL/6 animals were purchased from Charles River Laboratories and housed in the animal facility of the Biomedical Center Munich at least 1 week before use in experiments. *Lyz2*^{GFP}, *Tnfaip3*$^{fl/fl}$, and *Ly6g-Cre* tdTomato (23, 49, 55, 56) mice were generated as described before.

Generation of A20-overexpressing Hoxb8 cells and differentiation into neutrophil-like cells. The murine *pWPI-A20-IRES-EGFP* vector was a gift (University of California, San Francisco, San Francisco, California, USA). The *pMSCV-Puro* and *pCL-Eco* vectors were provided by Hans Häcker (St. Jude Children's Research Hospital, Memphis, Tennessee, USA). For viral transduction, the coding region of *A20-IRES-EGFP* was subcloned into the retroviral backbone *pMSCV-Puro*.

For virus production, HEK293T cells (ATCC CRL-11268) were transfected with *pMSCV-A20-IRES-EGFP* and *pCL-Eco* using Lipofectamine 2000 (Thermo Fisher Scientific) according to the manufacturer's protocol. Virus-containing supernatant was harvested 48 hours posttransfection, and Hoxb8-SCF cells, generated from C57BL/6 mice as described previously (57, 58), were transduced by

Table 3. Gestational ages and corresponding cell numbers used for microarray

Gestational age (weeks)	Cell number for microarray
32+4	2×10^6
32+0	2×10^6
30+5	2×10^6
40+2	1×10^7
38+0	2×10^6
38+6	6×10^5
Adult	3×10^6
Adult	5×10^6
Adult	4×10^6

spinocculation using Lipofectamine. Upon 72 hours posttransduction, puromycin-resistant cells were selected for the length of 7 days.

Differentiation of Hoxb8-SCF cells toward neutrophils was allowed by culture for 4 days in differentiation medium consisting of RPMI 1640 supplemented with 10% FCS, 1% penicillin/streptomycin, 20 ng/mL rmG-CSF (Peprotech), and 2% SCF-containing supernatant as described (59).

Purification of human and murine neutrophils. Human neutrophils were isolated from umbilical cord or peripheral venous blood by layering cells on a Polymorphprep density gradient (AXIS-SHIELD PoC AS) followed by centrifugation (500*g*, 30 minutes, room temperature). The neutrophil layer was harvested, then washed with Dulbecco's PBS, and erythrocytes were lysed with ammonium chloride lysis buffer. Subsequently, neutrophils were purified by EasySep Human Neutrophil Enrichment Kit (STEMCELL Technologies). Alternatively, the EasySep Direct Human Neutrophil Isolation Kit (STEMCELL Technologies) was used. For quantitative RT-PCR analysis, purity was investigated by flow cytometry and required to be more than 90%.

Murine neutrophils were isolated from fetal blood by decapitation of C57BL/6 fetuses on E13.5/E14.5 as well as E17.5/E18.5. Blood was layered on a Percoll density gradient (MilliporeSigma). The neutrophil layer was isolated, then washed with Dulbecco's PBS, and erythrocytes were lysed with ammonium chloride lysis buffer. To yield a highly pure cell population, neutrophils were further purified using the anti-mouse Ly6G–Pacific Blue antibody (BioLegend catalog 127612) by FACS, using a BD FACSAria III instrument.

RNA processing and quantitative RT-PCR. RNA of neutrophils (>90% purity) was extracted with the RNeasy Mini Kit (QIAGEN). RNA concentration was measured with a NanoDrop instrument (Thermo Fisher Scientific). Reverse transcription was conducted with High-Capacity cDNA Reverse Transcription Kit (Applied Biosystems), and quantitative RT-PCR was done using TaqMan Gene Expression Assays according to the manufacturer's protocol (Applied Biosystems). Expression levels were calculated relative to housekeeping genes. See Table 4 for further detail.

Western blot. Isolated human and murine neutrophils were homogenized in protein lysis buffer (150 mM NaCl, 1% Triton X-100) (AppliChem), 0.5% Na deoxycholate (MilliporeSigma), 50 mM Tris-HCl pH 7.3 (Merck), and 2 mM EDTA (Merck) supplemented with protease (Roche) and phosphatase inhibitors (MilliporeSigma), and proteins were resolved by SDS-PAGE and then electrophoretically transferred from the gels onto PVDF membranes, which were subsequently blocked in LI-COR blocking solution and incubated with antibodies. The following antibodies were used for detection: mouse/rabbit anti-A20 (Abcam catalog ab13597 and Santa Cruz Biotechnology catalog sc-166692), rabbit anti-p52 (Cell Signaling Technology catalog 4882S), rabbit anti-pIκB (catalog 2859) and rabbit anti-IκB (catalog 4814) (Cell Signaling Technology), and mouse anti-GAPDH (Calbiochem, catalog MAB374). IRDye 680RD (catalog 926-68070) and IRDye800CW (catalog 925-32210) secondary antibodies were purchased from LI-COR. Western blots were scanned using the Odyssey CLx Imaging System and analyzed with Image Studio software (both LI-COR).

Imaging flow cytometry. Human cord blood and peripheral blood neutrophils were isolated using the EasySep Direct Human Neutrophil Isolation Kit (STEMCELL Technologies). Afterward, cells were fixed and permeabilized with the Foxp3 Transcription Factor Staining Buffer Set (Affymetrix) according to the manufacturer's protocol. Intracellular NF-κB was stained with the following antibodies:

Table 4. TaqMan expression assays used for quantitative RT-PCR

TaqMan expression assay	Gene	Target species
Mm00518541_m1	IRAK-3	Mouse
Mm00437121_m1	TNFAIP3	Mouse
Mm00437762_m1	B2m	Mouse
Mm00433896_m1	Gyk	Mouse
Hs00936103_m1	IRAK-3	Human
Hs00234713_m1	TNFAIP3	Human
Hs02758991_g1	GAPDH	Human
Hs01060665_g1	ACTB	Human

mouse anti-p65 (F-6) (Santa Cruz Biotechnology catalog sc-8008 AF488) and mouse anti-RelB (Santa Cruz Biotechnology catalog sc-48366 AF488), both conjugated with Alexa Fluor 488. DAPI (Invitrogen) was used to stain the nucleus. Images were acquired using an Amnis ImageStream multispectral imaging flow cytometer. Image analysis was done using Image Data Exploration and Analysis Software (Amnis), applying the nuclear localization wizard. Similarity score defines the overlap of nuclear DAPI signal and NF-κB signal.

Flow cytometry. Surface expression of TLR4 (anti-mouse TLR4-PE, BioLegend, catalog 145403), LTβR (anti-mouse catalog 134403 or anti-human catalog 322008 LTβR-PE, BioLegend), TNFRI (TNFRI-APC, BioLegend catalog 369906), or TNFRII (anti-mouse catalog 113406 or anti-human catalog B293743 TNFRII-PE-Cy7, BioLegend) was assessed on neutrophils from human cord or peripheral blood or mouse peripheral blood using a Beckman Coulter Gallios or a Cytoflex S flow cytometer and analyzed with FlowJo Analysis Software. Surface expression of CD11b (Mac-1) (anti–mouse or anti–human Cd11b-AF700 BioLegend catalog 101222) and CD18 (integrin β2 subunit) (anti-human CD18-FITC, BioLegend catalog 302106) was assessed after 2 hours of incubation either with 20 ng/mL recombinant human TNF-α or HBSS as control using Cytoflex S flow cytometer and FlowJo Analysis Software for analysis. Gating of human neutrophils was performed using CD15 (anti-human CD15-APC, BioLegend catalog 323008) and CD66b (anti-human CD66b-PB, BioLegend catalog 305112). For the soluble ICAM-1 binding assay, please refer to Supplemental Methods.

Flow chamber. Ibidi flow chambers (0.5 μm Slide VI0.1) were coated with E selectin (rhCD62E-Fc chimera, 5 μg/mL; R&D Systems), ICAM-1 (rhICAM-1, 4 μg/mL; R&D Systems), and CXCL8 (rhCXCL-8, 10 μg/mL, Peprotech) overnight at 4°C. The next day, chambers were blocked with 5% casein. Prior to the start of experiments, isolated human adult neutrophils were incubated for 2 hours with either HBSS (control) or adult or fetal serum, washed twice, and then diluted in HBSS to 1×10^6 cells/mL. Perfusion through the flow chamber was conducted with a high-precision pump (Harvard Apparatus) at a shear stress level of 1 dyne/cm^2. Experiments were conducted on a ZEISS AXIOVERT 200 microscope, provided with a ZEISS LD Plan-neofluor objective (20×, 0.4 NA: and a SPOT RT ST Camera). MetaMorph software was used to generate movies for later analysis using Fiji software.

Phagocytosis. Human peripheral blood neutrophils were isolated using the EasySep Direct Human Neutrophil Isolation Kit (STEMCELL Technologies). Cells were stimulated for 2 hours with either RPMI (control) or fetal or adult serum, washed 2 times, afterward incubated with Zymosan particles for another 2 hours, and further processed as described in the data sheet (Phagocytosis Assay Kit, Green Zymosan). Samples were analyzed in the FL1 channel of a Cytoflex S flow cytometer and data analyzed by FlowJo Analysis Software.

LT-α ELISA. Serum was obtained from human cord and adult peripheral blood. The assay was performed according to the manufacturer's instructions (R&D Systems). Samples were run in duplicates and analyzed using a microplate reader (TECAN).

Surgical preparation of the yolk sac and intravital microscopy. Pregnant *Lyz2*^{GFP} mice (E14.5–E17.5) were anesthetized intraperitoneally with 5 mg/mL ketamine and 1 mg/mL xylazine in 10 mL/kg of normal saline. Two hours prior to intravital microscopy, the uterine horn was carefully exteriorized through an abdominal wall incision followed by the intrauterine injection of 100 μL LPS (1 μg/μL in 0.9% NaCl), 50 μL of TNF-α (10 ng/μL in 0.9% NaCl), or NaCl (0.9%). During the intrauterine injection between 2 fetuses, care was taken not to damage the fetuses or their surrounding yolk sacs. The site of injection between

2 fetuses was marked by a small knot using silk braided suture. Thereafter, the uterine horn was returned, and the abdominal wall incision was temporarily closed by a small metallic clamp. After 2 hours, intravital microscopy (La Vision Biotech and Olympus BX51) to analyze leukocyte recruitment was performed as previously described (8).

Intravital microscopy of TNF-α–stimulated mouse cremaster muscle venules. Mice were treated by intrascrotal injection of 500 ng TNF-α (R&D Systems) 2 hours prior to microscopy, anesthetized, and prepared for intravital microscopy, as described (60). Movies from cremasteric postcapillary venules ranging from 20 to 40 μm in diameter were recorded using BX51WI microscope (Olympus) with a water immersion objective ×40, 0.80 NA, and an Olympus charge-coupled device camera (CF8/1, Kappa). Blood samples were taken after the experiments, and WBC and neutrophil counts were determined using ProCyte Dx Hematology Analyzer (IDEXX). Rolling velocity and leukocyte adhesion efficiency (number of adherent cells/mm^2 divided by the systemic neutrophil count) were calculated on the basis of the recorded movies using Fiji software (61). Afterward, cremaster muscles were fixed with 4% PFA (AppliChem) and stained using Giemsa (MilliporeSigma). The number of perivascular cells/mm^2 was calculated with a Leica DM2500 microscope equipped with a DMC2900 CMOS camera and an HCX PL APO 100×/1.40 Oil Ph3.

Statistics. All data were analyzed and plotted using Graph Pad Prism Software. For pairwise comparison of experimental groups, a paired 2-tailed Student's *t* test was performed; for comparison of independent samples, the unpaired Student's *t* test was used. Depending on the condition, we used 1-way ANOVA with either Dunnett's post hoc test (comparison of experimental groups against control) or Tukey's post hoc test (comparison of all experimental groups against each other) or a 2-way ANOVA with Tukey's post hoc test (comparison of paired experimental groups against each other) for multiple comparison. *P* values less than 0.05 were considered statistically significant.

Study approval. All experiments using human cord blood were approved by the ethics committee of LMU Munich, project 249-08. All animal experiments were approved by the Regierung von Oberbayern, Munich, Germany (AZ 55.2-1-54-2531-80-76/12, 55.2-1-54-2532.102.2017 and 02-18-26).

Author contributions

IR, LMW, and KH designed and conducted experiments, analyzed data, and wrote the manuscript. AB, JA, MR, SB, and M Salvermoser acquired and analyzed data. CN and TK provided human cord blood samples, and MG, AM, and CS provided mice. MSS and BW provided critical reagents and their expertise. TS, KH, and MH analyzed data. M Sperandio designed experiments and wrote the manuscript.

Acknowledgments

We thank Dorothee Gössel, Sabine D'Avis, Anke Lübeck, and Nadine Schmidt for excellent technical assistance. We also thank Ludger Klein-Hitpass for his assistance with the transcriptome analysis. Work was supported by the German Research Foundation (DFG) collaborative research grant SFB914 and projects A02 (to BW), A10 (to CS), and B01 (to M Sperandio); the core facility flow cytometry as well as the core facility bioimaging at the Biomedical Center, LMU, Planegg-Martinsried, Germany; and the Cell Analysis Core Facility at the TranslaTUM, Center for Translational Cancer Research, TU Munich, Munich, Germany. CS, M Sperandio, BW, and MG also receive support from DFG Transregio TRR332 projects A06, C02, C03, and C06, respectively.

Address correspondence to: Markus Sperandio, Institute of Cardiovascular Physiology and Pathophysiology, Biomedizinisches Centrum München, Ludwig-Maximilians-Universität, Großhaderner Str. 9, 82152 Planegg-Martinsried, Germany. Phone: 49 89 2180 71515; Email: markus.sperandio@lmu.de.

1. Stoll BJ, et al. Late-onset sepsis in very low birth weight neonates: the experience of the NICHD Neonatal Research Network. *Pediatrics*. 2002;110(2 pt 1):285–291.
2. Liu L, et al. Global, regional, and national causes of under-5 mortality in 2000-15: an updated systematic analysis with implications for the sustainable development goals. *Lancet*. 2016;388(10063):3027–3035.
3. Levy O. Innate immunity of the newborn: basic mechanisms and clinical correlates. *Nat Rev Immunol*. 2007;7(5):379–390.
4. Henneke P, et al. Perinatal development of innate immune topology. *Elife*. 2021;10:e67793.
5. Burg ND, Pillinger MH. The neutrophil: function and regulation in innate and humoral immunity. *Clin Immunol*. 2001;99(1):7–17.
6. Németh T, et al. Neutrophils as emerging therapeutic targets. *Nat Rev Drug Discov*. 2020;19(4):253–275.
7. Nussbaum C, et al. Neutrophil and endothelial adhesive function during human fetal ontogeny. *J Leukoc Biol*. 2013;93(2):175–184.

8. Sperandio M, et al. Ontogenetic regulation of leukocyte recruitment in mouse yolk sac vessels. *Blood*. 2013;121(21):e118–e128.
9. Lee AH, et al. Dynamic molecular changes during the first week of human life follow a robust developmental trajectory. *Nat Commun*. 2019;10(1):1092.
10. Olin A, et al. Stereotypic immune system development in newborn children. *Cell*. 2018;174(5):1277–1292.
11. Zhong W, et al. Dramatic changes in blood protein levels during the first week of life in extremely preterm infants. *Pediatr Res*. 2020;89(3):604–612.
12. Zhang Q, et al. 30 years of NF-κB: a blossoming of relevance to human pathobiology. *Cell*. 2017;168(1–2):37–57.
13. Millet P, et al. RelB: an outlier in leukocyte biology. *J Leukoc Biol*. 2013;94(5):941–951.
14. Yilmaz ZB, et al. RelB is required for Peyer's patch development: differential regulation of p52-RelB by lymphotoxin and TNF. *EMBO J*. 2003;22(1):121–130.
15. Zhao B, et al. The NF-κB genomic landscape in lymphoblastoid B cells. *Cell Rep*. 2014;8(5):1595–1606.
16. Ma A, Malynn BA. A20: linking a complex regulator of ubiquitylation to immunity and human disease. *Nat Rev Immunol*. 2012;12(11):774–785.
17. Catrysse L, et al. A20 in inflammation and autoimmunity. *Trends Immunol*. 2014;35(1):22–31.
18. Shembade N, Harhaj EW. Regulation of NF-κB signaling by the A20 deubiquitinase. *Cell Mol Immunol*. 2012;9(2):123–130.
19. Lee EG, et al. Failure to regulate TNF-induced NF-kappaB and cell death responses in A20-deficient mice. *Science*. 2000;289(5488):2350–2354.
20. Matmati M, et al. A20 (TNFAIP3) deficiency in myeloid cells triggers erosive polyarthritis resembling rheumatoid arthritis. *Nat Genet*. 2011;43(9):908–912.
21. Blum KS, Pabst R. Keystones in lymph node development. *J Anat*. 2006;209(5):585–595.
22. Phillipson M, et al. Intraluminal crawling of neutrophils to emigration sites: a molecularly distinct process from adhesion in the recruitment cascade. *J Exp Med*. 2006;203(12):2569–2575.
23. Faust N, et al. Insertion of enhanced green fluorescent protein into the lysozyme gene creates mice with green fluorescent granulocytes and macrophages. *Blood*. 2000;96(2):719–726.
24. Orosz A, et al. In vivo functions of mouse neutrophils derived from HoxB8-transduced conditionally immortalized myeloid progenitors. *J Immunol*. 2021;206(2):432–445.
25. Sperandio M, et al. P-selectin glycoprotein ligand-1 mediates L-selectin-dependent leukocyte rolling in venules. *J Exp Med*. 2003;197(10):1355–1363.
26. Kan B, et al. An immunological perspective on neonatal sepsis. *Trends Mol Med*. 2016;22(4):290–302.
27. Van Den Berg JP, et al. Transplacental transport of IgG antibodies specific for pertussis, diphtheria, tetanus, haemophilus influenzae type b, and neisseria meningitidis serogroup C is lower in preterm compared with term infants. *Pediatr Infect Dis J*. 2010;29(9):801–805.
28. Sharma AA, et al. The developing human preterm neonatal immune system: a case for more research in this area. *Clin Immunol*. 2012;145(1):61–68.
29. Mariscalco MM, et al. P-Selectin support of neonatal neutrophil adherence under flow: contribution of L-selectin, LFA-1, and ligand(s) for P-selectin. *Blood*. 1998;91(12):4776–4785.
30. Yost CC, et al. Impaired neutrophil extracellular trap (NET) formation: a novel innate immune deficiency of human neonates. *Blood*. 2009;113(25):6419–6427.
31. Marcos V, et al. Delayed but functional neutrophil extracellular trap formation in neonates. *Blood*. 2009;114(23):4908–4911.
32. Weih F, et al. Multiorgan inflammation and hematopoietic abnormalities in mice with a targeted disruption of RelB, a member of the NF-kappaB/Rel family. *Cell*. 1995;80(2):331–340.
33. Weih F, et al. p50-NF-kappaB complexes partially compensate for the absence of RelB: Severely increased pathology in p50(-/-) relB(-/-)double-knockout mice. *J Exp Med*. 1997;185(7):1359–1370.
34. Förster-Waldl E, et al. Monocyte toll-like receptor 4 expression and LPS-induced cytokine production increase during gestational aging. *Pediatr Res*. 2005;58(1):121–124.
35. Sadeghi K, et al. Immaturity of infection control in preterm and term newborns is associated with impaired toll-like receptor signaling. *J Infect Dis*. 2007;195(2):296–302.
36. Al-Hertani W, et al. Human newborn polymorphonuclear neutrophils exhibit decreased levels of MyD88 and attenuated p38 phosphorylation in response to lipopolysaccharide. *Clin Invest Med*. 2007;30(2):E44–E53.
37. Sharma AA, et al. Impaired NLRP3 inflammasome activity during fetal development regulates IL-1β production in human monocytes. *Eur J Immunol*. 2015;45(1):238–249.
38. Dinarello CA. Immunological and inflammatory functions of the interleukin-1 family. *Annu Rev Immunol*. 2009;27:519–550.
39. Krikos A, et al. Transcriptional activation of the tumor necrosis factor alpha -inducible zinc finger protein, A20, is mediated by kappa B elements. *J Biol Chem*. 1992;267(25):17971–17976.
40. Song HY, et al. The tumor necrosis factor-inducible zinc finger protein A20 interacts with TRAF1/TRAF2 and inhibits NF-kappaB activation. *Proc Natl Acad Sci U S A*. 1996;93(13):6721–6725.
41. Heyninck K, Beyaert R. The cytokine-inducible zinc finger protein A20 inhibits IL-1-induced NF-kappaB activation at the level of TRAF6. *FEBS Lett*. 1999;442(2–3):147–150.
42. Yamaguchi N, et al. Involvement of A20 in the molecular switch that activates the non-canonical NF-κB pathway. *Sci Rep*. 2013;3:2568.
43. Vereecke L, et al. The ubiquitin-editing enzyme A20 (TNFAIP3) is a central regulator of immunopathology. *Trends Immunol*. 2009;30(8):383–391.
44. Lodolce JP, et al. African-derived genetic polymorphisms in TNFAIP3 mediate risk for autoimmunity. *J Immunol*. 2010;184(12):7001–7009.
45. Elsby LM, et al. Functional evaluation of TNFAIP3 (A20) in rheumatoid arthritis. *Clin Exp Rheumatol*. 2010;28(5):708–714.
46. Adrianto I, et al. Association of a functional variant downstream of TNFAIP3 with systemic lupus erythematosus. *Nat Genet*. 2011;43(3):253–258.
47. Walle L Vande, et al. Negative regulation of the NLRP3 inflammasome by A20 protects against arthritis. *Nature*.

2014;512(7512):69–73.
48. Das T, et al. A20/tumor necrosis factor α-induced protein 3 in immune cells controls development of autoinflammation and autoimmunity: lessons from mouse models. *Front Immunol*. 2018;9:104.
49. Tavares RM, et al. The ubiquitin modifying enayme A20 restricts B cell survival and prevents autoimmunity. *Immunity*. 2010;33(2):181–191.
50. Hammer GE, et al. Dendritic cell expression of A20 preserves immune homeostasis and prevents colitis and spondyloarthritis Gianna. *Nat Immunol*. 2011;12(12):1184–1193.
51. Duong BH, et al. A20 restricts ubiquitination of pro-interleukin-1β protein complexes and suppresses NLRP3 inflammasome activity. *Immunity*. 2015;42(1):55–67.
52. Carvalho BS, Irizarry RA. A framework for oligonucleotide microarray preprocessing. *Bioinformatics*. 2010;26(19):2363–2367.
53. Zhang B, et al. WebGestalt: an integrated system for exploring gene sets in various biological contexts. *Nucleic Acids Res*. 2005;33(suppl 2):W741–W748.
54. Wang J, et al. WEB-based GEne SeT AnaLysis Toolkit (WebGestalt): update 2013. *Nucleic Acids Res*. 2013;41(w1):W77–W83.
55. Hasenberg A, et al. Catchup: a mouse model for imaging-based tracking and modulation of neutrophil granulocytes. *Nat Methods*. 2015;12(5):445–452.
56. Stremmel C, et al. Yolk sac macrophage progenitors traffic to the embryo during defined stages of development. *Nat Commun*. 2018;9(1):75.
57. Wang GG, et al. Quantitative production of macrophages or neutrophils ex vivo using conditional Hoxb8. *Nat Methods*. 2006;3(4):287–293.
58. Redecke V, et al. Hematopoietic progenitor cell lines with myeloid and lymphoid potential. *Nat Methods*. 2013;10(8):795–803.
59. Zehrer A, et al. A fundamental role of Myh9 for neutrophil migration in innate immunity. *J Immunol*. 2018;201(6):1748–1764.
60. Pruenster M, et al. Extracellular MRP8/14 is a regulator of β2 integrin-dependent neutrophil slow rolling and adhesion. *Nat Commun*. 2015;6:6915.
61. Schindelin J, et al. Fiji: an open-source platform for biological-image analysis. *Nat Methods*. 2012;9(7):676–682.

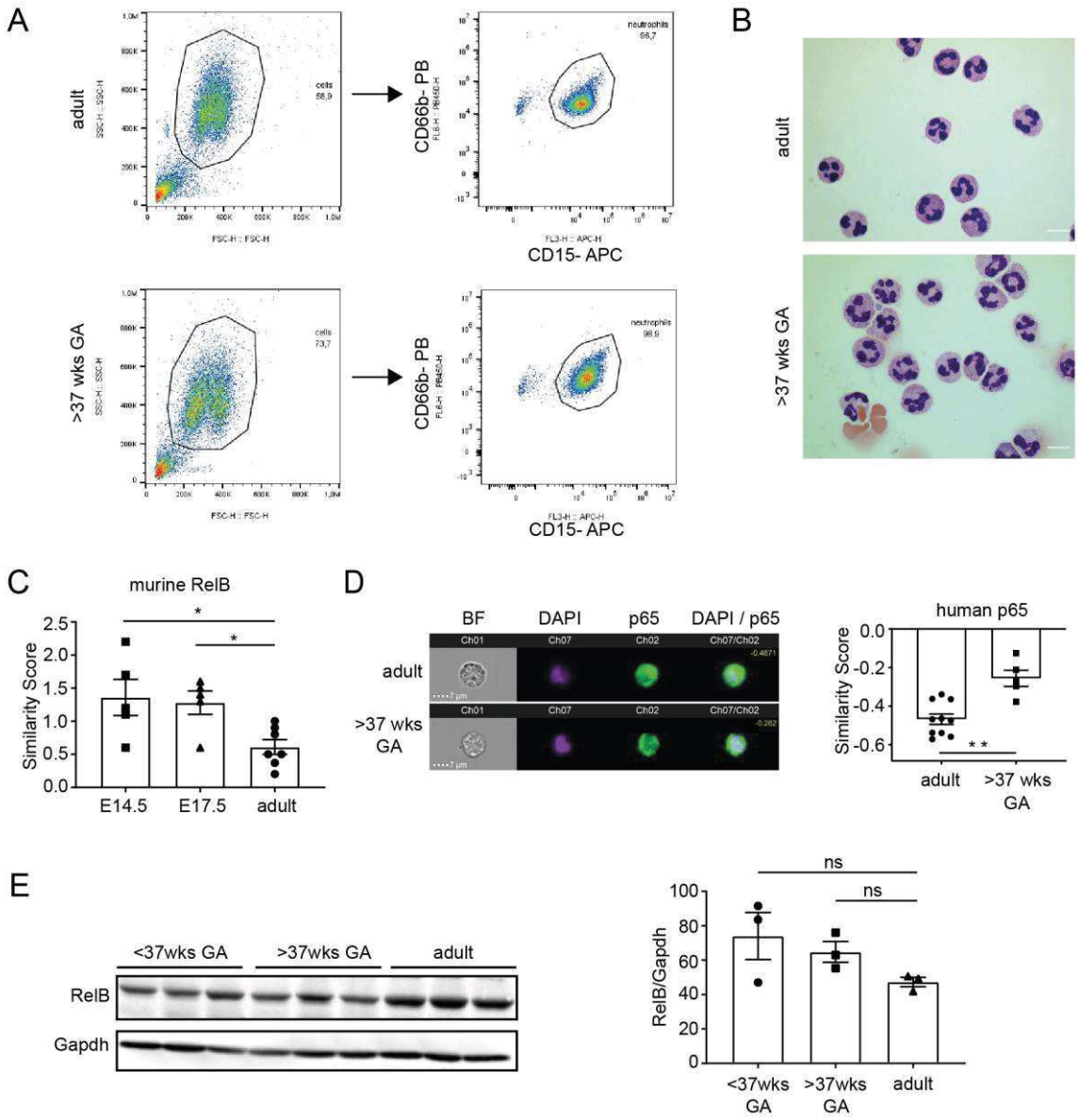

Supplemental Figure 1: Comparison of human adult and fetal neutrophils, RelB and p65 localization as well as RelB protein expression levels.

(A) Representative forward scatter vs. side scatter dot plots of isolated human adult and fetal (gestational age >37 weeks) neutrophils (left panels). Gating of human neutrophils was performed using CD15 and CD66b (right panels). Cytoflex S flow cytometer was used and data was analyzed with the FlowJo Analysis Software. (B) Representative images of May-Gruenwald Giemsa stained cytospin slides of isolated human adult and fetal (gestational age >37 weeks) neutrophils. Images were obtained using a Leica DM2500 microscope equipped with a DMC2900 CMOS camera and a HCX PL APO 100x/1.40 Oil Ph3. Scale bar: 10µm (C) Imaging flow cytometry was performed on murine adult and E14.5 and E17.5 fetal neutrophils and nuclear RelB was quantified. Similarity score defines overlap of nuclear DAPI signal and the respective NF-κB subunit. All data is presented as mean ± SEM. (* $p<0.05$, n= 5-7) Ordinary one-way ANOVA with Tukey's multiple comparisons test. (D) Imaging flow cytometry was performed on cord blood neutrophils from mature infants (gestational age >37 weeks) and peripheral blood from adult healthy donors. Nuclear signal was determined by DAPI and additionally the NF-κB subunit p65 was visualized. Representative pictures of fetal and adult neutrophils are shown as brightfield (BF) image, DAPI, NF-κB subunit p65 and a DAPI/p65 overlay. Respective similarity scores are displayed. Scale bar: 7µm. Similarity score defines overlap of nuclear DAPI signal and the respective

NF-κB subunit. All data is presented as mean ± SEM (** $p<0.005$, n= 5-10). Mann Whitney test. (E) Western blot and respective quantitative analysis of RelB in neutrophils isolated from premature (gestational age (GA) <37 weeks) and mature infants (gestational age >37 weeks) and peripheral blood from healthy adult donors. Band intensity was normalized to Gapdh. All data is presented as mean ± SEM. (ns= not significant; n= 3); Ordinary one-way ANOVA with Dunnett's multiple comparisons test.

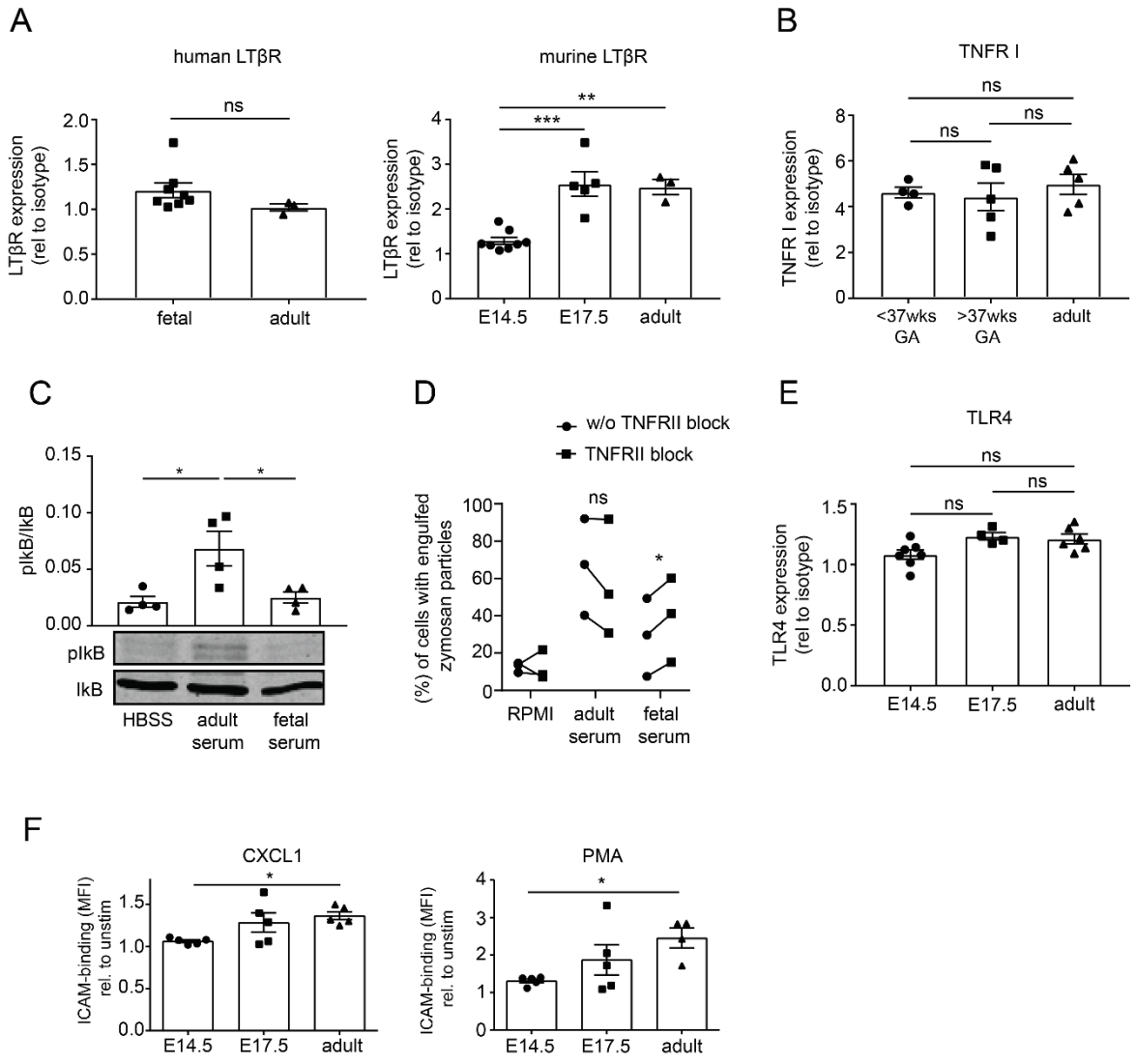

Supplemental Figure 2: Surface marker levels in fetal and adult neutrophils, stimulation of fetal neutrophils with adult and fetal serum as well as ICAM-1 binding assay

(A) Flow cytometry analysis of LTβR expression on human and murine neutrophils out of whole blood from indicated gestational ages. Median fluorescence intensity normalized to isotype control is displayed. All data is presented as mean ± SEM. (ns= not significant, ** p<0.005, *** p<0.001; n= 6). (B) Flow cytometry analysis of TNFR I expression on human neutrophils out of whole blood from indicated gestational ages. Median fluorescence intensity normalized to isotype control is displayed. All data is presented as mean ± SEM. (ns= not significant; n= 4-5/group). Ordinary one-way ANOVA with Dunnett's multiple comparisons test. (C) Western blot and respective quantitative analysis of phospho-IκB in fetal neutrophils after HBSS (control) incubation or stimulation with adult or fetal serum. Band intensities were normalized to total IκB protein. All data is presented as mean ± SEM. (* p<0.05; n= 4) Ordinary one-way ANOVA with Tukey's multiple comparisons test. (D) Quantitative analysis of phagocytosis of human adult neutrophils by measuring the amount of engulfed zymosan particles by flow cytometry after incubation with either RPMI (w/o TNFRII block) or blocking with anti-human TNRFII antibody (TNFRII block) for 2 h prior to stimulation without (RPMI) or with adult or fetal serum. All data is presented as mean ± SEM. (ns= not significant, * p<0.05; n= 3) Paired student´s t-test for each group (RPMI, adult serum and fetal serum). (E) Flow cytometry analysis of

the LPS receptor TLR4 expression on the cell surface of fetal and adult mouse neutrophils. Median expression levels relative to the respective isotype control are displayed. All data is presented as mean ± SEM. (ns = not significant; n=4-7). Ordinary one-way ANOVA with Dunnett's multiple comparisons test. (F) Soluble ICAM-1 binding to LFA-1 on murine neutrophils was investigated in vitro. Values of ICAM-1 binding to unstimulated control cells was set to one and results are shown relative to unstimulated controls. Data are presented as mean +SEM (* $p<0.05$, n=5-7). Ordinary one-way ANOVA with Tukey's multiple comparisons test.

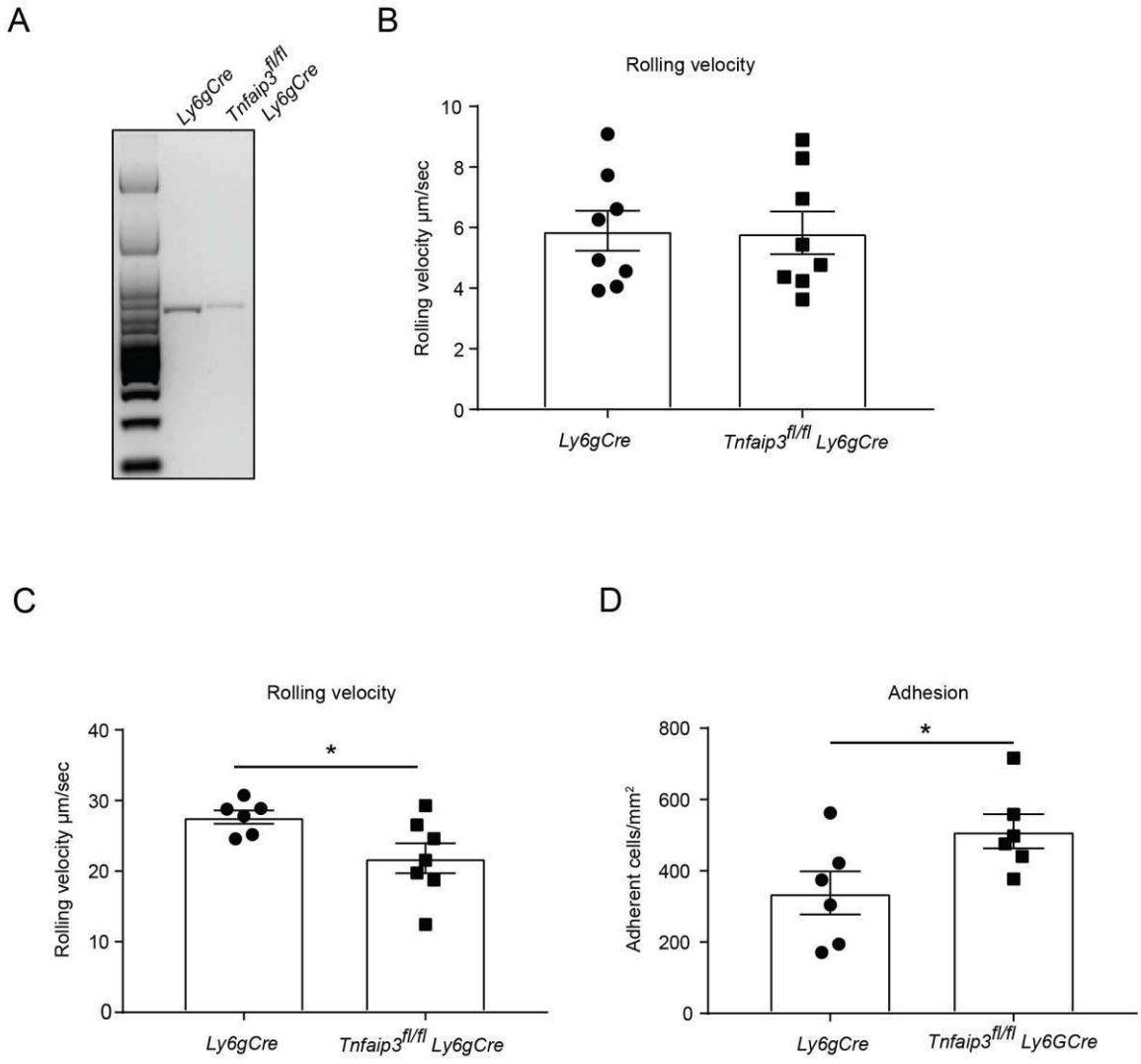

Supplemental Figure 3: Neutrophil adhesion in *Tnfaip3*$^{fl/fl}$ *Ly6gCre* mice.

(A) Representative images of A20 mRNA levels in *Ly6gCre* and *Tnfaip3*$^{fl/fl}$ *Ly6gCre* isolated neutrophils. (B) In vivo leukocyte rolling velocity was analyzed in 2h TNF-α -stimulated venules of mouse cremaster muscles in 8 *Ly6gCre* and 8 *Tnfaip3*$^{fl/fl}$ *Ly6gCre* mice. (C) In vivo leukocyte rolling velocity and (D) leukocyte adhesion was analyzed in surgically prepared venules of mouse cremaster muscles in 6 *Ly6gCre* and 6 *Tnfaip3*$^{fl/fl}$ *Ly6gCre* mice. Values are given as mean ± SEM; * $p<0.05$. Unpaired student´s t-test.

Supplemental Movie 1 and 2: In vivo imaging of E14.5 and E17.5 yolk sac vessels after LPS stimulation

Adhesion of fetal neutrophils at E14.5 (Movie 1) and E17.5 (Movie 2) in yolk sac vessels in vivo was assessed 2h after *Lyz2*^{GFP} mice received an intrauterine injection of 100ng LPS. Using fluorescence microscopy vessels were recorded for approximately 1 minute and neutrophils identified due to their GFP signal. Movies were analyzed using Fiji software. Scale bar: 30µm.

Supplemental Movie 3: In vivo imaging of inflamed cremaster muscle venules of *Tnfaip3*$^{fl/fl}$ *Ly6gCre* and *Ly6gCre* mice

In vivo leukocyte rolling and adhesion was analyzed in 2h TNF-α-stimulated venules of mouse cremaster muscles. Each vessel was recorded for approximately 1 min using BX51WI microscope with a water immersion objective ×40, 0.80 NA and a Olympus CCD camera (CF8/1, Kappa). Movies were analyzed using Fiji software. Scale bar: 30µm.

Supplemental Table 1: Candidate genes according to their function and association with biological processes

WEB-based Gene SeT AnaLysis Toolkit (WebGestalt) was applied, to group candidate genes according to their function and association with biological processes.

Supplemental Table 2: Overrepresentation of RelB subunit in promoters of upregulated genes

				Not regulated		Regulated	
Subunit	**Regulation**	**P-value**	**Odds ratio**	**not bound**	**bound**	**not bound**	**bound**
p65	down	0.00026281	2.82844308	4462	4042	16	41
RelB	down	5.19E-07	4.05754114	5383	3121	17	40
p50	down	5.72E-06	3.6366211	7087	1417	33	24
p52	down	0.00052564	2.54197721	5789	2715	26	31
p65	up	0.28319133	0.75556444	4436	4054	42	29
RelB	up	1	0.98692307	5355	3135	45	26
p50	up	0.00975615	0.29304986	7053	1437	67	4
p52	up	0.37327176	0.77222254	5763	2727	52	19

Supplemental Table 3: Table of RelB- up- and downregulated genes in cord blood neutrophils in comparison to adult neutrophils.

Upregulated in cord blood neutrophils	
Gene symbol	**Gene name**
JAG1	jagged 1
ALDH2	aldehyde dehydrogenase 2 family (mitochondrial)
ARG1	arginase 1
ENO1	enolase 1, (alpha)
HES1	hairy and enhancer of split 1, (Drosophila)
IGF1R	insulin-like growth factor 1 receptor
IL6ST	interleukin 6 signal transducer (gp130, oncostatin M receptor)
IL10RA	interleukin 10 receptor, alpha
LDLR	low density lipoprotein receptor
MAK	male germ cell-associated kinase
NFE2L2	nuclear factor, erythroid 2-like 2

P4HA1	prolyl 4-hydroxylase, alpha polypeptide I
PPP1CB	protein phosphatase 1, catalytic subunit, beta isozyme
PTPN7	protein tyrosine phosphatase, non-receptor type 7
RALGDS	ral guanine nucleotide dissociation stimulator
SKIL	SKI-like oncogene
SLC8A1	solute carrier family 8 (sodium/calcium exchanger), member 1
TFRC	transferrin receptor (p90, CD71)
KLF10	Kruppel-like factor 10
TNFAIP3	tumor necrosis factor, alpha-induced protein 3
UPP1	uridine phosphorylase 1
EZR	Ezrin
IL1R2	interleukin 1 receptor, type II
SLC7A5	solute carrier family 7 (amino acid transporter light chain, L system), member 5
GAS7	growth arrest-specific 7
DGKD	diacylglycerol kinase, delta 130kDa
BHLHE40	basic helix-loop-helix family, member e40
COX7A2L	cytochrome c oxidase subunit VIIa polypeptide 2 like
SF3A3	splicing factor 3a, subunit 3, 60kDa
IRAK3	interleukin-1 receptor-associated kinase 3
ELL2	elongation factor, RNA polymerase II, 2
ZNF292	zinc finger protein 292
CLIC4	chloride intracellular channel 4
TIAM2	T-cell lymphoma invasion and metastasis 2
RABGEF1	RAB guanine nucleotide exchange factor (GEF) 1
PAG1	phosphoprotein associated with glycosphingolipid microdomains 1
SAMSN1	SAM domain, SH3 domain and nuclear localization signals 1
RILPL2	Rab interacting lysosomal protein-like 2
IRF2BP2	interferon regulatory factor 2 binding protein 2
PIM3	pim-3 oncogene

Downregulated in cord blood neutrophils	
Gene symbol	**Gene name**
RHOB	ras homolog family member B
ATP6V0A1	ATPase H+ transporting VO subunit a1
CALM3	calmodulin 3
GBP1	guanylate binding protein 1
NFIC	nuclear factor I C
EIF3H	eukaryotic translation initiation factor 3 subunit Hrabaptin, RAB GTP
RABEP1	rabaptin, RAB GTPase binding effector protein 1
MED27	mediator complex subunit 27
VTI1B	vesicle transport through interaction with t-SNAREs 1B
TCFL5	transcription factor like 5
SP140	SP140 nuclear body protein
ZFYVE26	zinc finger FYVE-type containing 26

CCDC28A	coiled-coil domain containig 28A
P2RY10	P2Y receptor family member 10
BAZ2B	bromodomain adjacent to zinc finger domain 2B
TAPBPL	TAP binding protein like
C7orf43	chromosome 7 open reading frame 43
NAGK	N-acetylglucosamine kinase
PNRC2	proline rich nuclear receptor coactivator 2
PRRG4	proline rich and Gla domain 4
ASCC2	activating signal cointegrator 1 complex subunit 2
RAVER1	ribonucleoprotein, PTB binding 1
RPP25L	ribonuclease P/MRP subunit p25 like
MICA	MHC class I polypeptide-related sequence A

Supplemental Methods

Soluble ICAM-1 binding assay

Isolated murine neutrophils were resuspended in HBSS Buffer and stimulated with 100ng/ml rmCXCL1 (PeproTech), PMA (Calbiochem) or an equal amount of HBSS buffer in the presence of soluble rmICAM-1 (ICAM-1 hFC chimera; R&D Systems, 20µg/ml), goat anti-human Fcg-biotin (eBioscience) and streptavidin-PerCP-Cy5.5 (eBioscience) for 3 minutes at 37°C. Cells were fixed (FACS Lysing Solution; BD), stained with rat anti-mouse Ly6G-Pacific Blue antibody (1A8; BioLegend) and measured using a flow cytometer.

5. Paper II

nature immunology

Article

https://doi.org/10.1038/s41590-023-01656-1

E-selectin-mediated rapid NLRP3 inflammasome activation regulates S100A8/S100A9 release from neutrophils via transient gasdermin D pore formation

Received: 24 March 2021

Accepted: 18 September 2023

Published online: 30 October 2023

Check for updates

Monika Pruenster[1,8], Roland Immler[1,8], Jonas Roth[1], Tim Kuchler[1], Thomas Bromberger[2], Matteo Napoli[1], Katrin Nussbaumer[1], Ina Rohwedder[1], Lou Martha Wackerbarth[1], Chiara Piantoni[1], Konstantin Hennis[1], Diana Fink[3], Sebastian Kallabis[3], Tobias Schroll[1], Sergi Masgrau-Alsina[1], Agnes Budke[1], Wang Liu[1], Dietmar Vestweber[4], Christian Wahl-Schott[1], Johannes Roth[5], Felix Meissner[3], Markus Moser[2], Thomas Vogl[5], Veit Hornung[6], Petr Broz[7] & Markus Sperandio[1] ✉

S100A8/S100A9 is a proinflammatory mediator released by myeloid cells during many acute and chronic inflammatory disorders. However, the precise mechanism of its release from the cytosolic compartment of neutrophils is unclear. Here, we show that E-selectin-induced rapid S100A8/S100A9 release during inflammation occurs in an NLRP3 inflammasome-dependent fashion. Mechanistically, E-selectin engagement triggers Bruton's tyrosine kinase-dependent tyrosine phosphorylation of NLRP3. Concomitant potassium efflux via the voltage-gated potassium channel $K_V1.3$ mediates ASC oligomerization. This is followed by caspase 1 cleavage and downstream activation of pore-forming gasdermin D, enabling cytosolic release of S100A8/S100A9. Strikingly, E-selectin-mediated gasdermin D pore formation does not result in cell death but is a transient process involving activation of the ESCRT III membrane repair machinery. These data clarify molecular mechanisms of controlled S100A8/S100A9 release from neutrophils and identify the NLRP3/gasdermin D axis as a rapid and reversible activation system in neutrophils during inflammation.

Neutrophils comprise the largest fraction of circulating white blood cells in humans and are ready to sense infectious or sterile challenges in damaged tissue, thereby functioning as the first line of defense during the inflammatory response[1]. Activation of neutrophils triggers the secretion of intracellular components, including damage-associated molecular pattern molecules (DAMPs), to the extracellular microenvironment. S100A8/S100A9, also known as calprotectin or MRP8/MRP14, is such a DAMP that modulates immune responses after its release

[1]Walter Brendel Centre of Experimental Medicine, Biomedical Center, Institute of Cardiovascular Physiology and Pathophysiology, Ludwig-Maximilians-Universität München, Planegg-Martinsried, Germany. [2]Institute of Experimental Hematology, School of Medicine, Technical University Munich, Munich, Germany. [3]Department of Systems Immunology and Proteomics, Institute of Innate Immunity, Medical Faculty, University of Bonn, Bonn, Germany. [4]Max Planck Institute for Molecular Biomedicine, Münster, Münster, Germany. [5]Institute of Immunology, University of Münster, Münster, Germany. [6]Gene Center and Department of Biochemistry, Ludwig-Maximilians-Universität München, Munich, Germany. [7]Department of Immunobiology, University of Lausanne, Epalinges, Switzerland. [8]These authors contributed equally: M. Pruenster, R. Immler. ✉e-mail: markus.sperandio@lmu.de

https://doi.org/10.1038/s41590-023-01656-1

from the cytosol of myeloid cells[2]. In human neutrophils, S100A8/S100A9 represents about 40% of the total cytosolic protein content, rendering these cells the major source of this alarmin. Passive release of S100A8/S100A9 into the extracellular space is evoked through tissue damage and is also observed during NETosis. This is in contrast to active secretion triggered by cell stress that operates independently of cell death[2]. Neutrophils have been shown rolling along inflamed endothelium during their recruitment into inflamed tissue and rapidly secreting S100A8/S100A9 via an E-selectin-dependent mechanism[3,4]. This leads to a rise in S100A8/S100A9 levels in the blood circulation, contributing to high serum levels of S100A8/S100A9, which correlates with disease progression in diverse acute and chronic inflammatory disorders[2]. Hence, for many years, S100A8/S100A9 has been used as a valuable clinical biomarker for therapeutic response monitoring. Of note, S100A8/S100A9 serum levels are not only a biomarker but also a disease indicator of pathogenesis of various diseases, including coronavirus disease 2019, chronic tuberculosis and cancer metastasis[5–7].

Similar to interleukin-1β (IL-1β), S100A8/S100A9 lacks a signal peptide required for secretion via the conventional secretory pathway[2]. In 2015, pore-forming gasdermin D (GSDMD) was described as a critical component of IL-1β release from the cytosol into the extracellular space[8]. GSDMD pore formation requires upstream inflammasome activation and subsequent inflammatory caspase and GSDMD cleavage[9]. In contrast to IL-1β, S100A8/S100A9 is prestored within the cytosol in large amounts, and its release is a rapid process, taking place within minutes after stimulation. Here, we show that E-selectin triggers rapid NLRP3 inflammasome activation and caspase 1 cleavage in neutrophils, triggering transient GSDMD pore formation by which S100A8/S100A9 exits cells in a time-restricted manner, which contributes to successful neutrophil recruitment during the acute inflammatory response.

Results

E-selectin-induced S100A8/S100A9 release is GSDMD and caspase 1 dependent

Secretion of S100A8/S100A9 by neutrophils is triggered by an E-selectin-dependent process[3,4]. Because pore-forming GSDMD has been proposed to mediate unconventional protein release, we investigated whether rapid S100A8/S100A9 release may be dependent on GSDMD and its activating protease caspase 1. Therefore, we injected tumor necrosis factor (TNF) into the scrotum of C57BL/6 wild-type (WT) mice and mice deficient for GSDMD (*Gsdmd*$^{-/-}$) or caspase 1 and caspase 11 (*Casp1*$^{-/-}$*Casp11*$^{-/-}$; Fig. 1a). S100A8/S100A9 serum levels were determined by enzyme-linked immunosorbent assay (ELISA) before and 2 h after TNF treatment. Application of TNF, which directly induces upregulation of E-selectin on endothelial cells[10], significantly increased serum levels of S100A8/S100A9 in WT mice. This increase was absent in *Gsdmd*$^{-/-}$ and *Casp1*$^{-/-}$*Casp11*$^{-/-}$ animals (Fig. 1b). Consistent with the role of E-selectin in S100A8/S100A9 release, E-selectin-deficient (*Sele*$^{-/-}$) mice did not exhibit increased serum levels of S100A8/S100A9 after TNF stimulation (Extended Data Fig. 1a). For all mouse strains, numbers of blood neutrophils and monocytes did not differ from those observed in WT controls (Extended Data Fig. 1b–g). Next, we stimulated bone marrow neutrophils isolated from WT, *Gsdmd*$^{-/-}$ and *Casp1*$^{-/-}$*Casp11*$^{-/-}$ mice with E-selectin or PBS (control) for 10 min and determined the amount of secreted S100A8/S100A9 in the supernatants (Fig. 1a). E-selectin stimulation induced rapid S100A8/S100A9 release in WT cells, whereas lack of caspase 1/caspase 11 or GSDMD completely prevented its release (Fig. 1c). Importantly, the overall amount of cytosolic S100A8/S100A9 was similar between WT, *Gsdmd*$^{-/-}$ and *Casp1*$^{-/-}$*Casp11*$^{-/-}$ neutrophils (Extended Data Fig. 1h). We have shown before that secreted S100A8/S100A9 binds to Toll-like receptor 4 (TLR4) in an autocrine manner, thereby activating β_2-integrins on neutrophils[3]. This results in deceleration of rolling neutrophils along the inflamed vessel wall (slow rolling), facilitating firm leukocyte arrest. Therefore, we investigated to what degree loss of GSDMD and caspase 1/caspase 11 influences neutrophil

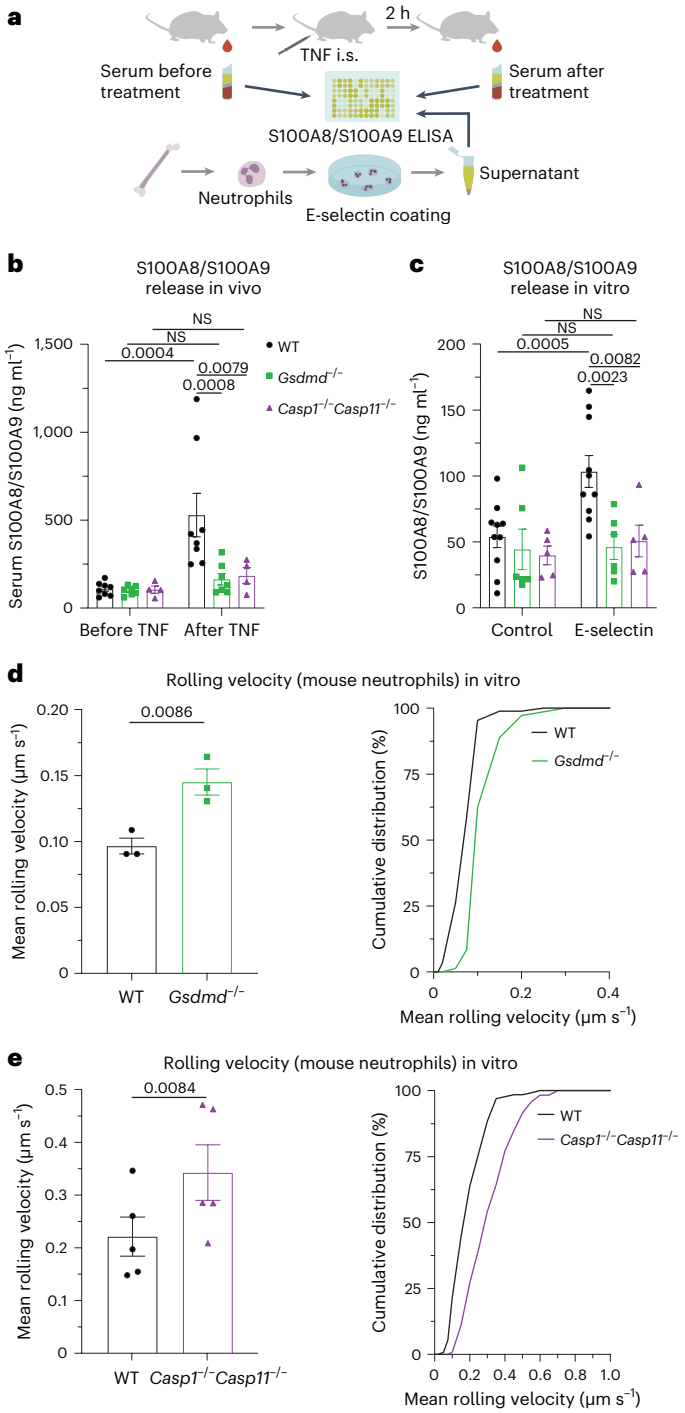

Fig. 1 | E-selectin-induced S100A8/S100A9 release is GSDMD and caspase 1 dependent. a, Schematic of the experimental design. **b**, Serum S100A8/S100A9 levels were analyzed by ELISA before and 2 h after intrascrotal (i.s.) TNF application to WT, *Gsdmd*$^{-/-}$ and *Casp1*$^{-/-}$*Casp11*$^{-/-}$ mice ($n = 8$ (WT), 7 (*Gsdmd*$^{-/-}$) and 4 (*Casp1*$^{-/-}$*Casp11*$^{-/-}$) mice per group); NS, not significant. **c**, Bone marrow neutrophils from WT, *Gsdmd*$^{-/-}$ and *Casp1*$^{-/-}$*Casp11*$^{-/-}$ mice were incubated with E-selectin or PBS for 10 min ($n = 10$ (WT), 6 (*Gsdmd*$^{-/-}$) and 5 (*Casp1*$^{-/-}$*Casp11*$^{-/-}$) mice per group). Supernatants were collected, and S100A8/S100A9 levels were analyzed. **d**,**e**, Rolling velocities of WT and *Gsdmd*$^{-/-}$ neutrophils (**d**; 87 (WT) and 72 (*Gsdmd*$^{-/-}$) cells from $n = 3$ mice per group) and WT and *Casp1*$^{-/-}$*Casp11*$^{-/-}$ neutrophils (**e**; 130 (WT) and 117 (*Casp1*$^{-/-}$*Casp11*$^{-/-}$) cells from $n = 5$ mice per group) were assessed in E-selectin/ICAM-1-coated flow chambers. Data are presented as mean ± s.e.m. and were analyzed by two-way repeated measures analysis of variance (RM ANOVA) with a Sidak's multiple comparison test (**b** and **c**) or are presented as mean ± s.e.m. and cumulative distribution and were analyzed by two-tailed paired Student's *t*-tests (**d** and **e**).

rolling velocities in vitro. *Gsdmd*$^{-/-}$ and *Casp1*$^{-/-}$*Casp11*$^{-/-}$ neutrophils rolled significantly faster than WT neutrophils (Fig. 1d,e), underlining the inability of *Gsdmd*$^{-/-}$ and *Casp1*$^{-/-}$*Casp11*$^{-/-}$ neutrophils to decelerate their rolling velocity through secretion of S100A8/S100A9. These results suggest that E-selectin-mediated rapid S100A8/S100A9 release is a process that relies on the expression of GSDMD and caspase 1/caspase 11 in neutrophils.

E-selectin induces NLRP3 inflammasome activation in neutrophils

The defect in S100A8/S100A9 release observed in *Gsdmd*$^{-/-}$ and *Casp1*$^{-/-}$*Casp11*$^{-/-}$ neutrophils suggests the involvement of an inflammasome-driven pathway in S100A8/S100A9 release. To investigate whether E-selectin stimulation mediates inflammasome activation and downstream caspase 1 cleavage in neutrophils, we stimulated primary human neutrophils with E-selectin or PBS (control) and performed Western blot analysis (Fig. 2a). To exclude that released S100A8/S100A9 induces TLR4-mediated inflammasome activation, we conducted these experiments in the presence of the TLR4 inhibitor TAC242 and paquinimod, an inhibitor of S100A8/S100A9–TLR4 interaction[3]. We detected cleaved caspase 1 (casp-1 p20/p22) in the supernatants of E-selectin-stimulated neutrophils within 10 min of incubation (Fig. 2b), independent of the presence of TAC242 and paquinimod, demonstrating that rapid caspase 1 cleavage is directly mediated by E-selectin and not by TLR4 signaling. In addition, the presence of the specific NLRP3 inflammasome inhibitor MCC950 prevented E-selectin-induced caspase 1 cleavage (Fig. 2c), suggesting an involvement of the NLRP3 inflammasome. Importantly, we also found increased amounts of cleaved caspase 1 in cell lysates of E-selectin-treated human neutrophils compared to that observed in control cells, demonstrating intracellular activity of caspase 1 downstream of E-selectin stimulation (Extended Data Fig. 2a).

To further validate caspase 1 activation after E-selectin stimulation, we used the fluorescent-labeled inhibitor of caspase 1 (FLICA) reagent (Fig. 2a). We found speck-like aggregates of active caspase 1 in human neutrophils within 10 min of E-selectin treatment (Fig. 2d,e). Furthermore, E-selectin induced an increase in the overall intensity of the FLICA signal compared to PBS (control; Fig. 2f), confirming rapid E-selectin-induced caspase 1 activation. Inhibition of caspase 1 activity using the inhibitor VX-765 prevented an increase in FLICA signal in E-selectin-stimulated cells compared to control-stimulated cells (Extended Data Fig. 2b,c), demonstrating the FLICA signal to be a proxy for intracellular caspase 1 activity.

To test whether E-selectin stimulation of neutrophils would also mediate rapid GSDMD cleavage, we stimulated human neutrophils for 10 min with E-selectin and determined the amount of full-length GSDMD and cleaved N-terminal GSDMD (GSDMD-NT) in the cellular lysates (Fig. 2g). Indeed, E-selectin stimulation induced rapid GSDMD-NT formation in neutrophils. Concomitant incubation of the cells with E-selectin and MCC950 prevented GSDMD cleavage. In addition, we visualized E-selectin-induced GSDMD cleavage and translocation to the cell surface by confocal microscopy using an antibody (clone EPR20829-408) that specifically recognizes GSDMD-NT but not non-active full-length GSDMD[11] (Fig. 2h,i). Both GSDMD cleavage and GSDMD-NT surface translocation were absent in unstimulated neutrophils and E-selectin-stimulated neutrophils pretreated with MCC950, suggesting that canonical NLRP3 activation contributes to GSDMD cleavage and GSDMD-NT surface mobilization following stimulation of neutrophils with E-selectin. To examine in more detail the subcellular localization of GSDMD in E-selectin-stimulated human neutrophils, we performed stimulated emission depletion (STED) microscopy and found colocalization of GSDMD and the plasma membrane marker wheat germ agglutinin (WGA) at the cell surface, suggesting GSDMD pore formation at the plasma membrane downstream of E-selectin stimulation (Extended Data Fig. 2d,e).

Finally, blockade of NLRP3 activation with MCC950 resulted in reduced S100A8/S100A9 release after E-selectin stimulation in vitro and in vivo, similar to the reduction observed in *Casp1*$^{-/-}$*Casp11*$^{-/-}$ mice (Extended Data Fig. 2f,g), suggesting a predominant role of the NLRP3 inflammasome pathway in E-selectin-triggered S100A8/S100A9 release. Accordingly, the presence of MCC950 resulted in higher rolling velocities than control cells when perfused through E-selectin- and ICAM-1-coated microflow chambers (Extended Data Fig. 2h,i). Together, the data provide evidence that E-selectin mediates GSDMD-NT pore formation in neutrophils in an NLRP3-dependent manner, resulting in S100A8/S100A9 release.

Rapid E-selectin-induced inflammasome activation is $K_V1.3$ dependent

K^+ efflux is a common trigger of NLRP3 inflammasome activation. Therefore, we wanted to investigate a potential role of K^+ efflux in E-selectin-induced rapid inflammasome activation. Indeed, high extracellular potassium (high $[K^+]_{ex}$), which prevents K^+ efflux, efficiently attenuated E-selectin-induced caspase 1 cleavage (Fig. 3a) and GSDMD-NT formation in human neutrophils (Extended Data Fig. 3a). Recently, we were able to show that the voltage-gated potassium channel $K_V1.3$ regulates neutrophil recruitment[12]. To study a potential role of $K_V1.3$ in E-selectin-mediated inflammasome activation, we stimulated human neutrophils with E-selectin in the absence and presence of the selective $K_V1.3$ inhibitor 5-(4-phenoxybutoxy) psoralen (PAP-1)[13]. We detected a significant reduction of cleaved caspase 1 in the supernatant of E-selectin-stimulated neutrophils when $K_V1.3$ was blocked (Fig. 3b). In line with human neutrophils, pharmacological inhibition of $K_V1.3$ with PAP-1 or genetic deletion of $K_V1.3$ (*Kcna3*$^{-/-}$ mice) in mouse neutrophils resulted in attenuated E-selectin-induced S100A8/S100A9 release in vitro (Fig. 3c,d), suggesting a critical role of $K_V1.3$ in rapid E-selectin-mediated NLRP3 inflammasome activation in neutrophils. Of note, the overall amount of cytosolic S100A8/S100A9 did not differ between WT and *Kcna3*$^{-/-}$ neutrophils (Extended Data Fig. 3b). To test whether K^+ efflux per se would mediate rapid inflammasome activation and caspase 1 cleavage resulting in S100A8/S100A9 release, we stimulated neutrophils with ATP and nigericin, two common inflammasome activators that mediate potassium efflux[14], and investigated the amount of S100A8/S100A9 in the supernatant. Interestingly, stimulation of neutrophils with ATP or nigericin alone was not sufficient to induce S100A8/S100A9 release within 10 min (Fig. 3e,f). Further, concomitant stimulation of neutrophils with lipopolysaccharide (LPS) and nigericin for 10 min did not result in remarkable S100A8/S100A9 release (Fig. 3f), pointing toward an exclusive role for E-selectin and $K_V1.3$ in mediating rapid NLRP3 inflammasome activation and GSDMD pore formation.

Next, we wanted to elucidate the specificity of E-selectin in inducing S100A8/S100A9 release through binding to its ligand on human neutrophils, L-selectin. Therefore, we stimulated human neutrophils with endoglycan and MAdCAM-1, two L-selectin ligands expressed on endothelial cells, which differ in their binding requirements to L-selectin compared to E-selectin[15]. Neither endoglycan nor MAdCAM-1 was able to induce S100A8/S100A9 release in vitro (Fig. 3g), underlining a unique role for E-selectin as a rapid inflammasome activator. In fact, we detected a time-dependent E-selectin-mediated S100A8/S100A9 release starting already after 1 min, demonstrating extremely rapid inflammasome activation and GSDMD pore formation in neutrophils (Extended Data Fig. 3c). Of note, rapid inflammasome activation did not result in IL-1β release in vitro (Fig. 3h), presumably due to low amounts of prestored IL-1β in unprimed neutrophils. However, as expected, classical priming of neutrophils with LPS for 2.5 h followed by 30 min of nigericin activation induced IL-1β release in neutrophils. Similar to nigericin, E-selectin stimulation induced IL-1β release in LPS-primed neutrophils (Fig. 3i), identifying E-selectin as an alternative and endogenous activation molecule for canonical inflammasome activation.

https://doi.org/10.1038/s41590-023-01656-1

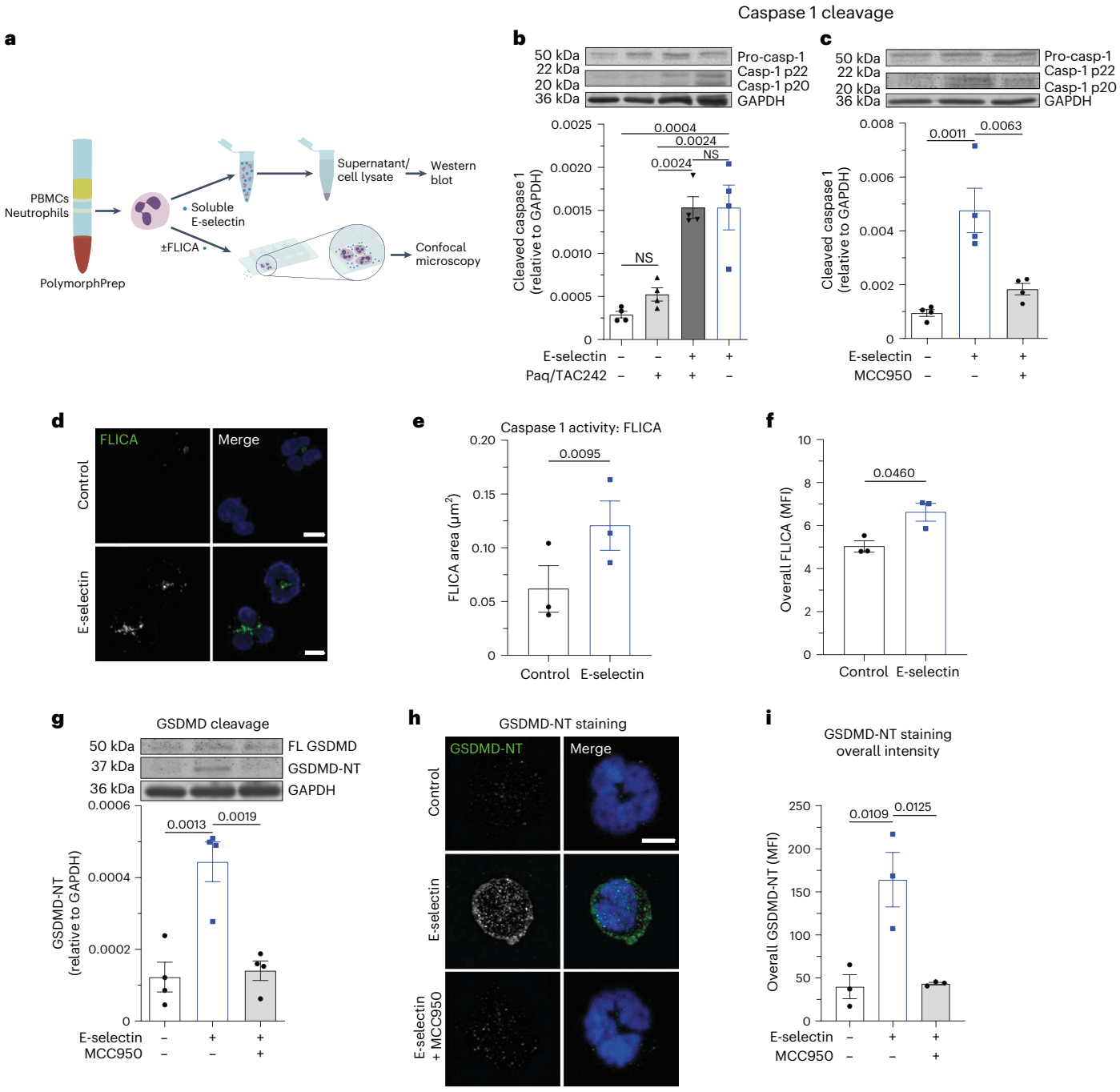

Fig. 2 | E-selectin induces NLRP3 inflammasome activation in neutrophils. **a**, Schematic of the experimental design; PBMCs, peripheral blood mononuclear cells. **b**,**c**, E-selectin-induced cleavage of caspase 1 was assessed in isolated human neutrophils treated for 10 min with PBS/paquinimod/TAC242, PBS (control), E-selectin or a combination of E-selectin/paquinimod/TAC242 (**b**) and with PBS, E-selectin and E-selectin in the presence MCC950 (**c**). The amount of processed caspase 1 (casp-1 p20 and casp-1 p22) was determined in the supernatants, and the amount of procaspase 1 and GAPDH was determined in cell lysates ($n = 4$ independent experiments); Paq, paquinimod. **d**–**f**, Caspase 1 activity was determined in isolated human neutrophils stimulated with E-selectin or PBS (control) for 10 min loaded with FLICA dye and analyzed by confocal microscopy. Representative confocal images (**d**), quantification of mean FLICA$^+$ area (**e**) and overall mean fluorescence intensity (MFI) of FLICA signal per cell (**f**; 76 (control) and 112 (E-selectin) cells of $n = 3$ independent experiments) are shown. **g**, Isolated human neutrophils were treated for 10 min with PBS (control), E-selectin or E-selectin in the presence of MCC950, and the amount of full-length GSDMD (FL GSDMD), GSDMD-NT and GAPDH was determined in the cell lysates ($n = 4$ independent experiments). **h**,**i**, Representative confocal images (**h**) and overall MFI of GSDMD-NT staining of human neutrophils (**i**) stimulated with PBS (control), E-selectin or E-selectin in the presence of MCC950 for 10 min (49 (control), 75 (E-selectin) and 62 (E-selectin + MCC950) cells of $n = 3$ independent experiments). Data are presented as representative western blots and mean ± s.e.m. (analyzed by one-way ANOVA with Tukey's multiple comparison tests; **b**, **c** and **g**), as mean ± s.e.m. (analyzed by two-tailed paired Student's t-tests (**e** and **f**) or one-way ANOVA with a Tukey's multiple comparison test (**i**)) and as representative confocal images (**d** and **h**); scale bars, 5 μm.

To investigate whether E-selectin-induced GSDMD pores act as a conduit for cytosolic small alarmins ($M_w \leq 50$ kDa) in general, we performed a secretome analysis of neutrophils stimulated with PBS or E-selectin for 10 min (ref. 16). Indeed, we were able to detect a significant increase in the amount of secreted cytosolic small alarmins after E-selectin stimulation (Extended Data Fig. 4). We detected

E-selectin-induced secretion of S100A8, S100A9 and macrophage migration-inhibitory factor in the supernatants and found a significant enrichment of the term 'cytosolic small alarmin' in an unbiased one-dimensional annotation enrichment (Extended Data Fig. 4c). S100A12 was identified in two of three samples and was therefore excluded from statistical analysis. In contrast to cytosolic small alarmins, alarmins located within the nucleus, like HMGB1, were not detected in the secretomes. Further, cytoplasmic alarmins with higher molecular weights, like HSP70 or HSP90, were either not detected in the secretome or secretion was not upregulated after E-selectin stimulation compared to control. In line with the findings shown in Fig. 3h, we did not detect proteins of the IL-1 family (IL-1α, IL-1β and IL-18) in the secretomes of control or E-selectin-stimulated neutrophils. Of note, we also did not observe the induction of granule release after 10 min of E-selectin stimulation as validated by secretome analysis (Extended Data Fig. 5a–c) and flow cytometry (Extended Data Fig. 5d–g), further underlining the specificity of E-selectin in inducing GSDMD pore formation in neutrophils within the vasculature, leading to the specific release of cytosolic small alarmins without an overall activation of neutrophils.

E-selectin induces NLRP3 tyrosine phosphorylation and ASC oligomerization

Next, we wanted to elucidate in more detail downstream signaling events linking E-selectin stimulation to K^+ efflux via $K_V1.3$ and NLRP3 inflammasome assembly. Mueller et al. showed a central role of the Tec family kinase Bruton's tyrosine kinase (BTK) in downstream signaling events induced by E-selectin[17]. Interestingly, BTK has been shown recently to positively regulate inflammasome activation by mediating tyrosine phosphorylation of NLRP3 at the PYD-NACHT linker domain[18,19]. Indeed, we detected tyrosine phosphorylation of NLRP3 in neutrophils after E-selectin stimulation, which was abolished in the presence of ibrutinib, a Food and Drug Administration-approved BTK inhibitor (Fig. 4a). Moreover, BTK inhibition efficiently abolished S100A8/S100A9 release in vitro (Fig. 4b). Interestingly, E-selectin-induced NLRP3 tyrosine phosphorylation was independent of $K_V1.3$ activity, as we detected NLRP3 tyrosine phosphorylation after E-selectin treatment in *Kcna3*$^{-/-}$ neutrophils (Fig. 4c). This implies that NLRP3 phosphorylation and K^+ efflux converge to induce oligomerization of the adaptor protein apoptosis-associated speck-like protein containing a CARD (ASC) and formation of the active inflammasome complex, promoting caspase 1 cleavage downstream of E-selectin treatment[14]. In fact, we detected an increase in ASC oligomers in neutrophils after stimulating the cells with E-selectin compared to treatment with PBS control (Fig. 4d,e). This was dependent on K^+ efflux via $K_V1.3$, as *Kcna3*$^{-/-}$ neutrophils stimulated with E-selectin were unable to form ASC oligomers (Fig. 4f,g), indicating that E-selectin stimulation mediates NLRP3 tyrosine phosphorylation and ASC oligomerization; however, only the latter was dependent on K^+ efflux via $K_V1.3$.

E-selectin-induced GSDMD pore formation is transient

To evaluate E-selectin-induced GSDMD pore formation, we used isolated human and mouse neutrophils and live-cell confocal microscopy to visualize the passive uptake of propidium iodide (PI) through GSDMD pores (Fig. 5a)[20]. Stimulation of human neutrophils with E-selectin induced PI uptake, leading to nuclear staining within minutes (Fig. 5b,c). After 10 min of E-selectin stimulation, almost 100% of neutrophils displayed positive PI staining (Fig. 5d). Pretreatment with MCC950 in turn completely prevented PI uptake (Fig. 5b–d). Accordingly, mouse WT neutrophils efficiently took up PI, and over 90% of WT neutrophils displayed positive staining for PI after 10 min of incubation with E-selectin (Fig. 5e–g). Lack of caspase 1 and caspase 11 completely prevented PI uptake (Fig. 5e–g and Supplementary Video 1), demonstrating the dependence of E-selectin-induced rapid pore formation on inflammatory caspases.

Next, we evaluated changes in membrane potential associated with E-selectin-induced pore formation using current clamp experiments (Extended Data Fig. 6a). To do so, we assessed the baseline membrane potential in human neutrophils before application of E-selectin (inset in Extended Data Fig. 6a). Neutrophils displayed a baseline membrane potential ranging from −11 mV to −49 mV with mean values of around −30 mV (Extended Data Fig. 6b). Neutrophils pretreated with PAP-1 or disulfiram, a GSDMD pore formation inhibitor[21], exhibited similar baseline levels. Application of E-selectin resulted in depolarization of membrane potential in neutrophils, which could be completely abolished by preincubation of the cells with PAP-1 or disulfiram, confirming that E-selectin-induced depolarization is dependent on $K_V1.3$ activation and subsequent GSDMD pore formation, allowing moderate, unspecific ion fluxes across the plasma membrane (Extended Data Fig. 6c).

Several reports implicated GSDMD pores to drive neutrophil pyroptosis[22] and to play a role in the generation of neutrophil extracellular traps[23,24]. However, considering the fact that neutrophils are not supposed to lose their cellular integrity during the intravascular phase of their recruitment into inflamed tissue, we hypothesized that GSDMD pores are formed only transiently. Non-lytic functions of GSDMD have emerged recently, including lysis-independent release of mature IL-1β and cytosolic small DAMPs[20,25,26]. To test for GSDMD pore formation without inducing neutrophil cell death, we assessed lactate dehydrogenase (LDH) concentrations as a proxy for lytic cell death in supernatants of neutrophils stimulated with E-selectin (Fig. 5a). LDH is too large to exit through GSDMD pores and can only leave the cell after membrane rupture. E-selectin stimulation of human neutrophils neither induced cell death after 10 min nor after 30 min or 180 min (Fig. 5h–j). In contrast to E-selectin, LPS priming for 2.5 h followed by 30 min of nigericin stimulation induced moderate LDH release in human neutrophils and high LDH release in human monocytes (positive control), respectively (Extended Data Fig. 6d–g). These findings show that E-selectin stimulation, although inducing GSDMD pore formation and S100A8/S100A9 release, does not mediate any form of cell death in neutrophils. To investigate whether E-selectin-induced GSDMD pore formation might be a transient process, we activated isolated human neutrophils with E-selectin and added PI after 5, 10, 15 or 20 min of stimulation (Fig. 5k). Interestingly, continuous stimulation of neutrophils with E-selectin reduced PI uptake in a time-dependent manner (Fig. 5l,m). Prestimulation of cells with E-selectin for 10 min before the addition of PI reduced the amount of PI^+ cells to around 70%. After 15 min or 20 min of E-selectin stimulation, respectively, PI uptake was completely abolished. These results suggest that E-selectin-induced GSDMD pore formation in neutrophils is a time-limited and reversible process.

Recently, the endosomal sorting complexes required for transport (ESCRT) machinery was shown to trigger repair programs to remove GSDMD pores from the plasma membrane, thereby counterbalancing cell death[27]. To elucidate a potential role of the ESCRT machinery in this self-repair program, we investigated subcellular localization of CHMP4B, an ESCRT III-associated protein, after E-selectin stimulation for 15 min. ESCRT proteins form a punctate pattern during membrane repair and translocate to the plasma membrane[27,28]. Consistently, stimulation of human neutrophils with E-selectin resulted in the formation of CHMP4B puncta, presumably corresponding to functional assemblies of ESCRT III, whereas unstimulated neutrophils (control cells) displayed a weak and rather diffuse cytoplasmic staining of CHMP4B (Fig. 5n,o). These findings suggest the induction of membrane repair processes in E-selectin-stimulated neutrophils to clear the surface membrane of GSDMD pores.

GSDMD-dependent pore formation supports neutrophil recruitment

Finally, we wanted to test if GSDMD pore formation supports neutrophil recruitment during acute inflammation in vivo. Therefore, we studied leukocyte recruitment in an acute, predominantly neutrophil-driven,

https://doi.org/10.1038/s41590-023-01656-1

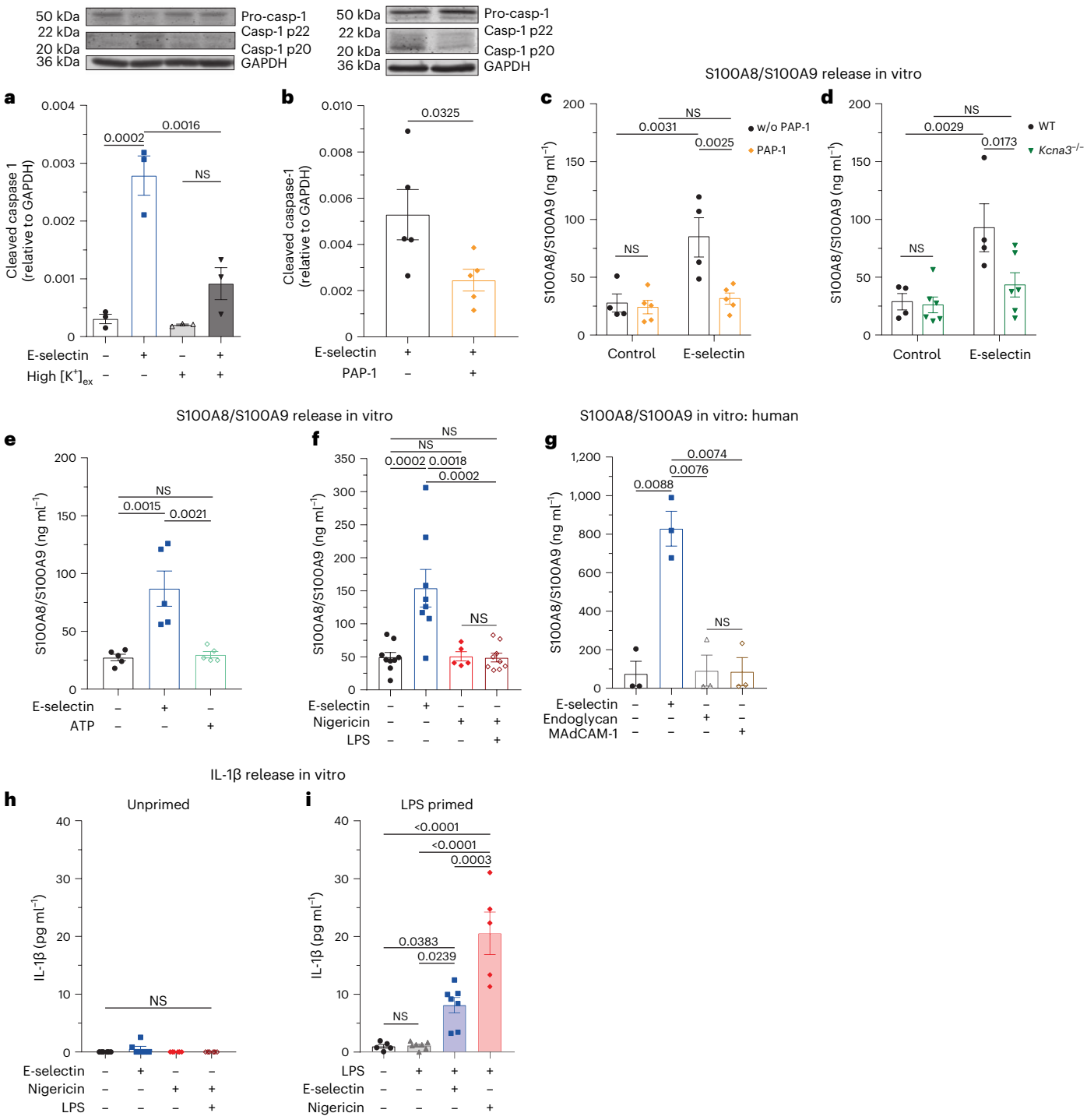

Fig. 3 | Rapid E-selectin-induced inflammasome activation is $K_v1.3$ dependent. a,**b**, Caspase 1 cleavage was assessed in isolated human neutrophils resuspended in normal HBSS and HBSS with high $[K^+]_{ex}$ (**a**) and pretreated with $K_v1.3$ inhibitor PAP-1 (**b**; 50 nM) or vehicle control and stimulated with E-selectin for 10 min. The amount of processed caspase 1 (casp-1 p20 and casp-1 p22) was determined in the supernatants, and the amounts of procaspase 1 and GAPDH were determined in cell lysates ($n = 3$ and 5 independent experiments, respectively). **c**,**d**, Bone marrow neutrophils from WT mice pretreated with PAP-1 (50 nM) or vehicle control (**c**) or from WT and *Kcna3*$^{-/-}$ mice (**d**) were incubated with E-selectin or PBS (control) for 10 min ($n = 4$ (control), 5 (PAP-1), 4 (WT) and 6 (*Kcna3*$^{-/-}$) mice per group); w/o, without. **e**,**f**, Bone marrow neutrophils from WT mice were incubated with PBS, E-selectin or ATP (**e**) or with PBS, E-selectin, nigericin or a combination of LPS and nigericin (**f**) for 10 min ($n = 5$ (control (**e**), E-selectin (**e**), ATP (**e**) and nigericin (**f**)), 9 (control (**f**), LPS and nigericin (**f**)) and 8 (E-selectin (**f**)) mice per group). **g**, Isolated human neutrophils were stimulated with PBS, E-selectin, MAdCAM-1 or endoglycan for 10 min ($n = 3$ independent experiments). In **c**–**g**, supernatants were collected, and S100A8/S100A9 levels were analyzed by ELISA. **h**,**i**, IL-1β levels were analyzed by ELISA in the supernatants from WT bone marrow neutrophils stimulated with PBS, E-selectin, nigericin or a combination of LPS and nigericin for 10 min (**h**; $n = 6$ mice per group) or primed with PBS or LPS for 2.5 h and subsequently stimulated for 30 min with PBS, E-selectin or nigericin (**i**; $n = 5$ (control, LPS/nigericin) and 7 (LPS, LPS/E-selectin) mice per group). Data are presented as representative western blots and mean ± s.e.m. (**a** and **b**; data were analyzed by one-way ANOVA with a Tukey's multiple comparison test or two-tailed paired Student's *t*-tests, respectively) or mean ± s.e.m. (**c**–**i**; data were analyzed by two-way RM ANOVA with a Sidak's multiple comparison test (**c** and **d**) or one-way ANOVA with Tukey's multiple comparison tests (**e**–**i**)).

https://doi.org/10.1038/s41590-023-01656-1

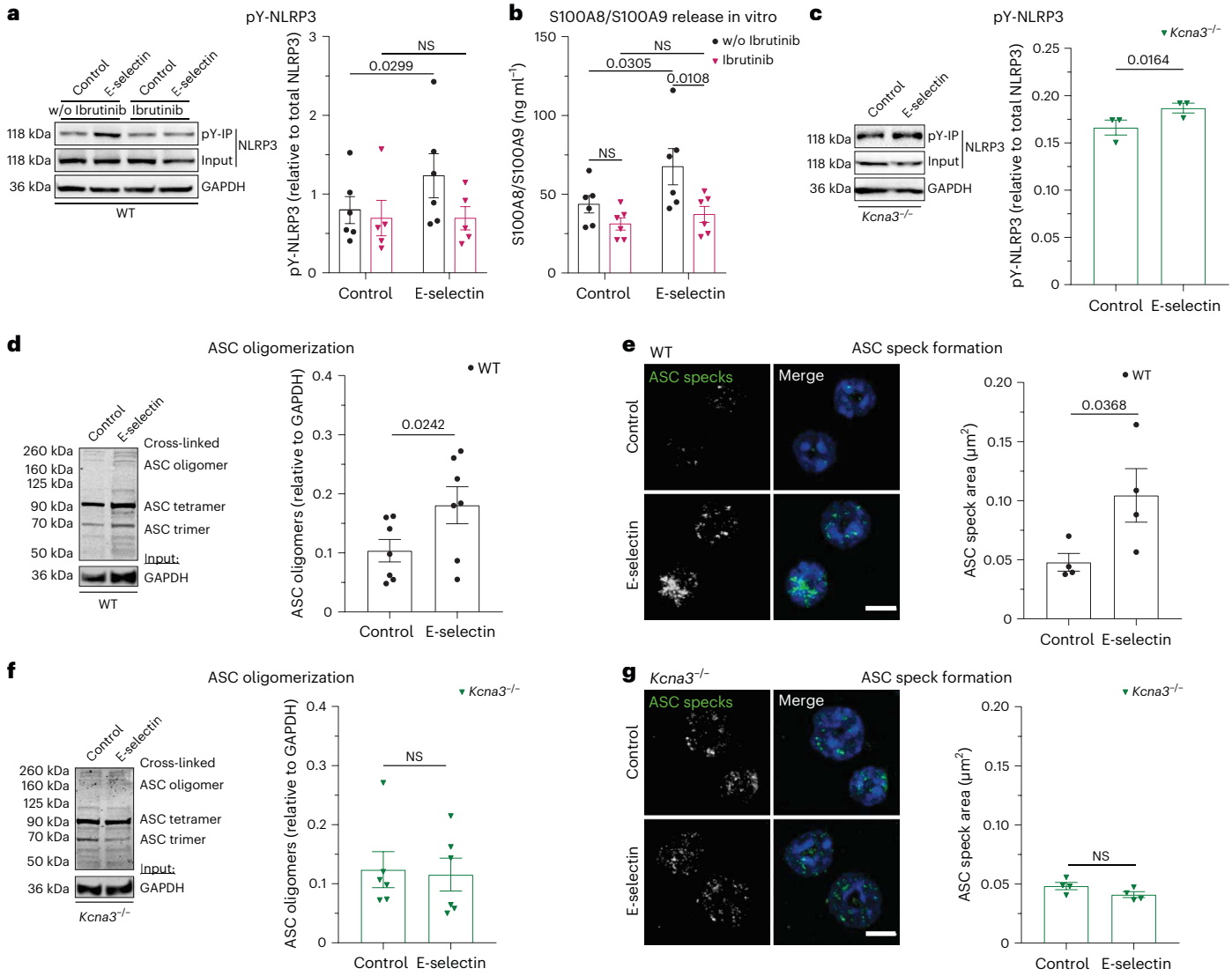

Fig. 4 | E-selectin induces NLRP3 tyrosine phosphorylation and ASC oligomerization. a, Tyrosine phosphorylation of NLPR3 after 5 min of PBS or E-selectin stimulation was assessed via phospho-tyrosine immunoprecipitation (pY-IP) in WT bone marrow neutrophils pretreated with the BTK inhibitor ibrutinib (0.6 µM) or vehicle control ($n = 5$ (ibrutinib) and 6 (without ibrutinib) independent experiments). **b**, Bone marrow neutrophils from WT mice were incubated with ibrutinib (0.6 µM) or vehicle control and subsequently stimulated with E-selectin or PBS (control) for 10 min ($n = 6$ mice per group). Supernatants were collected, and S100A8/S100A9 levels were analyzed by ELISA. **c**, Bone marrow *Kcna3*$^{-/-}$ neutrophils were stimulated for 5 min with PBS or E-selectin, and tyrosine phosphorylation of NLRP3 was analyzed by pY-IP ($n = 3$ independent experiments). **d**–**g**, Bone marrow neutrophils from WT (**d** and **e**) and *Kcna3*$^{-/-}$ (**f** and **g**) mice were stimulated with E-selectin or PBS (control) for 10 min, and ASC oligomerization was analyzed by western blotting ($n = 7$ (WT) and 6 (*Kcna3*$^{-/-}$) mice per group) and confocal microscopy (WT: 38 (control) and 32 (E-selectin) cells; *Kcna3*$^{-/-}$: 41 (control) and 34 (E-selectin) cells of $n = 4$ mice per group). Data are presented as representative western blots and mean ± s.e.m. (**a**, **c**, **d** and **f**; data were analyzed by two-way RM ANOVA and a Sidak's multiple comparison test (**a**) or two-tailed paired Student's *t*-tests (**c**, **d** and **f**)), mean ± s.e.m. (**b**; data were analyzed by two-way RM ANOVA and a Sidak's multiple comparison test) and representative micrographs and mean ± s.e.m. (**e** and **g**; 51 (WT control), 64 (WT E-selectin), 46 (*Kcna3*$^{-/-}$ control) and 48 (*Kcna3*$^{-/-}$ E-selectin) cells of $n = 4$ mice per group; data were analyzed by paired Student's *t*-tests); scale bars, 5 µm.

inflammatory setting[29] and assessed leukocyte rolling, leukocyte rolling velocities and number of adherent leukocytes in postcapillary venules of the TNF-stimulated mouse cremaster muscle using intravital microscopy. In addition, we analyzed the number of extravasated neutrophils in the TNF-stimulated cremaster muscle (Fig. 6a). Rolling flux fraction was not affected in the absence of GSDMD (Fig. 6b), demonstrating that GSDMD pores and release of cytosolic proteins are not regulating the number of rolling neutrophils. However, and in line with the flow chamber experiments (Fig. 1d), *Gsdmd*$^{-/-}$ cells rolled significantly faster in vivo (Fig. 6c and Supplementary Video 2), indicating that pore formation and release of S100A8/S100A9 is important for the deceleration of leukocyte rolling velocities in vivo. Furthermore, in the absence of GSDMD, leukocytes were unable to adhere efficiently (Fig. 6d and Supplementary Video 2), and the number of perivascular neutrophils was decreased (Fig. 6e). Notably, overall surface expression of adhesion and extravasation-relevant molecules, such as Mac-1 (CD11b/α_M), LFA-1 (CD11a, α_L), CD18 (β_2) and CXCR2 (CD182), on neutrophils was similar between WT and *Gsdmd*$^{-/-}$ mice under baseline conditions (Extended Data Fig. 7). Consistently, MCC950 injection into WT mice 1 h before TNF application increased leukocyte rolling velocity and significantly reduced the number of adherent and extravasated cells in the inflamed cremaster muscle (Extended Data Fig. 8). Importantly, microvascular parameters did not differ between respective groups (Extended Data Table 1). Of note, genetic deletion of *Gsdmd* or pharmacological

https://doi.org/10.1038/s41590-023-01656-1

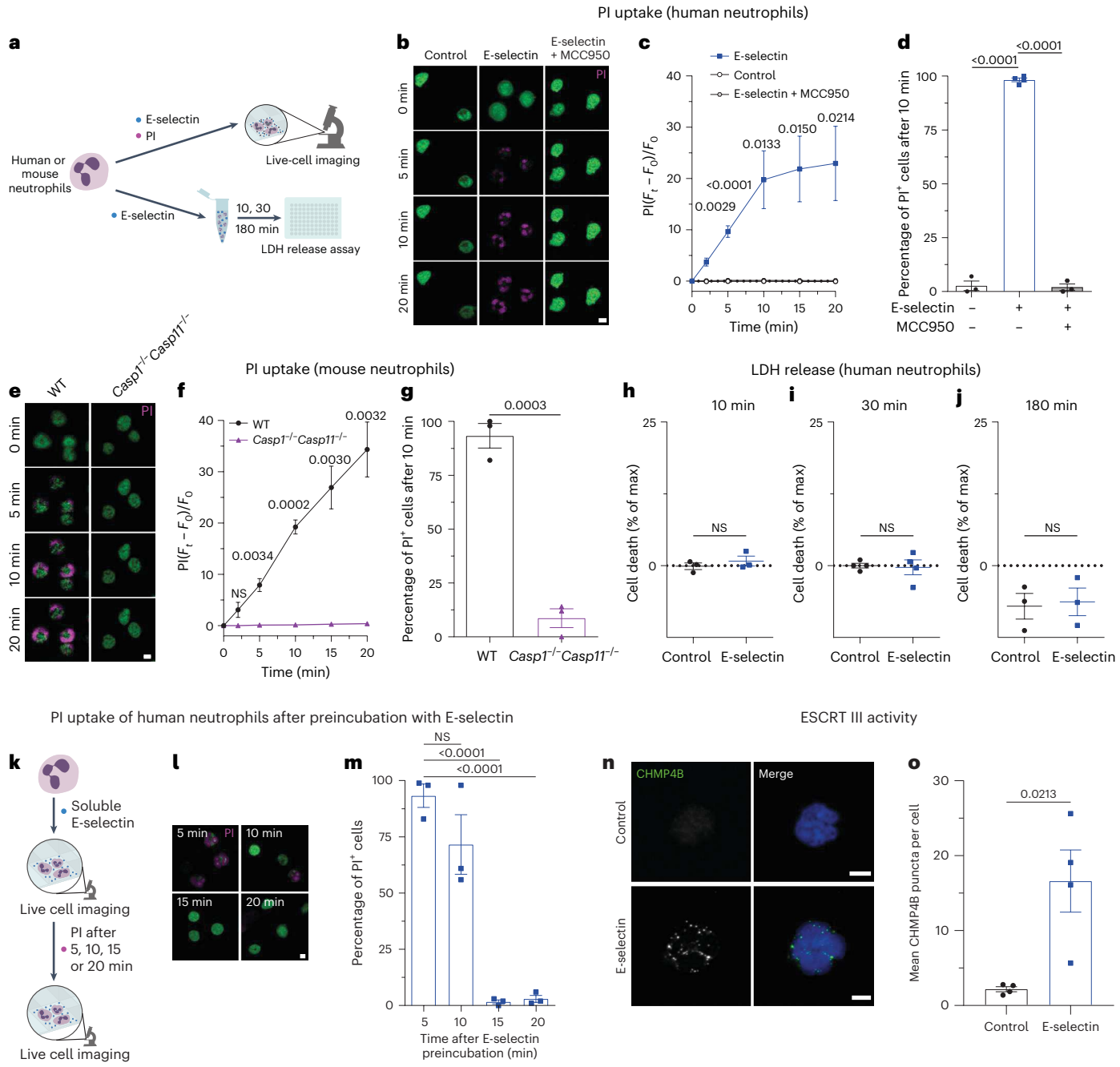

Fig. 5 | E-selectin-induced GSDMD pore formation is transient. a, Schematic of the experimental design. **b**, Representative confocal images of PI uptake in isolated human neutrophils stimulated with PBS, E-selectin or E-selectin in the presence of MCC950. **c**,**d**, Time course analysis (**c**) and percentage of PI$^+$ cells after 10 min of stimulation (**d**; 1,029 (PBS), 429 (E-selectin) and 315 (E-selectin/MCC950) cells of $n = 3$ (control and E-selectin + MCC950) and 4 (E-selectin) independent experiments); F_t, fluorescence at the respective time point; F_0, fluorescence at t_0. **e**, Representative confocal images of PI uptake in bone marrow neutrophils from WT and *Casp1*$^{-/-}$*Casp11*$^{-/-}$ mice treated with E-selectin. **f**,**g**, Time course (**f**) and percentage of PI$^+$ WT and *Casp1*$^{-/-}$*Casp11*$^{-/-}$ neutrophils after 10 min of stimulation (**g**; 190 (WT) and 351 (*Casp1*$^{-/-}$*Casp11*$^{-/-}$) cells of $n = 3$ mice per group). **h**–**j**, Cell death of human neutrophils was assessed via LDH release after stimulation with PBS or E-selectin for 10 min (**h**), 30 min (**i**) and 180 min (**j**; $n = 3$ (10 min and 180 min) and 4 (30 min) independent experiments). **k**–**m**, PI uptake was measured in isolated human neutrophils after pretreatment of cells with E-selectin for the specified amounts of time (**k**). Representative confocal images of PI uptake (**l**) and percentage of PI$^+$ neutrophils (**m**) are shown (274 (5 min), 313 (10 min), 358 (15 min) and 466 (20 min) cells of $n = 3$ independent experiments). **n**,**o**, CHMP4B expression was investigated in isolated human neutrophils stimulated with PBS or E-selectin for 15 min. Representative confocal images of CHMP4B localization (**n**) and number of CHMP4B puncta per cell (**o**; 24 (control) and 47 (E-selectin) cells of $n = 4$ independent experiments) are shown. Data are presented as mean ± s.e.m. (**c**, **d**, **f**–**j**, **m** and **o**; data were analyzed by one-way ANOVA with a Dunnetts's multiple comparison test (**c**, **d** and **m**), two-tailed unpaired Student's *t*-tests (**f**–**j**) or two-tailed paired Student's *t*-tests (**m** and **o**)) and representative micrographs (**b**, **e**, **l** and **n**); scale bars, 5 µm.

inhibition of NLRP3 inflammasome activation will also affect inflammasome activation in cell types other than neutrophils, which might additionally contribute to the reduction in the inflammatory response observed in the in vivo setting.

Discussion

Neutrophils comprise the major part of circulating white blood cells in humans and are critically involved in the early inflammatory response exerted by the innate immune system. The importance of

https://doi.org/10.1038/s41590-023-01656-1

inflammasome activation in neutrophils during the inflammatory response has been rather neglected in the past, and inflammasome research has focused primarily on monocytes and macrophages. However, neutrophils express and store key components of the inflammasome machinery and are a major source of IL-1β secretion; so the idea of targeting inflammasome activation in neutrophils as a potential anti-inflammatory strategy during overwhelming immune responses or autoimmune disorders became more and more appreciated over the last decade[30–34]. With our present study, we expand the knowledge on inflammasome activation in neutrophils and identify an E-selectin-induced mechanism leading to rapid, but transient, GSDMD pore formation accompanied by S100A8/S100A9 release during inflammation. In contrast to other cell types that need to be 'converted' into a proinflammatory phenotype or primed before being able to secret high amounts of cytokines and other proinflammatory mediators, neutrophils are fast-reacting cells and are fully equipped with the receptor and protein machinery needed to effectively fight against invading pathogens. S100A8/S100A9 is one of the major components within the cytosol of circulating blood neutrophils and an important mediator of inflammation[2]. In its cytosolic form, S100A8/S100A9 is abundantly expressed and completely processed and does not require upregulation by de novo protein synthesis. Instead, IL-1β secretion is a rather slow process that relies on de novo synthesis during the priming phase[9]. Before IL-1β secretion, the inflammasome is primed through engagement of pattern recognition receptors or cytokines to upregulate inflammasome components like NLRP3 and caspase 1. Priming is followed by an activation step, which can be induced by bacterial, viral and fungal products, sterile inflammation or cellular stress. Upstream signals of NLRP3 activation are thought to include efflux of K^+ or chloride, calcium influx, lysosomal disruption, metabolic changes, *trans*-Golgi disassembly and mitochondrial dysfunction[14]. Here, we describe a rapid activation process for GSDMD pore formation in neutrophils triggered by E-selectin, which is expressed on inflamed endothelial cells. Importantly, this fast activation process is independent of TLR4 engagement, as disruption of TLR4 downstream signaling with a TLR4 inhibitor and paquinimod does not affect the amount of cleaved caspase 1 within the supernatant of E-selectin-stimulated neutrophils.

Similar to conventional inflammasome activation, E-selectin-induced rapid inflammasome activation and subsequent S100A8/S100A9 release in neutrophils is dependent on K^+ efflux, which is provided via the voltage-sensitive K^+ channel $K_V1.3$. Interestingly, stimulation of neutrophils over 10 min with nigericin or ATP alone (two known inducers of K^+ efflux) or in combination with LPS[35,36] was unable to trigger rapid S100A8/S100A9 release from neutrophils. These findings suggest that E-selectin stimulation not only mediates K^+ efflux by $K_V1.3$ but also induces signaling events leading to post-translational NLRP3 modifications, a process required for proper NLRP3 activation[14,37,38]. Indeed, we were able to demonstrate that E-selectin triggers BTK-dependent NLRP3 tyrosine phosphorylation. Accordingly, BTK was reported to positively regulate NLRP3 inflammasome activation by phosphorylating four conserved tyrosine residues on NLRP3. This promoted formation of NLRP3 oligomers and complexes with ASC, which resulted in IL-1β secretion in LPS/nigericin- or LPS/monosodium urate crystal-treated primary immune cells[18]. We show here that E-selectin induces post-translational modifications of NLRP3 independent of K^+ efflux, as E-selectin-mediated NLRP3 tyrosine phosphorylation was still present in the absence of $K_V1.3$. However, and in line with LPS/ATP-induced inflammasome activation[39], ASC speck formation occurred downstream of K^+ efflux in rapid E-selectin-induced inflammasome activation, as ASC oligomerization and ASC speck formation were absent in E-selectin-stimulated KCNA3-deficient neutrophils.

During NLRP3 inflammasome activation, the 52-kDa GSDMD is processed to the 31-kDa GSDMD-NT fragment, which oligomerizes at the plasma membrane and forms pores, thereby increasing permeability for macromolecules and the release of IL-1β in macrophages, dendritic cells and neutrophils[11,25,40]. The pores have an inner diameter of around 20 nm (refs. 41,42) and are predominantly negatively charged, thus predominantly allowing passage of neutral or positively charged proteins[40,42]. With a molecular weight of 24 kDa, S100A8/S100A9 is suitable to exit through GSDMD pores. However, the net charge of released S100A8 and S100A9 is currently unclear but might be influenced by the local influx of Ca^{2+} ions through the open GSDMD pores, favoring Ca^{2+} binding to S100A8/S100A9 and enhancing hydrophobicity and positive charge, as previously reported[43].

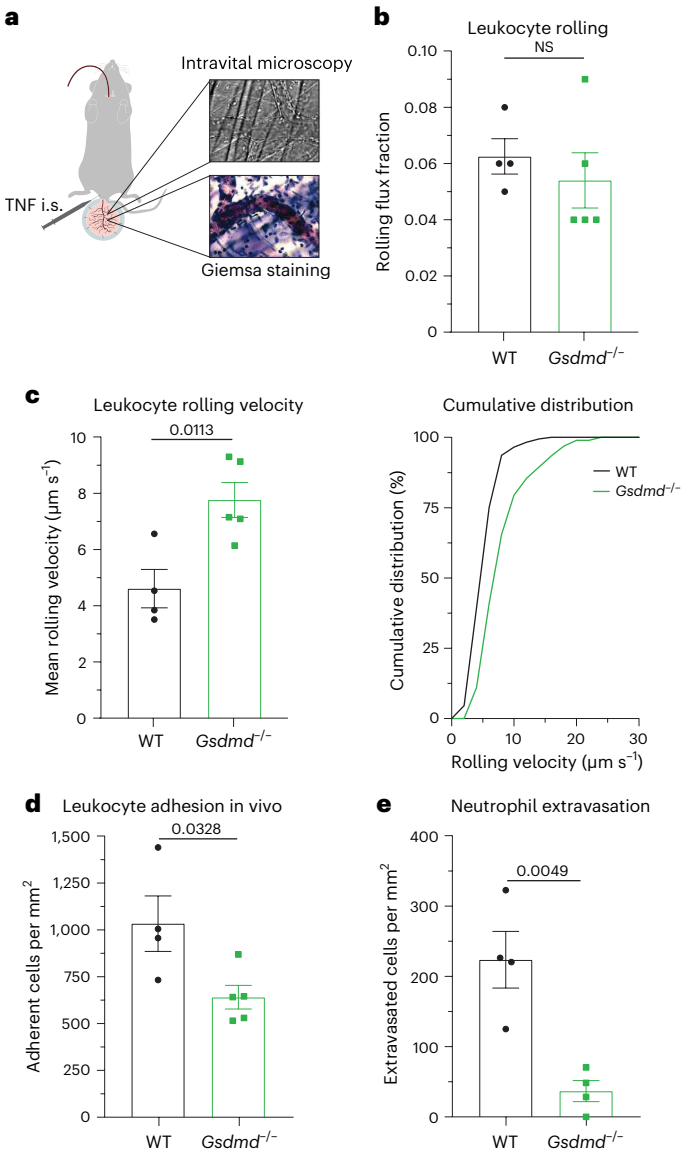

Fig. 6 | GSDMD-dependent pore formation supports neutrophil recruitment. **a**, Schematic of the experimental design. Male WT and *Gsdmd*$^{-/-}$ mice were stimulated after intrascrotal administration of TNF (500 ng) 2 h before intravital microscopy of postcapillary venules of the mouse cremaster muscle. **b**–**d**, Neutrophil rolling (**b**), neutrophil rolling velocity (**c**) and number of adherent neutrophils per vessel surface (**d**) were analyzed (18 and 24 vessels, respectively, of $n = 4$ (WT) and 5 (*Gsdmd*$^{-/-}$) mice per group). **e**, TNF-stimulated cremaster muscles were stained with Giemsa, and the number of perivascular neutrophils was quantified (52 and 31 vessels, respectively, of $n = 4$ mice per group). Data are presented as mean ± s.e.m. (**b**–**e**) and as cumulative distribution (**c**; right) and were analyzed by two-tailed unpaired Student's *t*-tests.

Our findings provide evidence that E-selectin-driven S100A8/S100A9 release requires canonical NLRP3 inflammasome activation and GSDMD pores, as inhibition of the NLRP3 inflammasome by MCC950 and genetic deletion of *Gsdmd* completely abolished its release from neutrophils in vitro and in vivo. Initially, cell death has been proposed to be a direct and unavoidable consequence of GSDMD pore formation[44,45]. However, non-lytic functions of GSDMD emerged, such as promoting lysis-independent release of mature IL-1β and cytosolic small DAMPs[20,25,26,46]. Accordingly, the ESCRT machinery was shown to trigger repair programs to remove GSDMD pores from the plasma membrane, thereby counterbalancing cell death[27]. Neutrophils rolling on inflamed endothelium are not supposed to undergo cell death within the vasculature, as neutrophils need to extravasate into inflamed tissue. Within the tissue, neutrophils fight against invading pathogens and clear the area from cell debris or injured tissue during sterile inflammation together with other innate immune cells, like tissue-resident macrophages or dendritic cells. We show that, although almost all neutrophils stimulated with E-selectin displayed positive staining for PI, the amount of LDH release was rather low, suggesting protective mechanisms that allow neutrophils to close/remove GSDMD pores from their surface. In general, neutrophils seem to be less prone to undergo cell death, in particular after canonical inflammasome activation[23,26]. After NLRC4 inflammasome activation, for example, neutrophils are resistant to pyroptotic cell death[26], and GSDMD-independent secretion pathways were described for IL-1β from non-pyroptotic cells, such as neutrophils[40]. Karmakar et al. recently described an additional IL-1β secretory mechanism in neutrophils via an autophagy-dependent, non-lytic pathway. They showed that p31 GSDMD pores do not accumulate in the plasma membrane of neutrophils but associate with azurophilic granules, leading to neutrophil elastase release into the cytosol, mediating a secondary cascade of serine protease dependent-GSDMD processing[11]. In 2018, Rühl et al. showed that calcium influx through GSDMD pores initiates a membrane repair program by recruiting the ESCRT machinery to damaged membrane areas[27]. We detected CHMP4B puncta after stimulating the cells with E-selectin, implying the formation of the ESCRT III membrane repair machinery following rapid E-selectin-induced GSDMD pore formation. These findings support our notion that GSDMD pores appear in a transient fashion, enabling the release of S100A8/S100A9 from recruited neutrophils within the vasculature while preserving their integrity, a prerequisite for subsequent diapedesis.

Taken together, we uncovered a rapid, endogenous and transient E-selectin-dependent activation system for neutrophils within inflamed microvessels, which triggers NLRP3 inflammasome assembly, leading to transient GSDMD pore formation and S100A8/S100A9 release from neutrophils without inducing cell death. Although triggering inflammation within the vasculature, neutrophils remain capable of extravasation and functional to fulfill their role in subsequent immune responses within tissues. Modulating this E-selectin/NLRP3 inflammasome/GSDMD-dependent activation pathway in neutrophils might therefore offer an interesting therapeutic approach for the treatment of acute and chronic inflammatory disorders with unwanted neutrophil accumulation.

Online content

Any methods, additional references, Nature Portfolio reporting summaries, source data, extended data, supplementary information, acknowledgements, peer review information; details of author contributions and competing interests; and statements of data and code availability are available at https://doi.org/10.1038/s41590-023-01656-1.

References

1. Amulic, B., Cazalet, C., Hayes, G. L., Metzler, K. D. & Zychlinsky, A. Neutrophil function: from mechanisms to disease. *Annu. Rev. Immunol.* **30**, 459–489 (2012).
2. Pruenster, M., Vogl, T., Roth, J. & Sperandio, M. S100A8/A9: from basic science to clinical application. *Pharmacol. Ther.* **167**, 120–131 (2016).
3. Pruenster, M. et al. Extracellular MRP8/14 is a regulator of β_2 integrin-dependent neutrophil slow rolling and adhesion. *Nat. Commun.* **6**, 6915 (2015).
4. Morikis, V. A. et al. Selectin catch-bonds mechanotransduce integrin activation and neutrophil arrest on inflamed endothelium under shear flow. *Blood* **130**, 2101–2110 (2017).
5. Silvin, A. et al. Elevated calprotectin and abnormal myeloid cell subsets discriminate severe from mild COVID-19. *Cell* **182**, 1401–1418 (2020).
6. Scott, N. R. et al. S100A8/A9 regulates CD11b expression and neutrophil recruitment during chronic tuberculosis. *J. Clin. Invest.* **130**, 3098–3112 (2020).
7. Perego, M. et al. Reactivation of dormant tumor cells by modified lipids derived from stress-activated neutrophils. *Sci. Transl. Med.* **12**, eabb5817 (2020).
8. He, W. T. et al. Gasdermin D is an executor of pyroptosis and required for interleukin-1β secretion. *Cell Res.* **25**, 1285–1298 (2015).
9. Broz, P. & Dixit, V. M. Inflammasomes: mechanism of assembly, regulation and signalling. *Nat. Rev. Immunol.* **16**, 407–420 (2016).
10. Read, M. A. et al. Tumor necrosis factor α-induced E-selectin expression is activated by the nuclear factor-κB and c-JUN N-terminal kinase/p38 mitogen-activated protein kinase pathways. *J. Biol. Chem.* **272**, 2753–2761 (1997).
11. Karmakar, M. et al. N-GSDMD trafficking to neutrophil organelles facilitates IL-1β release independently of plasma membrane pores and pyroptosis. *Nat. Commun.* **11**, 2212 (2020).
12. Immler, R. et al. The voltage-gated potassium channel $K_v1.3$ regulates neutrophil recruitment during inflammation. *Cardiovasc. Res.* **118**, 1289–1302 (2021).
13. Schmitz, A. et al. Design of PAP-1, a selective small molecule $K_v1.3$ blocker, for the suppression of effector memory T cells in autoimmune diseases. *Mol. Pharmacol.* **68**, 1254–1270 (2005).
14. Swanson, K. V., Deng, M. & Ting, J. P. The NLRP3 inflammasome: molecular activation and regulation to therapeutics. *Nat. Rev. Immunol.* **19**, 477–489 (2019).
15. Rosen, S. D. Ligands for L-selectin: homing, inflammation, and beyond. *Annu. Rev. Immunol.* **22**, 129–156 (2004).
16. Meissner, F., Scheltema, R. A., Mollenkopf, H. J. & Mann, M. Direct proteomic quantification of the secretome of activated immune cells. *Science* **340**, 475–478 (2013).
17. Mueller, H. et al. Tyrosine kinase BTK regulates E-selectin-mediated integrin activation and neutrophil recruitment by controlling phospholipase C (PLC) γ2 and PI3Kγ pathways. *Blood* **115**, 3118–3127 (2010).
18. Bittner, Z. A. et al. BTK operates a phospho-tyrosine switch to regulate NLRP3 inflammasome activity. *J. Exp. Med.* **218**, e20201656 (2021).
19. Ito, M. et al. Bruton's tyrosine kinase is essential for NLRP3 inflammasome activation and contributes to ischaemic brain injury. *Nat. Commun.* **6**, 7360 (2015).
20. Evavold, C. L. et al. The pore-forming protein gasdermin D regulates interleukin-1 secretion from living macrophages. *Immunity* **48**, 35–44 (2018).
21. Hu, J. J. et al. FDA-approved disulfiram inhibits pyroptosis by blocking gasdermin D pore formation. *Nat. Immunol.* **21**, 736–745 (2020).
22. Chauhan, D. et al. GSDMD drives canonical inflammasome-induced neutrophil pyroptosis and is dispensable for NETosis. *EMBO Rep.* **23**, e54277 (2022).
23. Chen, K. W. et al. Noncanonical inflammasome signaling elicits gasdermin D-dependent neutrophil extracellular traps. *Sci. Immunol.* **3**, eaar6676 (2018).

24. Sollberger, G. et al. Gasdermin D plays a vital role in the generation of neutrophil extracellular traps. *Sci. Immunol.* **3**, eaar6689 (2018).
25. Heilig, R. et al. The gasdermin-D pore acts as a conduit for IL-1β secretion in mice. *Eur. J. Immunol.* **48**, 584–592 (2018).
26. Chen, K. W. et al. The neutrophil NLRC4 inflammasome selectively promotes IL-1β maturation without pyroptosis during acute *Salmonella* challenge. *Cell Rep.* **8**, 570–582 (2014).
27. Ruhl, S. et al. ESCRT-dependent membrane repair negatively regulates pyroptosis downstream of GSDMD activation. *Science* **362**, 956–960 (2018).
28. Jimenez, A. J. et al. ESCRT machinery is required for plasma membrane repair. *Science* **343**, 1247136 (2014).
29. Sperandio, M., Pickard, J., Unnikrishnan, S., Acton, S. T. & Ley, K. Analysis of leukocyte rolling in vivo and in vitro. *Methods Enzymol.* **416**, 346–371 (2006).
30. Bakele, M. et al. Localization and functionality of the inflammasome in neutrophils. *J. Biol. Chem.* **289**, 5320–5329 (2014).
31. Karmakar, M. et al. Neutrophil IL-1β processing induced by pneumolysin is mediated by the NLRP3/ASC inflammasome and caspase-1 activation and is dependent on K^+ efflux. *J. Immunol.* **194**, 1763–1775 (2015).
32. Mankan, A. K., Dau, T., Jenne, D. & Hornung, V. The NLRP3/ASC/caspase-1 axis regulates IL-1β processing in neutrophils. *Eur. J. Immunol.* **42**, 710–715 (2012).
33. Tyrkalska, S. D., Candel, S. & Mulero, V. The neutrophil inflammasome. *Dev. Comp. Immunol.* **115**, 103874 (2021).
34. Sreejit, G. et al. Retention of the NLRP3 inflammasome-primed neutrophils in the bone marrow is essential for myocardial infarction-induced granulopoiesis. *Circulation* **145**, 31–44 (2022).
35. Karmakar, M., Katsnelson, M. A., Dubyak, G. R. & Pearlman, E. Neutrophil P2X7 receptors mediate NLRP3 inflammasome-dependent IL-1β secretion in response to ATP. *Nat. Commun.* **7**, 10555 (2016).
36. Di, A. et al. The TWIK2 potassium efflux channel in macrophages mediates NLRP3 inflammasome-induced inflammation. *Immunity* **49**, 56–65 (2018).
37. Song, N. et al. NLRP3 phosphorylation is an essential priming event for inflammasome activation. *Mol. Cell* **68**, 185–197 (2017).
38. McKee, C. M. & Coll, R. C. NLRP3 inflammasome priming: a riddle wrapped in a mystery inside an enigma. *J. Leukoc. Biol.* **108**, 937–952 (2020).
39. He, Y., Zeng, M. Y., Yang, D., Motro, B. & Nunez, G. NEK7 is an essential mediator of NLRP3 activation downstream of potassium efflux. *Nature* **530**, 354–357 (2016).
40. Monteleone, M. et al. Interleukin-1β maturation triggers its relocation to the plasma membrane for gasdermin-D-dependent and -independent secretion. *Cell Rep.* **24**, 1425–1433 (2018).
41. Gaidt, M. M. & Hornung, V. Pore formation by GSDMD is the effector mechanism of pyroptosis. *EMBO J.* **35**, 2167–2169 (2016).
42. Xia, S. et al. Gasdermin D pore structure reveals preferential release of mature interleukin-1. *Nature* **593**, 607–611 (2021).
43. Champaiboon, C., Sappington, K. J., Guenther, B. D., Ross, K. F. & Herzberg, M. C. Calprotectin S100A9 calcium-binding loops I and II are essential for keratinocyte resistance to bacterial invasion. *J. Biol. Chem.* **284**, 7078–7090 (2009).
44. Liu, X. et al. Inflammasome-activated gasdermin D causes pyroptosis by forming membrane pores. *Nature* **535**, 153–158 (2016).
45. Sborgi, L. et al. GSDMD membrane pore formation constitutes the mechanism of pyroptotic cell death. *EMBO J.* **35**, 1766–1778 (2016).
46. Kayagaki, N. et al. NINJ1 mediates plasma membrane rupture during lytic cell death. *Nature* **591**, 131–136 (2021).

Methods

Mice

C57BL/6NCrl (WT) mice were purchased from Charles River Laboratories. *Gsdmd*$^{-/-}$ (ref. 47) mice were from P. Broz (University of Lausanne, Switzerland), *Casp1*$^{-/-}$*Casp11*$^{-/-}$ (ref. 48) mice were from V. Hornung (LMU München, Germany), *Sele*$^{-/-}$ (ref. 49) mice were from D. Vestweber (Max Planck Institute for Molecular Biomedicine, Münster, Germany) and *Mrp14*$^{-/-}$ mice were from Johannes Roth (University of Münster, Germany). *Kcna3*$^{-/-}$ mice[50] were purchased from Jackson Laboratories and maintained on a C57BL/6NCrl background. WT, *Mrp14*$^{-/-}$ and *Kcna3*$^{-/-}$ mice were housed at 20 to 22 °C with a humidity of 45–55% and a 12-h light/12-h dark cycle. Eight- to 25-week-old male and female were used for all experiments. Mice of similar age and sex were used for all experiments except for intravital microscopy studies in the cremaster muscle, where only male mice were used. The allocation of animals to groups was performed randomly or on the basis of their genotype. Animal experiments were approved by the Government of Oberbayern (AZ: ROB-55.2-2532.Vet_02-18-22 and ROB-55.2-2532.Vet_02-17-102) and were performed in accordance with the guidelines from Directive 2010/63/EU. For in vivo experiments, mice were anesthetized via intraperitoneal injection using a combination of ketamine/xylazine (125 mg per kg (body weight) and 12.5 mg per kg (body weight), respectively, in a volume of 0.1 ml per 8 g body weight). All mice were killed by cervical dislocation.

Human blood sampling

Blood sampling from healthy volunteers was approved by the ethical committee of Ludwig-Maximilians-Universität München (AZ 611-15), in agreement with the Declaration of Helsinki. Recruitment was randomly performed at the Biomedical Center at Ludwig-Maximilians-Universität Munich, and samples were allocated randomly to groups with no relevant covariates. Informed consent was obtained from all participants.

Isolation of human and mouse neutrophils

Human neutrophils were isolated from healthy blood donors using either Polymorphprep (Axis Shield) or an EasySep direct human neutrophil isolation kit (StemCell Technologies) according to the manufacturers' protocols. Bone marrow mouse neutrophils were isolated using an EasySep mouse neutrophil enrichment kit (StemCell Technologies) according to manufacturer's protocol.

S100A8/S100A9 release

For the in vivo release assay, recombinant mouse TNF (500 ng per mouse; R&D Systems) was injected into the scrotums of anesthetized male WT, *Gsdmd*$^{-/-}$, *Casp1*$^{-/-}$*Casp11*$^{-/-}$ and *Sele*$^{-/-}$ mice, as previously described[3]. In a second set of experiments, WT mice were pretreated with an intraperitoneal injection of MCC950 (10 mg per kg (body weight); Invivogen) or vehicle control 1 h before TNF injection. Mouse blood was collected via retroorbital bleeding before and 2 h after TNF application.

In vitro release of S100A8/S100A9 was assessed as described previously[3]. Briefly, bone marrow neutrophils were isolated from WT, *Gsdmd*$^{-/-}$, *Casp1*$^{-/-}$*Casp11*$^{-/-}$ and *Kcna3*$^{-/-}$ mice. Glass cover slips were coated with recombinant mouse E-selectin (rmCD62E-Fc chimera, 10 µg ml^{-1}; R&D Systems) or PBS/0.1% bovine serum albumin (BSA) at 4 °C overnight, blocked with 5% casein (Sigma-Aldrich) and washed with PBS. Neutrophils (5×10^5) were reconstituted in 500 µl of HBSS and incubated under shaking conditions on coated slides for 10 min at 37 °C with 5% CO_2. Depending on the specific groups, cells were pretreated with MCC950 (1 µM, 30 min), PAP-1 (50 nM, 10 min; Sigma-Aldrich), ibrutinib (0.6 µM, 30 min; SelleckChem) or respective vehicle controls at 37 °C and 5% CO_2 and/or stimulated with ATP (3 mM; Sigma-Aldrich), nigericin (10 µM; InvivoGen) or a combination of LPS and nigericin (1 µg ml^{-1} and 10 µM, respectively; both InvivoGen). For human in vitro release assays, 5×10^5 neutrophils were stimulated with recombinant human E-selectin, recombinant human endoglycan, recombinant human MAdCAM (all 1 µg ml^{-1}; R&D Systems) or PBS. Finally, cellular supernatants and serum probes were analyzed by ELISA to determine the concentrations of S100A8/S100A9, as previously described[51].

Quantification of intracellular S100A8/S100A9 levels

Isolated bone marrow neutrophils (1×10^6 cells per 100 µl) were lysed with modified RIPA lysing buffer (150 mM NaCl, 1% Triton X-100 (Applichem), 0.5% sodium deoxycholate (Sigma-Aldrich), 50 mM Tris-HCl (pH 7.3; Merck Millipore) and 2 mM EDTA (Merck Millipore) supplemented with protease/phosphatase inhibitors (Cell Signaling) and 1× Laemmli sample buffer), homogenized and boiled (95 °C, 5 min). Proteins were resolved by SDS–PAGE and electrophoretically transferred to PVDF membranes. After blocking in LI-COR blocking solution, membranes were incubated overnight with primary antibodies. The following primary antibodies were used for detection: polyclonal rabbit anti-mouse S100A8 and polyclonal rabbit anti-mouse S100A9 (1 µg ml^{-1} and 5 µg ml^{-1}, respectively; provided by T. Vogl, University of Münster, Germany) and mouse anti-GAPDH (0.15 µg ml^{-1}; Calbiochem). Goat anti-rabbit IRDye 800CW and goat anti-mouse IRDye 680RD (0.1 µg ml^{-1}; both LI-COR Bioscience) secondary antibodies were used to detect the respective proteins on an Odyssey CLx (LI-COR Bioscience). Blots were analyzed with Image Studio software, and intensities of S100A8/S100A9 were normalized to that of the loading control (GAPDH).

Mouse and human neutrophil rolling velocities

Ibidi flow chambers (µ Slide VI$^{0.1}$) were coated with recombinant mouse E-selectin/recombinant human E-selectin (20 µg ml^{-1} and 5 µg ml^{-1}, respectively; both R&D Systems) and recombinant mouse ICAM-1/recombinant human ICAM-1 (15 µg ml^{-1} and 4 µg ml^{-1}, respectively; both R&D Systems) for 3 h at room temperature and blocked with 5% casein overnight at 4 °C. Isolated mouse bone marrow neutrophils (5×10^5 cells per ml) or isolated human neutrophils (5×10^5 cells per ml) were diluted in prewarmed HBSS (37 °C) and perfused through the flow chamber with a high precision pump (Harvard Apparatus) at a shear stress level of 2 dyn cm^{-2}. For NLRP3 inflammasome inhibition, cells were preincubated for 30 min with MCC950 (1 µM) or vehicle control at 37 °C and 5% CO_2 before the experiment. Flow assays were conducted as previously described[12].

Caspase 1 and GSDMD cleavage

Isolated human neutrophils (1×10^7) were stimulated for 10 min with soluble recombinant human E-selectin (1 µg ml^{-1}) or PBS as a control. To inhibit TRL4 receptor signaling, cells were treated with both the TLR4 inhibitor TAC242 (1 µg ml^{-1}; Merck Millipore) and paquinimod (10 µg ml^{-1}; Active Biotech) or vehicle control 5 min before stimulation. For NLRP3 inflammasome inhibition, cells were preincubated with MCC950 (1 µM) or vehicle control for 30 min at 37 °C and 5% CO_2. To analyze the contribution of K^+ efflux or of $K_V1.3$ on rapid caspase 1 and GSDMD cleavage, neutrophils were stimulated in high K^+-containing PBS (137 mM KCl) or were pretreated with PAP-1 (50 nM) for 10 min at 37 °C and 5% CO_2, respectively. Stimulation was stopped by the addition of ice-cold HBSS, and supernatants and cell pellets were collected. Cell pellets were homogenized in lysis buffer, and protein extraction of supernatants was performed with chloroform–methanol or trichloracetate (Sigma-Aldrich) precipitation. Samples were resolved by SDS–PAGE gels and electrophoretically transferred onto PVDF membranes. The following primary and secondary antibodies were used: polyclonal rabbit anti-human caspase 1 (1:1,000; Cell Signaling), polyclonal rabbit anti-human GSDMD (1:2,000; Cell Signaling) and mouse anti-human GAPDH (0.15 µg ml^{-1}). Goat anti-mouse IRDye 680RD- and goat anti-rabbit IRDye 800CW-coupled secondary antibodies (0.1 µg ml^{-1}) were used for detection. Intensities of processed forms of GSDMD or caspase 1 were normalized to the expression of the loading control (GAPDH).

Confocal and STED microscopy of fixed neutrophils

To test E-selectin-dependent caspase 1 activation, we used the FAM-FLICA dye (ImmunoChemistry Technologies). Briefly, 3×10^5 isolated human neutrophils were loaded with FLICA in HBSS buffer for 30 min at 37 °C and 5% CO_2 and stimulated with soluble recombinant human E-selectin (1 µg ml^{-1}) or PBS for 10 min. To block caspase 1 activity, cells were incubated with VX-765 (10 µM; InvivoGen) for 10 min before application of FLICA dye. Stimulation was stopped by the addition of ice-cold 5 mM EDTA/HBSS. Cells were washed, transferred onto Ibidi eight-well removable slides precoated with 0.01% poly-L-lysine solution (Sigma-Aldrich) for 45 min and allowed to settle for 20 min. Cells were fixed for 15 min using the provided fixative, stained at room temperature with DyLight 649-conjugated WGA (10 µg ml^{-1}; EY Laboratories) for 10 min and DAPI (1 µg ml^{-1}; Invitrogen) for 5 min and embedded using VectaShield Antifade mounting medium (Vector Laboratories).

For studying GSDMD cleavage, ASC oligomerization or CHMP4B localization, 3×10^5 isolated neutrophils were transferred onto poly-L-lysine-coated Ibidi eight-well removable slides and allowed to settle for 20 min. For GSDMD cleavage experiments, cells were preincubated with MCC950 (1 µM) or vehicle control for 30 min at 37 °C and 5% CO_2. E-selectin (mouse or human, 1 µg ml^{-1}) or PBS (control) was added for 10 min before cells were fixed with 2% paraformaldehyde for 15 min, followed by permeabilization with 0.1% Triton X-100/2% BSA for 1 h. Slides were then incubated with monoclonal rabbit anti-human cleaved GSDMD-NT (2 µg ml^{-1}; Abcam), polyclonal rabbit anti-mouse ASC (5 µg ml^{-1}; Adipogen) or polyclonal rabbit anti-human CHMP4B (5 µg ml^{-1}; Abcam) in antibody diluent solution (Dako) at 4 °C overnight, washed and incubated with donkey anti-rabbit Alexa 488 (5 µg ml^{-1}; Thermo Fisher Scientific) or goat anti-rabbit abberior STAR 635P (2 µg ml^{-1}; Abberior), respectively, for 1 h at room temperature. Cell nuclei were stained with DAPI (1 µg ml^{-1}), and slides were embedded with VectaShield Antifade mounting medium. All images were acquired on a Leica SP8X WLL microscope (equipped with HC PL APO ×93/1.3-NA glycerol immersion, HC PL APO ×63/1.20-NA water immersion and HC PL APO ×40/1.30-NA oil immersion objectives), and semiautomated single-cell analysis was performed using ImageJ software[52]. For analysis of caspase 1 activity, WGA signal was used to define single-cell masks, and overall mean FLICA signal was analyzed in each cell. Average FLICA and ASC speck areas per cell were determined after automatic thresholding (RenyiEntropy) in the FLICA/ASC channels, respectively. GSDMD and CHMP4B intensities/puncta were analyzed on a single-cell basis using ImageJ. All representative micrographs were processed (including background subtraction and noise reduction) using ImageJ.

To analyze GSDMD-NT localization via STED microscopy, human neutrophils were stimulated with PBS (control) or E-selectin and fixed on poly-L-lysine-coated Ibidi slides, followed by incubation with CF594-labeled WGA (2 µg ml^{-1}; Biotium) in antibody diluent solution for 10 min at room temperature. Cells were permeabilized with 0.1% Triton X-100/2% BSA for 1 h and incubated with anti-GSDMD-NT (2 µg ml^{-1}) in antibody diluent solution at 4 °C overnight and secondary goat anti-rabbit abberior STAR 635P (2 µg ml^{-1}) for 1 h at room temperature. Samples were embedded in VectaShield Antifade mounting medium. *Z*-stack images of 0.33-µm step size were acquired on a Leica SP8X WLL super-resolution microscope (STED module) equipped with an HC PL APO CS2 ×100/1.4-NA oil immersion STED white objective and STED 592 and STED 775 depletion lasers. Tau (τ)-STED images were obtained with LASX software adopting FLIM to improve STED resolution. Single-cell analysis was performed using ImageJ software[52]. MFI values for GSDMD-NT signal were analyzed per *z* plane in the plasma membrane compartment and in the cytosol and averaged. A plasma membrane translocation index was calculated for each cell ($MFI_{GSDMD\text{-}NT}$ (plasma membrane)/$MFI_{GSDMD\text{-}NT}$ (cytosol)) and statistically analyzed. All representative micrographs were processed (including background subtraction and noise reduction, filtering and contrast enhancing) using ImageJ.

IL-1β release

Glass cover slips were coated and handled as described for the S100A8/S100A9 release assay. IL-1β concentrations in supernatants were analyzed by ELISA according to the manufacturer's protocol (Quantkine, R&D Systems).

Sample preparation for mass spectrometry

Neutrophils (1×10^6 ml^{-1}) were stimulated with PBS or E-selectin in HBSS buffer (BSA free), and supernatants were collected. Proteins in the supernatant were precipitated at −20 °C overnight with acetone (1:4 (sample:acetone)) and washed twice with ice-cold 80% acetone. Precipitated proteins were dissolved in 8 M urea in 50 mM Tris (pH 8), and disulfide bridges were reduced and alkylated with 10 mM Bond-Breaker TCEP solution and 30 mM chloroacetamide. Digestion was performed overnight at a concentration of 2 M urea with LysC/trypsin mixture (1:50 (enzyme:protein)). Protein digestion was stopped with 1% formic acid, and peptides were desalted on in-house-produced SDB-RPS StageTips.

Liquid chromatography–tandem mass spectrometry measurements

Samples were measured by liquid chromatography–tandem mass spectrometry. For each sample, 300 ng of tryptic peptides was loaded on an in-house-packed C18 analytical column. Peptides were separated on a nanoflow ultrahigh performance liquid chromatography system (EASY-nLC 1200, Thermo Scientific) using a 120-min non-linear gradient. Eluting peptides were transferred on-line to the quadrupole orbitrap tandem mass spectrometer (Orbitrap Exploris 480, Thermo Scientific) by a nanoelectrospray ionization source (Thermo Scientific). The mass spectrometer was operated in data-independent acquisition mode. Full spectra were recorded with a scan range of 300–1,650 *m*/*z* and a resolution of 120,000. The automatic gain control target was set to 3×10^6 ions and a maximum injection time of 60 ms. MS2 data-independent acquisition scans were acquired at a resolution of 30,000, an automatic gain control target of 1×10^6 and a maximum injection time of 54 ms. Data-independent acquisition isolation windows were of variable sizes ranging from 16 to 524 *m*/*z* and were fragmented with a higher-energy collisional dissociation energy of 27%.

Quantification and statistical analysis of mass spectrometry data

Peptide identification and protein quantification were performed in library-free mode using DIA-NN 1.8.1 (ref. 53). Data-independent acquisition tandem mass spectrometry spectra were searched against the UniProt SWISSPROT human proteome (version from 15 February 2023) and filtered on peptide level at a false discovery rate of 1%. Trypsin was set as the digestion enzyme with peptide lengths set from 7 to 30 amino acids, a fixed modification of cysteines (carbamidomethylation) and a maximum of one missed cleavage. The match-between-runs option was enabled. Using the DIA-NN main output table, identified precursors were filtered for Lib.QValue and Lib.PG.Value of <1%. Label-free quantification was performed with the R plugin diann using the maxLFQ algorithm[54] for proteotypic peptides only.

Statistical analyses were performed with the Perseus computational platform (version 1.6.15)[55], and protein LFQ intensities were $\log_2$ transformed and filtered for at least three valid values in at least one condition. Random values were used to impute missing data drawn from normal distributions with a 1.8 standard deviation downshift and 0.3 standard deviation spread for each sample. Significantly released proteins were identified by Welch's two-sample *t*-tests (significance: false discovery rate > 0.05, fudge factor S0 = 0.1). Secretory signatures were functionally characterized by one-dimensional annotation enrichment analysis (Benjamin–Hochberg false discovery rate = 0.02).

The following annotations were manually added: alarmins, cytosolic small alarmins, cytosolic big alarmins, granules, azurophilic granules, specific granules and gelatinase granules. The mass spectrometry proteomics data have been deposited to the ProteomeXchange Consortium via the PRIDE[56] partner repository with the dataset identifier PXD041652.

Detection of granule release via flow cytometry

Isolated human neutrophils (1×10^6) were stimulated with PBS (control), E-selectin or phorbol myristate acetate (positive control; 100 nM; Sigma-Aldrich) in HBSS for 10 min at 37 °C under shaking conditions. The reaction was stopped by the addition of FACS Lysing solution (BD Bioscience), and cells were stained with antibodies to CD15, CD63, CD66 and CD11b and their corresponding isotype controls (all Biolegend; 5 μg ml^{-1}). Translocation of granule components was assessed using a CytoFlex S flow cytometer (Beckmann Coulter) and FlowJo software.

ASC oligomerization

Isolated bone marrow neutrophils were stimulated with recombinant mouse E-selectin (1 μg ml^{-1}) in BSA-free HBSS for 10 min at 37 °C under shaking conditions and subsequently centrifuged for 5 min at 300*g* and 4 °C. Cells were processed as described elsewhere[57]. The following primary and secondary antibodies were used: polyclonal rabbit anti-mouse ASC (1 μg ml^{-1}; Adipogen), mouse anti-mouse GAPDH (0.15 μg ml^{-1}), goat anti-rabbit IRDye 800CW and goat anti-mouse IRDye 680RD (0.1 μg ml^{-1}). Intensities of ASC oligomers were normalized to those of GAPDH in non-cross-linked loading controls.

Patch-clamp recordings of human neutrophils

Membrane potential (V_m) recordings of isolated human neutrophils were performed in current clamp mode at room temperature using the whole-cell variation of the patch-clamp technique and a HEKA EPC10 USB patch-clamp amplifier (HEKA Elektronik) in combination with Patchmaster software. Origin Pro 2019G software was used for data analysis. Pipettes with a resistance of 4–6 MΩ were fabricated with a DMZ Universal Microelectrode Puller (Zeitz-Instrumente Vertriebs) and filled with intracellular solution (consisting of 140 mM KF, 10 mM NaCl, 2.0 mM $MgCl_2$, 1.0 mM $CaCl_2$, 10 mM HEPES and 10 mM EGT, pH 7.2 KOH). After isolation, cells were transferred into extracellular solution (containing 140 mM NaCl, 2.8 mM KCl, 2.0 mM $MgCl_2$, 1.0 mM $CaCl_2$, 10 mM HEPES and 11 mM glucose, pH 7.4 NaOH). Once the whole-cell configuration was established, baseline membrane potential was recorded for 1–2 min. Cells were then superfused with extracellular solution containing recombinant human E-selectin (1 μg ml^{-1}) in the presence or absence of PAP-1 (50 nM) or disulfiram (30 μM) for 1 min, and the membrane potential was recorded for an additional 3.5 min. The starting membrane potential was calculated as the 30-s mean V_m value immediately before superfusion of E-selectin. Changes in membrane potential after E-selectin stimulation were calculated as ΔV_m between the 30-s mean values at different time intervals as indicated and the starting membrane potential (−30 to 0 s). V_m values were corrected for liquid junction potential.

NLRP3 pY-IP

Tyrosine phosphorylation of NLRP3 was assessed by pY-IP and subsequent western blotting, as previously described[18]. Isolated bone marrow neutrophils (20×10^6 cells) were preincubated with ibrutinib (0.6 μM) or DMSO for 30 min at 37 °C and 5% CO_2 and subsequently stimulated with E-selectin (1 μg ml^{-1}) or PBS (control) for 7 min. Cells were washed with PBS and lysed in 1 ml of mammalian protein extraction reagent buffer (Thermo Fisher Scientific) supplemented with phosphatase inhibitors (phosphatase inhibitor cocktails 2 + 3; Sigma-Aldrich) and complete Mini EDTA-free protease inhibitors (Roche). IP of tyrosine-phosphorylated proteins was performed by incubating the lysates with 20 μl of pY-MultiMab rabbit mAb mix conjugated to magnetic beads (P-Tyr-1000, Cell Signaling) for 2 h at 4 °C with gentle mixing. After washing, bound protein was retained by incubation in 2× Laemmli buffer (Roti-Load 1, reducing, 4× stock, Carl Roth) at 95 °C for 5 min. IP and input control samples were subjected to SDS–PAGE and western blotting. Western blots were probed with the following antibodies diluted in 5% milk/ TBS plus 0.1% Tween20: mouse anti-NLRP3/NALP3 (1:1,000; Adipogen), mouse anti-GAPDH (0.15 μg ml^{-1}) and goat anti-mouse-HRP (1:15,000; Jackson ImmunoResearch). NLRP3 signal was quantified by densitometry using ImageJ. pY-NLRP3 signals as measured in IP samples were normalized to relative expression levels quantified from input controls.

Live imaging of neutrophils

Isolated neutrophils were stained with Cell Tracker Green CMFDA (Invitrogen) according to the manufacturer's protocol. For NLRP3 inflammasome inhibition, cells were preincubated with MCC950 (1 μM) for 30 min at 37 °C and 5% CO_2. Neutrophils (1×10^6) in 300 μl of HBSS were transferred onto poly-L-lysine-coated Ibidi eight-well glass-bottom slides and allowed to settle for 20 min before soluble recombinant mouse E-selectin/recombinant human E-selectin (both 1 μg ml^{-1}) was added to the samples. PI (0.33 μg ml^{-1}; Invitrogen) was used to track pore formation and was applied to the samples concomitantly with E-selectin or with a time delay, as indicated. Samples were imaged for 20 min with 20-s frame intervals by confocal microscopy with a Leica SP8X WLL microscope equipped with an HC PL APO ×40/1.30-NA oil immersion objective. Images were analyzed using ImageJ. PI intensity was quantified by subtracting the PI intensity at time zero (F_0) from the PI intensity at the depicted time point (F_t) and dividing by the PI intensity at time zero: $PI = (F_t - F_0)/F_0$.

LDH release assay

Isolated human neutrophils (5×10^5) were stimulated with PBS or soluble recombinant human E-selectin (1 μg ml^{-1}) in 500 μl of HBSS for 10, 30 or 180 min. In additional experiments, 5×10^5 human neutrophils or monocytes were stimulated with PBS or LPS/nigericin (1 μg ml^{-1} and 10 μM, respectively) for 30 min. Furthermore, 5×10^5 human neutrophils or monocytes were primed with LPS for 2.5 h and stimulated with nigericin for 30 min (180-min stimulation). LDH levels in the supernatants were quantified using a CyQuant LDH Cytotoxicity Assay (Thermo Fisher Scientific), according to the manufacturer's protocol, and measured using a Tecan SPARK 10M microplate reader.

Mouse model of acute inflammation in the cremaster muscle

Intravital microscopy of the mouse cremaster muscle was performed as previously described[3]. Rolling flux fraction (number of rolling cells normalized to complete leukocyte flux[29]), leukocyte rolling velocities, number of adherent cells per mm^2, vessel diameter and vessel length were determined on the basis of the generated movies using ImageJ software.

To assess neutrophil extravasation, cremaster muscles were dissected 2 h after intrascrotal TNF application and stained for perivascular neutrophils as previously described[12].

Surface expression of adhesion-relevant molecules in mouse neutrophils

Neutrophils were stained with antibodies to CD11a (eBioscience), CD11b (BioLegend), CD18 (Pharmingen) and CXCR2 (R&D Systems) or their corresponding isotype controls (all 5 μg ml^{-1}). Samples were fixed with FACS Lysing solution and analyzed using a Beckman Coulter Gallios flow cytometer with Kaluza Flow analysis software (Beckman Coulter). Neutrophils were defined as Ly6G$^+$ cells (5 μg ml^{-1}; Biolegend).

Statistics

Data are presented as mean ± s.e.m., cumulative frequency or representative images, as detailed in the figure legends. Group sizes were

chosen based on previous experiments. GraphPad Prism 7 software (GraphPad Software) and Adobe Illustrator were used to analyze data and illustrate graphs. Statistical tests were performed according to the number of groups being compared. Data collection and analysis were not performed blind to the conditions of the experiments. No data were excluded from statistical analyses. For pairwise comparisons, an unpaired or paired Student's *t*-test was performed, and for more than two experimental groups, either a one-way or two-way ANOVA with a Tukey's, Dunnetts's or Sidak's post hoc test was performed. Data distribution was assumed to be normal, but this was not formally tested. *P* values of <0.05 were considered statistically significant. No statistical methods were used to predetermine sample sizes, but our sample sizes are similar to those reported in previous publications[3,12].

Reporting summary

Further information on research design is available in the Nature Portfolio Reporting Summary linked to this article.

Data availability

Data-independent acquisition tandem mass spectrometry spectra were searched against the UniProt SWISSPROT human proteome (version from 15 February 2023). Mass spectrometry proteomics data have been deposited in the ProteomeXchange Consortium via the PRIDE partner repository with the dataset identifier PXD041652. Source data are provided with this paper. All other data that support the findings of this study are present in the article and Supplementary Information or from the corresponding author upon reasonable request.

References

47. Shi, J. et al. Cleavage of GSDMD by inflammatory caspases determines pyroptotic cell death. *Nature* **526**, 660–665 (2015).
48. Kuida, K. et al. Altered cytokine export and apoptosis in mice deficient in interleukin-1 β converting enzyme. *Science* **267**, 2000–2003 (1995).
49. Labow, M. A. et al. Characterization of E-selectin-deficient mice: demonstration of overlapping function of the endothelial selectins. *Immunity* **1**, 709–720 (1994).
50. Koni, P. A. et al. Compensatory anion currents in $K_v1.3$ channel-deficient thymocytes. *J. Biol. Chem.* **278**, 39443–39451 (2003).
51. Vogl, T. et al. Alarmin S100A8/S100A9 as a biomarker for molecular imaging of local inflammatory activity. *Nat. Commun.* **5**, 4593 (2014).
52. Schindelin, J. et al. Fiji: an open-source platform for biological-image analysis. *Nat. Methods* **9**, 676–682 (2012).
53. Demichev, V., Messner, C. B., Vernardis, S. I., Lilley, K. S. & Ralser, M. DIA-NN: neural networks and interference correction enable deep proteome coverage in high throughput. *Nat. Methods* **17**, 41–44 (2020).
54. Cox, J. et al. Accurate proteome-wide label-free quantification by delayed normalization and maximal peptide ratio extraction, termed MaxLFQ. *Mol. Cell. Proteomics* **13**, 2513–2526 (2014).
55. Tyanova, S. et al. The Perseus computational platform for comprehensive analysis of (prote)omics data. *Nat. Methods* **13**, 731–740 (2016).
56. Perez-Riverol, Y. et al. The PRIDE database resources in 2022: a hub for mass spectrometry-based proteomics evidences. *Nucleic Acids Res.* **50**, D543–D552 (2022).
57. Hoss, F., Rolfes, V., Davanso, M. R., Braga, T. T. & Franklin, B. S. Detection of ASC speck formation by flow cytometry and chemical cross-linking. *Methods Mol. Biol.* **1714**, 149–165 (2018).

Acknowledgements

This work was supported by the German Research Foundation collaborative research grants CRC914 (projects A01 (M.M.), B01 (M.S.) and B11N (M.P.)), TRR332 (# 449437943; projects B5 (Johannes Roth), C2 (M.S.) and C7 (T.V.)), TRR359 (#491676693; project B02 (M.S. and R.I.)), CRC1450 (projects C01 (Johannes Roth) and C03 (T.S.)) and CRU342 (projects P3 (Johannes Roth) and P5 (T.S.)). We thank D. Jenne (Comprehensive Pneumology Center, Institute of Lung Biology and Disease, German Center for Lung Research) and S. Zierler (Institute of Pharmacology, Johannes Keppler University) for fruitful discussions, T. Leandersson (Immunology Group, University of Lund) for providing paquinimod and C. Scheiermann (Geneva Centre for Inflammation Research) for providing animals. In addition, we thank D. Gössel, A. Lübeck and S. D'Avis for excellent technical assistance. We are indebted to the core facilities Bioimaging and Flow Cytometry and Animal Models at the Biomedical Center (Ludwig-Maximilians-University Munich) and U. Schillinger (Gene Center and Department of Biochemistry, Ludwig-Maximilians-University Munich) for their support.

Author contributions

M.P. and R.I. designed and performed experiments, analyzed data and wrote the manuscript. Jonas Roth, T.K., T.B., M.N., K.N., I.R., L.M.W., C.P., K.H., D.F., S.K., T.S., S.M.-A., A.B., W.L., M.M., T.V. and F.M. performed experiments and analyzed data. D.V., C.W.-S., Johannes Roth, V.H. and P.B. provided their expertise and critical reagents. M.S. designed experiments and wrote the manuscript.

Competing interests

V.H. serves on the Scientific Advisory Board of Inflazome, Ltd. All other authors have no competing interests.

Additional information

Extended data is available for this paper at https://doi.org/10.1038/s41590-023-01656-1.

Supplementary information The online version contains supplementary material available at https://doi.org/10.1038/s41590-023-01656-1.

Correspondence and requests for materials should be addressed to Markus Sperandio.

Peer review information *Nature Immunology* thanks Seth Masters, Kate Schroder and the other, anonymous, reviewer(s) for their contribution to the peer review of this work. Primary Handling Editor: N. Bernard, in collaboration with the *Nature Immunology* team.

https://doi.org/10.1038/s41590-023-01656-1

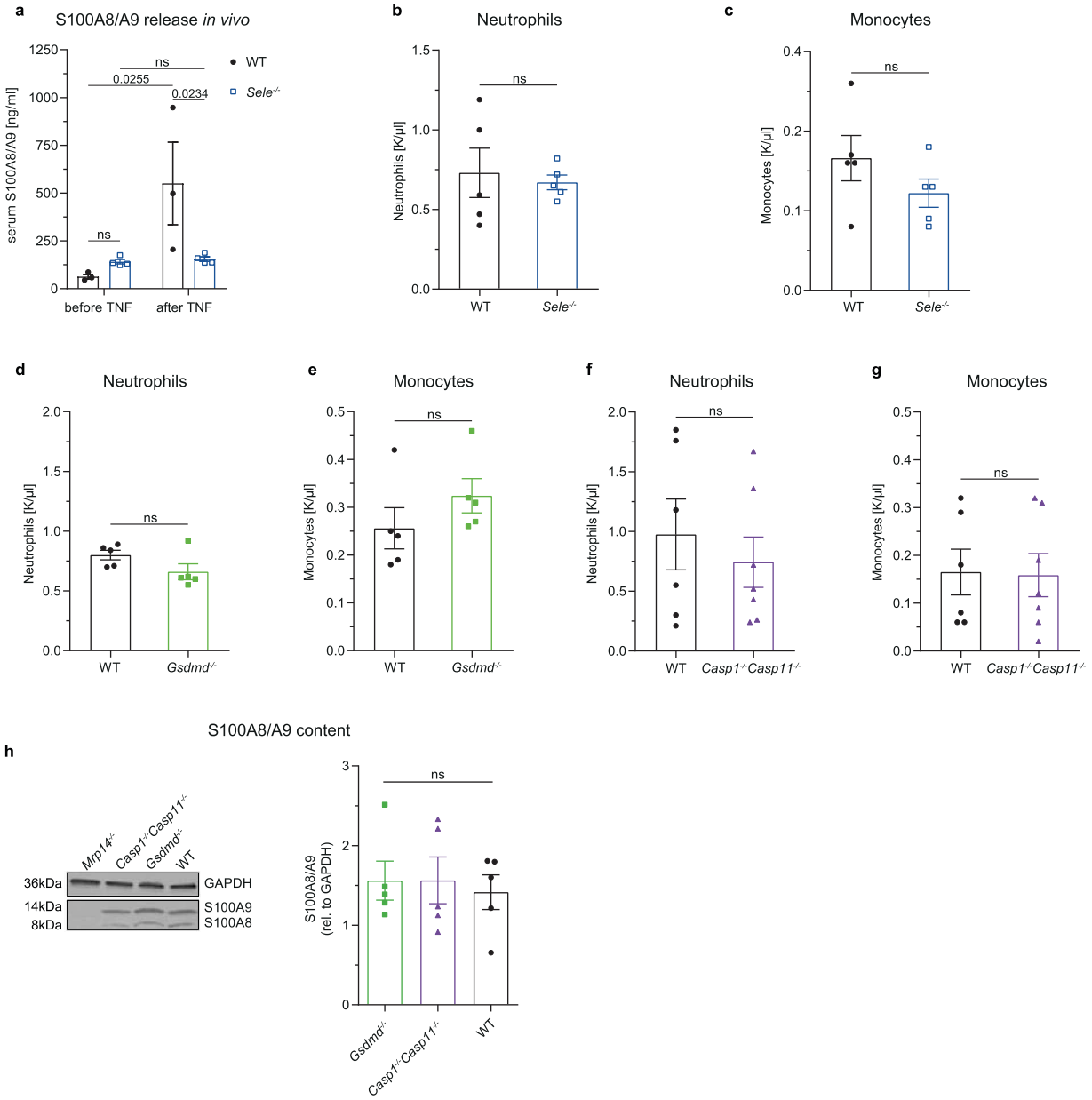

Extended Data Fig. 1 | S100A8/A9 release depends on E-selectin, GSDMD and inflammatory caspases. a Serum S100A8/A9 levels were determined by ELISA before and 2 h after intrascrotal TNF application to WT and *Sele*$^{-/-}$ mice (n = 3 (WT), 4 (*Sele*$^{-/-}$) mice/group). **b-g** Neutrophil and monocyte counts were analyzed in peripheral blood samples from untreated WT, *Sele*$^{-/-}$, *Gsdmd*$^{-/-}$ and *Casp1*$^{-/-}$*Casp11*$^{-/-}$ mice (n = 5 (WT **b**, **c**, **d**, **e**, *Sele*$^{-/-}$, *Gsdmd*$^{-/-}$), 6 (WT **f**,**g**, *Casp1*$^{-/-}$*Casp11*$^{-/-}$) mice/group). **h** Overall intracellular S100A8/A9 content in bone marrow neutrophils from WT, *Gsdmd*$^{-/-}$ and *Casp1*$^{-/-}$*Casp11*$^{-/-}$ mice was assessed and quantified by western blotting. *Mrp14*$^{-/-}$ neutrophils, which exhibit a loss of both S100A8 and A9, were used as negative control (representative western blot, n = 5 mice/group). Data are presented as mean ± s.e.m. (two-tailed unpaired student's t-test **for b-g**; one-way ANOVA, Tukey's comparison for **h** and two-way RM ANOVA, Sidak's multiple comparison for **a**) and representative Western blot for **h**; ns: not significant.

https://doi.org/10.1038/s41590-023-01656-1

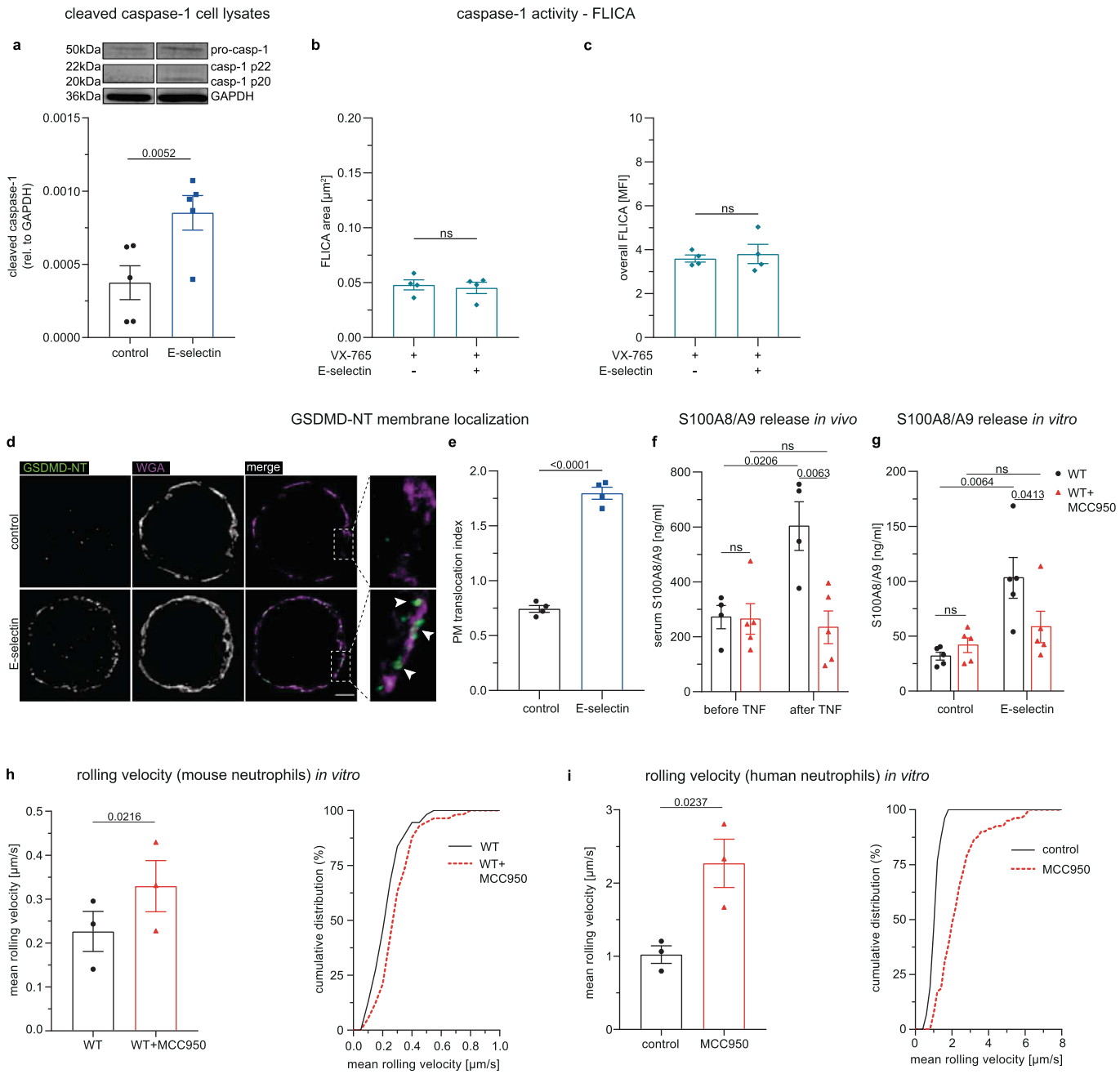

Extended Data Fig. 2 | S100A8/A9 release is dependent on NLRP3 inflammasome. a Amount of processed caspase-1 (casp-1 p20/casp-1 p22) in lysates of human neutrophils was determined and normalized to GAPDH (n = 5 independent experiments). **b**-**c** Caspase-1 activity was determined in FLICA dye-loaded, human neutrophils pretreated with VX-765 (10 µM) upon stimulation with E-selectin or PBS (control) for 10 min. Cells were analyzed by confocal microscopy. Quantification of **b** mean FLICA positive area and **c** overall mean fluorescence intensities (MFI) of FLICA signal/cell (47 (control) and 57 (E-selectin) cells of n = 4 independent experiments). **d** Representative super-resolution micrographs (maximum projection of 10 planes around cell centers; arrows: GSDMD-NT (green) at the plasma membrane (magenta)) and **e** Plasma membrane (PM) translocation index (PM vs cytosol GSDMD-NT MFI ratio) of human neutrophils treated with PBS and E-selectin (19 (control) and 19 (E-selectin) cells of n = 4 independent experiments). **f** WT mice were i.p. injected with NLRP3-inhibitor MCC950 or vehicle control 1 h prior to intrascrotal TNF application. Serum S100A8/A9 levels were analyzed by ELISA before and 2 h after TNF stimulation (n = 4 (WT), 5 (WT + MCC950) mice/group). **g** Bone marrow neutrophils from WT mice pretreated with MCC950 (1 µM, 30 min) or vehicle control were incubated with E-selectin or PBS. (n = 5 mice/group). S100A8/A9 levels were analyzed in supernatants by ELISA. Rolling velocities of **h** MCC950 (1 µM, 30 min) or vehicle control (65 control and 68 MCC950 treated cells from n = 3 mice/group) pretreated WT neutrophils were assessed in E-selectin/ICAM-1-coated flow chambers. Rolling velocities were determined in **i** MCC950 (1 µM, 30 min) or vehicle control (104 (control) and 81 (MCC950) cells from n = 3 independent experiments/group) pretreated human neutrophils. Data are presented as mean ± s.e.m., (two-tailed paired student's t-test for **a**-**c**, **e**, **h** and **i**, two-way ANOVA, Sidak's multiple comparison for **f**; two-way RM ANOVA, Sidak's multiple comparison for **g**), as representative Western blot for **a**, as representative micrographs for **d** and as cumulative distribution for **h** and **i**. ns: not significant.

https://doi.org/10.1038/s41590-023-01656-1

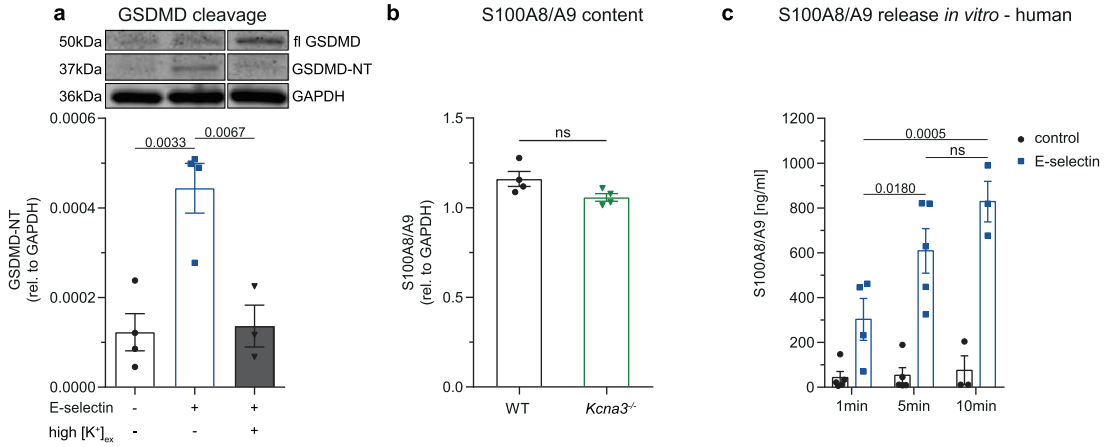

Extended Data Fig. 3 | E-selectin triggers rapid S100A8/A9 release. a Isolated neutrophils were treated for 10 min with PBS, E-selectin or E-selectin in the presence of high $[K^+]_{ex}$ and the amount of full length GSDMD, GSDMD-NT and GAPDH was determined in the cell lysates (PBS control group and E-selectin stimulated group values and representative blot are the same as in Fig. 2g; n = 4 (control, E-selectin), 3 (E-selectin/ high $[K^+]_{ex}$) independent experiments). **b** Overall intracellular S100A8/A9 content was assessed by Western blotting in bone marrow neutrophils of WT and *Kcna3*$^{-/-}$ mice (n = 4 mice/group). **c** Isolated human neutrophils were stimulated with PBS (control) or E-selectin (1 µg ml^{-1}) for 1 min, 5 min or 10 min and S100A8/A9 levels in the supernatants were assessed by ELISA (n = 3 (control 10 min, E-selectin 10 min), 4 (E-selectin 1 min), 5 (control 1 min, control 5 min, E-selectin 5 min) individual experiments. Values from the 10 min time point (control and E-selectin) are the same as in Fig. 3g. Data are presented as mean ± s.e.m. (one-way ANOVA, Tukey's comparison for **a**, two-tailed unpaired student's t-test for **b** and two-way ANOVA, Sidak's multiple comparison for **c**), as representative Western blot for **a**, ns: not significant.

https://doi.org/10.1038/s41590-023-01656-1

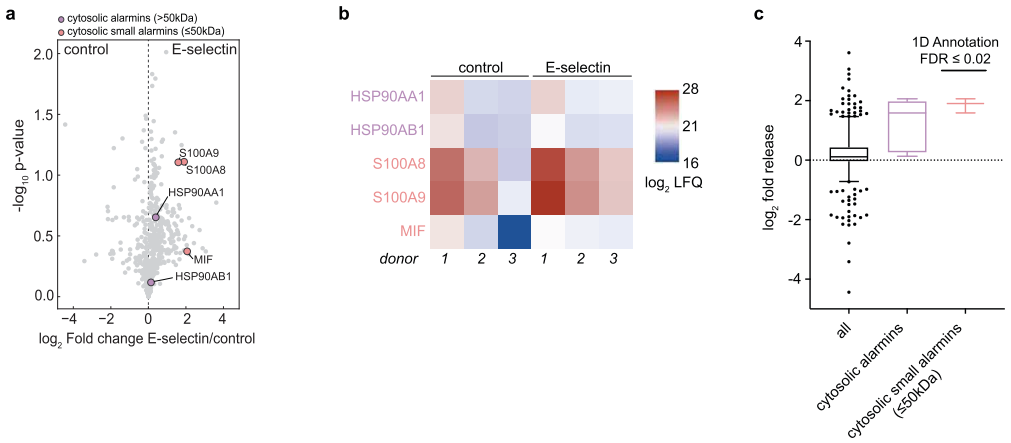

Extended Data Fig. 4 | E-selectin stimulates secretion of cytosolic small alarmins. Protein release analyzed by mass spectrometry-based proteomics of supernatants from E-selectin-activated versus PBS-treated isolated human neutrophils (n = 3 independent experiments). **a** Volcano plot showing differentially released proteins, cytosolic small alarmins (M_w≤50 kDa) and cytosolic alarmins (M_w>50 kDa) as indicated. **b** Release of indicated proteins for each donor, **c** release of all proteins, cytosolic alarmins (no size threshold) and cytosolic small alarmins (M_w≤50 kDa). Data are presented as volcano plot for **a**, as heat map for **b**, as box-whisker-plots for **c** (50% interquartile range (IQR), median center, whiskers ranging from 5-95 percentiles and dots indicating outliers). -$\log_{10}$ transformed p-values depicted in the volcano plots were determined by Welch's two-sided t-test. Enrichment of alarmins in **c** was determined by a 1D annotation enrichment with Benjamin-Hochberg FDR = 0.02, ns: not significant.

https://doi.org/10.1038/s41590-023-01656-1

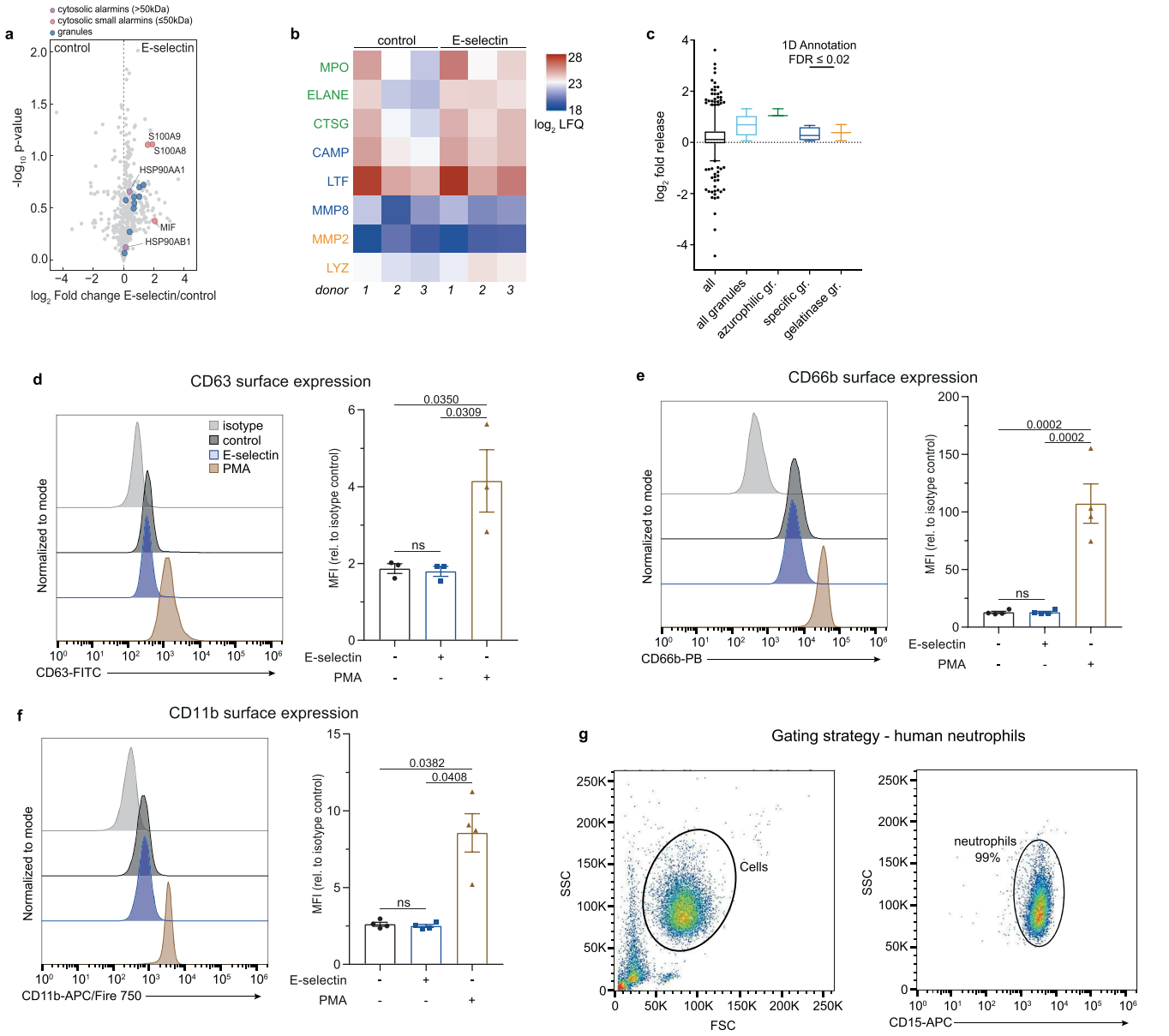

Extended Data Fig. 5 | E-selectin stimulation does not result in granule release. Enrichment of granule content (azurophilic gr., specific gr., gelatinase gr.) in supernatants of E-selectin (1 µg ml^{-1}) and PBS (control) stimulated human neutrophils was analyzed by mass spectrometry (n = 3 independent experiments). **a** Volcano plot showing differentially released proteins, cytosolic small alarmins (M_w≤50 kDa), cytosolic alarmins (M_w>50 kDa) and granules are indicated. **b** Release of indicated proteins for each donor, **c** release of all proteins, all granules, azurophilic granules, specific granules and gelatinase granules. **d**-**g** Isolated human neutrophils were stimulated with E-selectin (1 µg ml^{-1}), PMA (100 nM, positive control) or PBS (control) for 10 min. Surface expression of **d** CD63, **e** CD66b and **f** CD11b was assessed using flow cytometry (n = 4 independent experiments). **g** gating strategy. Data are presented as mean ± s.e.m. (one-way ANOVA, Tukey's comparison for **d**-**f**, as volcano plot for **a**, as heat map for **b**, as box-whisker-plots for **c** (50% IQR, median center, whiskers ranging from 5-95 percentiles and dots indicating outliers), as representative flow cytometry dot blot image for **g**, and as representative histograms for **d**-**f**. -log$_{10}$ transformed p-values depicted in the volcano plots were determined by Welch's two-sided t-test. Enrichment of granule content in **c** was determined by a 1D annotation enrichment with Benjamin-Hochberg FDR = 0.02. ns: not significant.

https://doi.org/10.1038/s41590-023-01656-1

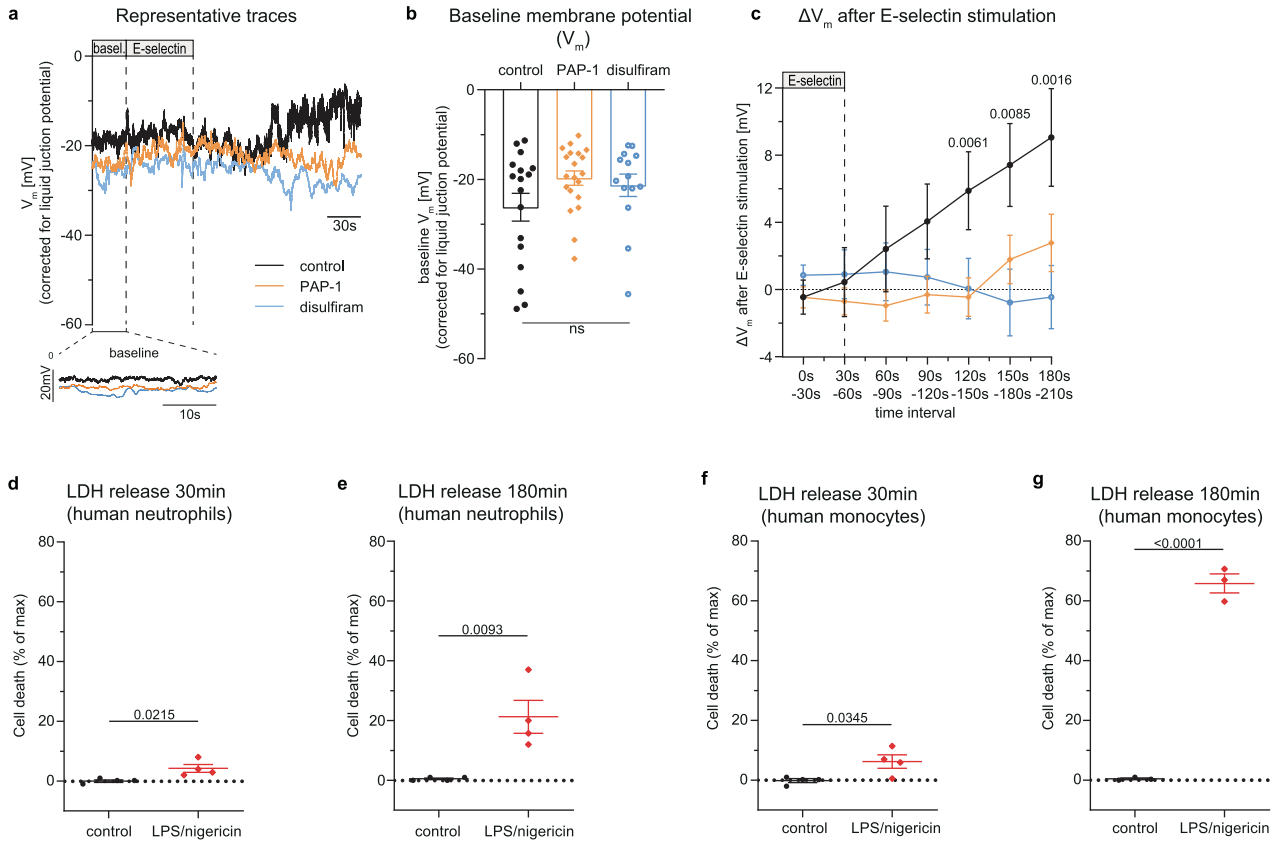

Extended Data Fig. 6 | E-selectin induces depolarization of membrane potential in neutrophils. a-c Changes in membrane potential of isolated human neutrophil pretreated with PAP-1 (50 nM), disulfiram (30 µM) or vehicle (control) before (baseline) and after E-selectin stimulation was measured by current clamp, **a** representative voltage membrane traces (n = 14 (disulfiram), 17 (control), 20 (Pap-1) cells of 7 different blood donors). **b** Mean baseline membrane potential V_m (averaged from $t_{(-30)}$-$t_{(0)}$) and **c** changes in V_m compared to baseline (ΔV_m) upon E-selectin stimulation were analyzed. **d** and **e** Cell death of human neutrophils and **f** and **g** monocytes was assessed by LDH release after stimulation with LPS/nigericin for 30 min and 180 min (n = 3 (monocytes 180 min), 4 (neutrophils 30 min, 180 min, monocytes 30 min) independent experiments). Data are presented as mean ± s.e.m. (two-tailed unpaired student's t-test for **d**-**g**, one-way ANOVA, Tukey's multiple comparison for **b** and two-way ANOVA, Tukey's multiple comparison for **c**) and as representative traces for **a**, ns: not significant.

https://doi.org/10.1038/s41590-023-01656-1

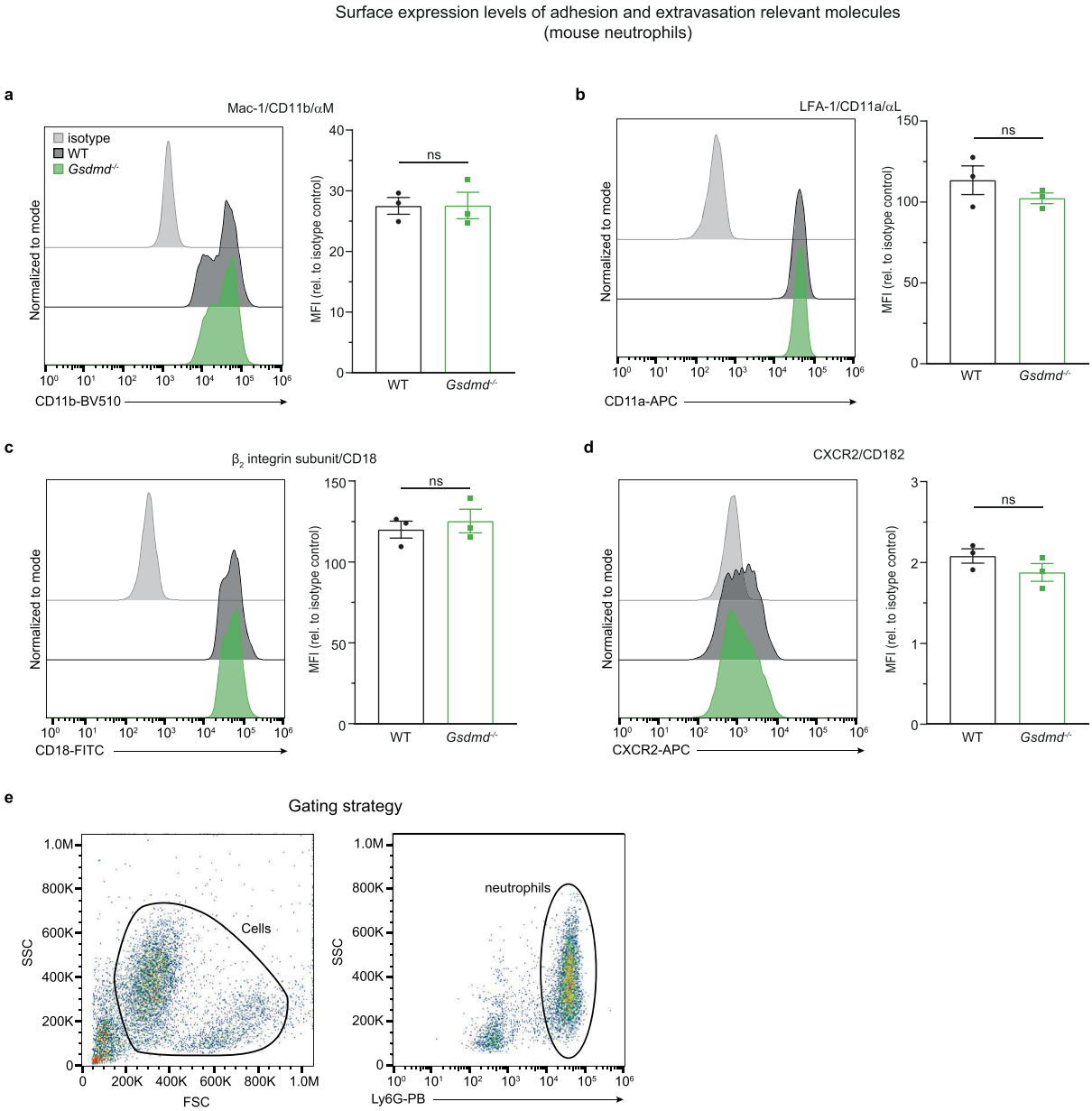

Extended Data Fig. 7 | Receptor expression of WT and *Gsdmd*$^{-/-}$ neutrophils. Surface expression levels of **a** Mac-1/CD11b/αM, **b** LFA-1/CD11a/αL, **c** β2 integrin subunit/CD18 and **d** CXCR2/CD182 were determined on bone marrow neutrophils from WT and *Gsdmd*$^{-/-}$ mice by flow cytometry (n = 3 mice/group). **e** Mouse neutrophils were defined as Ly6G positive cells using a PB conjugated rat anti-mouse Ly6G antibody. Data are presented as mean ± s.e.m. (two-tailed unpaired student's t-test) and as representative histograms for **a-d** and as representative flow cytometry dot blot image for **e**. ns: not significant.

https://doi.org/10.1038/s41590-023-01656-1

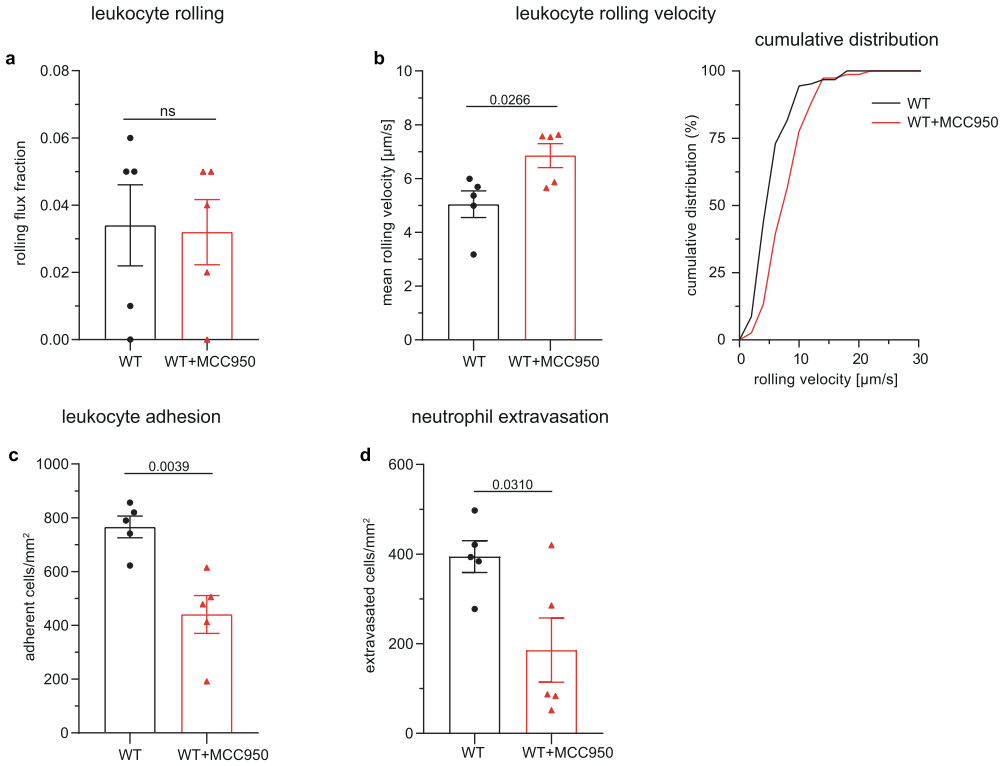

Extended Data Fig. 8 | Neutrophil recruitment *in vivo* requires NLRP3 inflammasome activity. Male WT mice were injected i.p. with MCC950 (10 mg kg^{-1}) or vehicle control 1 h before i.s. application of TNF (500 ng $mouse^{-1}$). Two hours later, intravital microscopy of postcapillary venules of the mouse cremaster muscle was performed and **a** neutrophil rolling, **b** neutrophil rolling velocity and **c** number of adherent neutrophils per vessel surface was analyzed (26 and 24 vessels, respectively, of n = 5 mice/group). **d** TNF stimulated cremaster muscles were stained with Giemsa and number of perivascular neutrophils was quantified (35 and 25 vessels, respectively, of n = 5 mice/group). Data are presented as mean ± s.e.m. (two-tailed unpaired student's t-test for **a**, **b**, **c** and **d**) and as cumulative distribution for **b**; ns: not significant.

https://doi.org/10.1038/s41590-023-01656-1

Extended Data Table 1 | Microvascular parameters of cremaster experiments

	n (mice)	n (venules)	Diameter [µm]	Centerline velocity [µm s^{-1}]	Wall shear rate [s^{-1}]	WBC [$µl^{-1}$]
WT	4	18	30±1	2000±216	1606±160	3500±726
Gsdmd$^{-/-}$	5	24	30±1	1929±269	1574±137	3796±375
			ns. (p=0.9309)	ns. (p=0.6076)	ns. (p=0.9543)	ns. (p=0.3173)
WT	5	26	31±1	1918±120	1598±132	2044±258
WT + MCC950	5	24	31±1	1738±135	1420±141	1978±216
			ns. (p=0.6320)	ns. (p=0.3214)	ns. (p=0.3594)	ns. (p=0.8494)

Vessel diameter, centerline velocity, wall shear rate and white blood cell count (WBC) of TNF-stimulated WT and *Gsdmd*$^{-/-}$ mice and TNF-stimulated WT mice pretreated with either MCC950 or vehicle control (mean±s.e.m.; data were analyzed by two-tailed unpaired Student's I-test).

Appendix A: Paper III

frontiers | Frontiers in Immunology

TYPE Original Research
PUBLISHED 23 December 2022
DOI 10.3389/fimmu.2022.1038936

OPEN ACCESS

EDITED BY
Michael Stürzl,
Universitätsklinikum Erlangen,
Germany

REVIEWED BY
Chang-Won Hong,
Kyungpook National University, South Korea
Mingjie Xia,
Nanjing Medical University, China

*CORRESPONDENCE
Markus Sperandio
markus.sperandio@lmu.de

SPECIALTY SECTION
This article was submitted to Inflammation, a section of the journal Frontiers in Immunology

RECEIVED 07 September 2022
ACCEPTED 08 December 2022
PUBLISHED 23 December 2022

CITATION
Masgrau-Alsina S, Wackerbarth LM, Lim D-s and Sperandio M (2022) MST1 controls murine neutrophil homeostasis *via* the G-CSFR/STAT3 axis. *Front. Immunol.* 13:1038936. doi: 10.3389/fimmu.2022.1038936

MST1 controls murine neutrophil homeostasis *via* the G-CSFR/STAT3 axis

Sergi Masgrau-Alsina[1], Lou Martha Wackerbarth[1], Dae-sik Lim[2] and Markus Sperandio[1*]

[1]Institute of Cardiovascular Physiology and Pathophysiology, Walter Brendel Center of Experimental Medicine, Ludwig-Maximilians University Munich, Munich, Germany, [2]Department of Biological Sciences, Korea Advanced Institute of Science and Technology (KAIST), Daejeon, Republic of Korea

The release of neutrophils from the bone marrow into the blood circulation is essential for neutrophil homeostasis and the protection of the organism from invading microorganisms. Granulocyte colony-stimulating factor (G-CSF) plays a pivotal role in this process and guides granulopoiesis as well as the release of bone marrow neutrophils into the blood stream both during homeostasis and in case of infection through activation of the G-CSF receptor/signal transduction and activation of transcription 3 (STAT3) signaling pathway. Here, we investigated the role of the mammalian sterile 20-like kinase 1 (MST1) for neutrophil homeostasis and neutrophil mobilization. We found increased plasma levels of G-CSF in *Mst1*$^{-/-}$ mice compared to wild type mice both under homeostatic conditions as well as after stimulation with the proinflammatory cytokine TNF-α. In addition, G-CSF-induced mobilization of neutrophils from the bone marrow into the blood circulation *in vivo* was markedly reduced in the absence of MST1. Interestingly, this was not accompanied by differences in the number of blood neutrophils. Addressing the underlying molecular mechanism of MST1-regulated neutrophil mobilization, we found reduced STAT3 phosphorylation and impaired upregulation of CXCR2 in *Mst1*$^{-/-}$ bone marrow neutrophils compared to wild type cells, while JAK2 phosphorylation was not altered. Taken together, we identify MST1 as a critical modulator of neutrophil homeostasis and neutrophil mobilization from the bone marrow, which adds another important aspect to the complex role of MST1 in regulating innate immunity.

KEYWORDS

MST1, neutrophils, G-CSF, STAT3, granulocytes

1 Introduction

In humans, neutrophils are the most abundant leukocyte in the blood circulation. They have a rather short life span of 10 – 12 hours (1) before they either get activated and recruited into inflamed tissue or become senescent and are cleared from the circulation by the spleen, bone marrow or lung (2). Consequently, mechanisms controlling

neutrophil homeostasis ranging from neutrophil generation in the bone marrow (granulopoiesis), its subsequent release into the bloodstream, and finally its clearance from the blood circulation need to function properly to ensure appropriate levels of circulating neutrophils to protect the organism.

In case of inflammation, the increased neutrophil demand requires emergency granulopoiesis and neutrophil mobilisation. Granulocyte-colony stimulating factor (G-CSF) has been identified as the principal cytokine regulating both processes (3). In humans, G-CSF serum levels are nearly undetectable under baseline conditions but rapidly increase during inflammation (4). Changes in G-CSF serum levels is under control of interleukin (IL) lL-23 and IL-17. Production and release of IL-23 from macrophages or dendritic cells induces neutrophil-regulatory T cells (Tn) to produce IL-17 that finally induces the release of G-CSF by endothelial cells, fibroblasts, bone marrow stroma cells and several immune cells (5, 6). Upon binding of G-CSF to the G-CSF receptor (G-CSFR), G-CSFR homodimerizes and activates a signaling transduction cascade leading to the induction of enhanced granulopoiesis and neutrophil mobilization into the blood stream. The JAK2-STAT3 axis is the principal signaling pathway activated upon G-CSFR stimulation in granulocyte-monocyte progenitors (GMPs) and downstream neutrophil precursor cells in the bone marrow (7). Hereby, STAT3 acts as a double-edged sword in granulopoiesis. On the one hand, STAT3 promotes neutrophil differentiation by inducing the expression of members of the C/EBP family of transcription factors (8). On the other hand, STAT3 has a negative role in emergency granulopoiesis through the promotion of SOCS3 expression, a STAT-induced STAT inhibitor (SSI) that suppresses G-CSF induced signaling (9). STAT3 has also a leading role in G-CSF-dependent neutrophil mobilization by controlling expression of chemokine receptors CXCR4 and CXCR2. While CXCR4 confers a strong retaining signal by binding to CXCL-12 (also known as SDF-1), CXCR2 engagement by CXCL8 in humans (and CXCL1 in mice) has the opposite effect promoting neutrophil mobilization into the blood circulation. Accordingly, activated STAT3 induces the release of neutrophil proteases that break CXCR4/CXCL12 bonds (10) and at the same time promotes the upregulation of CXCR2 expression on the neutrophil surface through Raf/MEK/ERK dependent signaling pathways (11).

Once in the blood circulation, neutrophils get recruited to sites of inflammation in a multistep process that requires the sequential action of a whole array of adhesion relevant molecules (12, 13). Recently, mammalian sterile 20-like kinase 1 (MST1, also known as serine/threonine kinase 4, STK4) has been reported to play an essential role in penetration of the vascular basement membrane, the last step along the neutrophil recruitment cascade, by controlling VLA-3, VLA-6, and neutrophil elastase-containing vesicle mobilization to the neutrophil surface (14). MST1 is widely known to be the central kinase of the mammalian Hippo pathway, first described as a major regulator of organ size during development (15) and later also found to be involved in the control of cell proliferation, apoptosis (16, 17), and differentiation (18). Through phosphorylation of substrates other than those from its canonical pathway, MST1 also emerged as important modulator of immune cell function such as leukocyte adhesion (19) or the aforementioned neutrophil vascular basement membrane penetration (14). Here, we report a novel function of MST1 in neutrophil homeostasis affecting neutrophil mobilization and release from the bone marrow to the circulation, triggered by a regulatory role of MST1 in G-CSF/G-CSFR-dependent activation of the JAK2/STAT3 signaling pathway.

2 Methods

2.1 Animal models

All experiments were performed in mice with a C57BL/6 background. The knockin strain *Lyz2*^{eEGP} (neutrophil reporter strain) and the knockout strain *Mst1*$^{-/-}$ were generously provided by Dr. Thomas Graf (Center for Genomic Regulation, Barcelona, ES) and Dr. Dae Sik Lim (KAIST, Daejeon, KR), respectively (20, 21). *Mst1*$^{-/-}$*Lyz2*^{eEGP} mice were generated by crossing the two aforementioned mouse lines. All animals were bred in the animal facility of the Biomedical Centre of Munich (BMC) and experiments were conducted under the approval of the Regierung von Oberbayern (ROB) and local authorities (project number ROB-55.2-2532.Vet_02-17-102).

2.2 Neutrophil release assay

C57BL/6 and *Mst1*$^{-/-}$ mice were anesthetised with a combined intraperitoneal injection of 125mg·kg^{-1} ketamine (Zoetis) and 12,5mg/kg^{-1} xylazin (Bayer) for blood collection and intravenous injection of NaCl 0.9% (control) or 2.5µg of recombinant murine G-CSF (ImmunoTools). Four hours after injection of NaCl 0.9% or G-CSF, mice were bled again and sacrificed. Blood was further processed and analyzed by flow cytometry.

2.3 Multi-photon imaging

Lyz2^{eEGP} and *Mst1*$^{-/-}$*Lyz2*^{eEGP} mice were first stimulated with an intravenous injection of 2.5µg of recombinant murine G-CSF to induce neutrophil mobilisation from the bone marrow into the blood circulation (22). Shortly before imaging, mice were anaesthetised with 125mg·kg^{-1} ketamine (Zoetis) and 12,5mg/kg^{-1} xylazin. The skull bone was then exposed by removing the hair and the skin over it, as well as the pericranium with the gentle help of a scalpel. A metal ring was glued on the skull bone and firmly fixed to the imaging stage in order to prevent any breathing movement. To visualize the bone marrow

microvasculature, 10µL of QTracker™ 705 (Thermo Fisher Scientific) was administrated intravenously. Imaging was carried out with the TCS SP8 MP Multiphoton Microscope (Leica) using the objective HC IRAPO L (25x, NA1.00 W, Leica) and started 2 hours after G-CSF injection. For each mouse, an area of analysis of 70x170µm was defined surrounding a vessel. Imaging was acquired in 512x512 pixels with a step size of 4µm for intervals of 15s from hour 2 to hour 4 post G-CSF injection. Analysis was performed using Imaris 8 Cell Imaging Software (Oxford Instruments).

2.4 Supplemental methods

Further experiments including bromodeoxyuridine cell proliferation assay, TNF-α induced peritonitis and serum G-CSF detection, as well as general procedures for flow cytometry and western blot can be found in Supplemental Methods.

2.5 Statistics

All statistical analyses and graphs were generated with GraphPad 9 (Prism) software. Statistical tests were performed according to the number of groups being compared. For pairwise comparison of experimental groups, an unpaired student's t-test was performed. For more than two groups, a one-way or two-way analysis of variance (ANOVA) with either Tukey's (one-way ANOVA) or Sidak's (two-way ANOVA) post-hoc test was used, respectively. P-values <0.05 were considered statistically significant.

2.6 Data availability statement

For original data, please contact markus.sperandio@lmu.de.

3 Results

3.1 *Mst1*$^{-/-}$ mice show increased numbers and proliferation of neutrophils in the bone marrow

First, we analysed absolute numbers of bone marrow cells by flow cytometry and found that bone marrow resident neutrophils were significantly increased in *Mst1*$^{-/-}$ mice compared to wild type (WT) mice (Figure 1A). Next, we assessed neutrophil numbers in the peripheral blood. Here, we could not detect any difference in the number of circulating neutrophils between WT and *Mst1*$^{-/-}$ mice (Figure 1B). After 10-12 hours in circulation, neutrophils enter senescence and migrate mostly towards the spleen to get cleared from the circulation. Comparable to the blood compartment, we found similar numbers of neutrophils in the spleen of WT and *Mst1*$^{-/-}$ mice (Figure 1C) suggesting that neutrophil clearance in the periphery is not significantly affected in *Mst1*$^{-/-}$ mice.

The lack of MST1 has been previously reported to cause higher numbers of hematopoietic stem and progenitor cells (HSPCs) in the bone marrow due to increased proliferation (17). In order to determine whether this was also the case for bone marrow-resident neutrophils, we injected mice intravenously with 2.5mg of BrdU followed by 2.5µg of G-CSF one hour later to stimulate neutrophil differentiation and release (23). Two days later, we analyzed the number of newly generated neutrophils in the bone marrow and blood using flow cytometry. We observed a higher ratio of BrdU^{+} neutrophils in *Mst1*$^{-/-}$ bone marrow (Figure 1D) suggesting that (similar to HSPCs) bone marrow-resident neutrophils were also more proliferative. This tendency could not be observed in circulating neutrophils (Figure 1E). After having shown an increase in number and proliferative capacity of neutrophils in the bone marrow, we became interested whether this observation is due to defective maturation of neutrophils from the granulocyte-macrophage progenitor (GMP) state to mature neutrophils. Therefore, we assessed the various neutrophil precursor subsets as recently described by Evrard and colleagues (24). Interestingly, neutrophil subset frequencies were similar in *Mst1*$^{-/-}$ compared to WT mice (Figure 1F) ruling out a maturation stop during neutrophil differentiation in the bone marrow. After bone marrow neutrophils get released to the circulation they experience a process of aging that affects their function (25). Recently, it was shown that an increase in Ly6G expression correlates with neutrophil aging (26). We found decreased expression of Ly6G on circulating *Mst1*$^{-/-}$ neutrophils (Figure 1G), suggesting a reduction of aged neutrophils in the blood circulation of mice lacking MST1.

3.2 *Mst1*$^{-/-}$ mice have increased levels of plasma G-CSF under normal conditions and during inflammation

Our observation of an increase in neutrophils and its precursors in the bone marrow of *Mst1*$^{-/-}$ mice did not translate into higher numbers of circulating neutrophils. One potential explanation for this might be that neutrophil mobilization and release into the blood circulation are impaired in the absence of MST1. To address this, we first assessed serum G-CSF levels in the blood circulation. G-CSF is not only the most important factor for neutrophil differentiation but also critical for the mobilization and release of neutrophils into the circulation (27). Serum G-CSF levels were investigated in unstimulated mice and in mice stimulated with intraperitoneal injection of TNF-α. We found that *Mst1*$^{-/-}$ mice had higher baseline serum levels of G-CSF compared to

10.3389/fimmu.2022.1038936

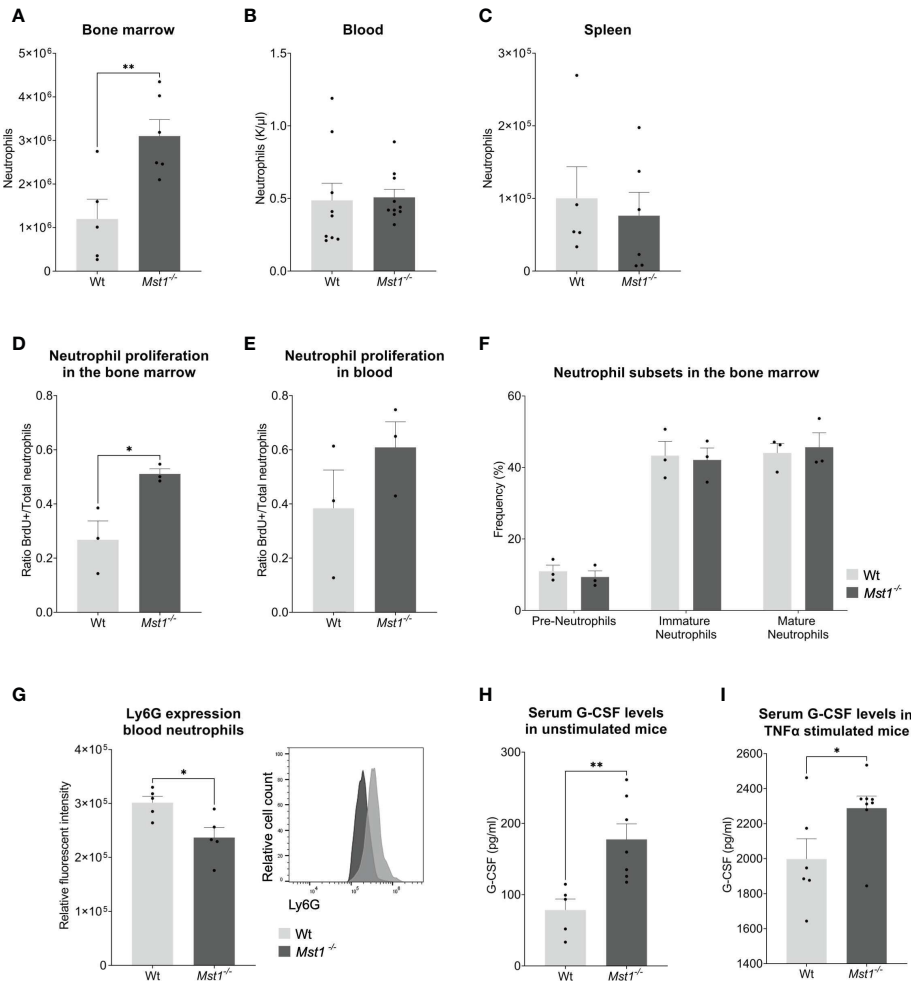

FIGURE 1
Mst1$^{-/-}$ mice show increased numbers of neutrophils in the bone marrow and higher levels of G-CSF under normal conditions and after TNF-α stimulation. **(A–C)** Neutrophil counts measured from blood with a haematology analyser **(B)** or from two femurs and whole spleen with flow cytometry **(A, C)**; **(A, C)** n=5/6, **(B)** n=9/10, **(D, E)** Ratio of BrdU^{+} neutrophils per total number of neutrophils (Ly6G^{+}) in bone marrow **(D)** and peripheral blood **(E)** 2 days after BrdU/G-CSF i.v. injection; n=3. **(F)** Frequencies of neutrophil subsets in the bone marrow obtained by flow cytometry; n=3. **(G)** Expression of Ly6G on peripheral blood neutrophils; n=5. **(H, I)** Serum G-CSF levels from unstimulated and stimulated mice measured by ELISA. **(H)** n=5/7, **(I)** n=6/8. Unpaired t-test; *p<0.05, **p<0.01.

WT mice (Figure 1H). In addition, we observed an increase in serum G-CSF levels 4 hours after intraperitoneal injection of TNF-α which was more pronounced in *Mst1*$^{-/-}$ mice compared to WT mice (Figure 1I) implying defective G-CSF signaling in neutrophils and its precursors in the absence of MST1.

3.3 G-CSF-induced mobilization of bone marrow neutrophils into the circulation is impaired in the absence of MST1

In order to confirm the defective response of *Mst1*$^{-/-}$ neutrophils to G-CSF, we injected 2.5µg of G-CSF intravenously and counted peripheral blood neutrophils 4 hours after injection (Figure 2A). While G-CSF-injection provoked a significant increase of circulating neutrophils in WT mice, we found no significant increase in *Mst1*$^{-/-}$ mice (Figures 2B, C). Using intravital multiphoton laser scanning microscopy and a murine skull bone marrow window model (Figure 2D), we next investigated the defective G-CSF-induced mobilization of neutrophils from the bone marrow into the circulation in the absence of MST1. To visualize neutrophils in *Mst1*$^{-/-}$ mice, we crossed *Lyz2*^{eGFP} mice with *Mst1*$^{-/-}$ mice (*Mst1*$^{-/-}$*Lyz2*^{eGFP} mice) and used *Lyz2*^{eGFP} as controls. While no mobilisation could be perceived in unstimulated mice (Video 1), we observed GFP^{+} cell mobilization within the bone marrow and intravasation 2 to 4 hours after G-CSF injection. During that time we assessed how many GFP^{+} cells showed a migratory behaviour within the bone

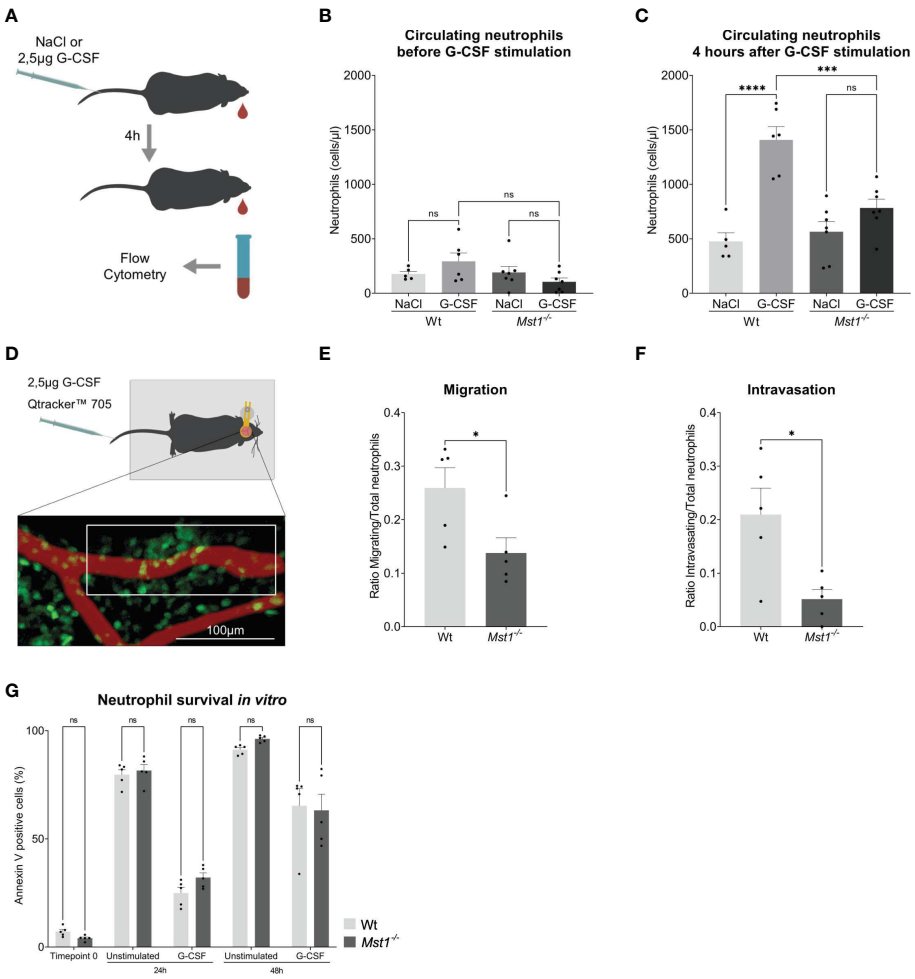

FIGURE 2
Mst1$^{-/-}$ neutrophils show an impaired response to G-CSF stimulation. **(A)** Schematic representation of the neutrophil release assay. **(B, C)** Flow cytometry analysis of blood circulating neutrophils before and after G-CSF stimulation; n=5-7. **(D)** Schematic representation of the two-photon skull imaging. The highlighted area of analysis is 70x170µm. **(E, F)** Number of cells migrating **(E)** and intravasating the vessel **(F)** relative to the total number of cells at T_0 in the area of analysis; n=5. **(G)** Flow cytometry analysis of Annexin V staining in unstimulated and G-CSF stimulated isolated neutrophils; n=5. One-way ANOVA; ns, non significant; ***p<0.001, ****p<0.0001 **(B, C)**, unpaired t-test; *p<0.05 **(E, F)** and two-way ANOVA **(G)**.

marrow and quantified the numbers of GFP$^+$ cells intravasated into the microvasculature. Interestingly, the number of migratory GFP$^+$ cells within the bone marrow was significantly decreased in *Mst1*$^{-/-}$*Lyz2*^{eEGP} mice compared to *Lyz2*^{eEGP} mice (Figure 2E, Videos 2 and 3). In addition, we found significantly reduced numbers of intravasating neutrophils in *Mst1*$^{-/-}$*Lyz2*^{eEGP} mice compared to *Lyz2*^{eEGP} mice (Figure 2F) suggesting that neutrophil trafficking from the bone marrow into the circulation is impaired in the absence of MST1.

Finally, we were testing whether regulation of granulopoiesis of bone marrow isolated Ly6G positive cells stimulated with G-CSF for 48h was different on the level of apoptosis induction between WT and *Mst1*$^{-/-}$ mice. G-CSF had been reported to prolong neutrophil survival by blocking apoptosis (28). Accordingly, we analyzed Annexin V staining of untreated and G-CSF-treated bone marrow derived neutrophils and observed the described protective role of G-CSF on neutrophil survival, but no differences were found in the rate of apoptosis between WT and *Mst1*$^{-/-}$ mice for all timepoints tested (Figure 2G). This suggests that MST1 does not regulate apoptosis in unstimulated or G-CSF-stimulated bone marrow derived neutrophils.

3.4 G-CSF-induced JAK2/STAT3 signaling axis is impaired in *Mst1*$^{-/-}$ mice

To elucidate the molecular mechanisms responsible for defective neutrophil mobilization of bone marrow neutrophils

into the circulation in the absence of MST1, we investigated G-CSFR dependent signaling events in neutrophils from *Mst1*$^{-/-}$ and WT mice. We first assessed overall G-CSFR levels in isolated bone marrow neutrophils by western blot. We found no difference in total G-CSFR expression in neutrophils that were either unstimulated or stimulated with G-CSF for 15, 30 and 60 minutes (Figure 3A). Upon binding of G-CSF to G-CSFR, G-CSFR is internalized and can be recycled in a process that highly depends on vesicular trafficking (29). Since MST1 was previously reported to regulate vesicle trafficking (14, 30), we hypothesized that the recycling route could be altered and plasma membrane levels of G-CSFR were altered after exposure to G-CSF. Therefore we investigated membrane levels of G-CSFR in neutrophils that were exposed to G-CSF for 15, 30, 60 and 120 minutes using flow cytometry. We did not find a significant difference in the levels of surface G-CSFR for

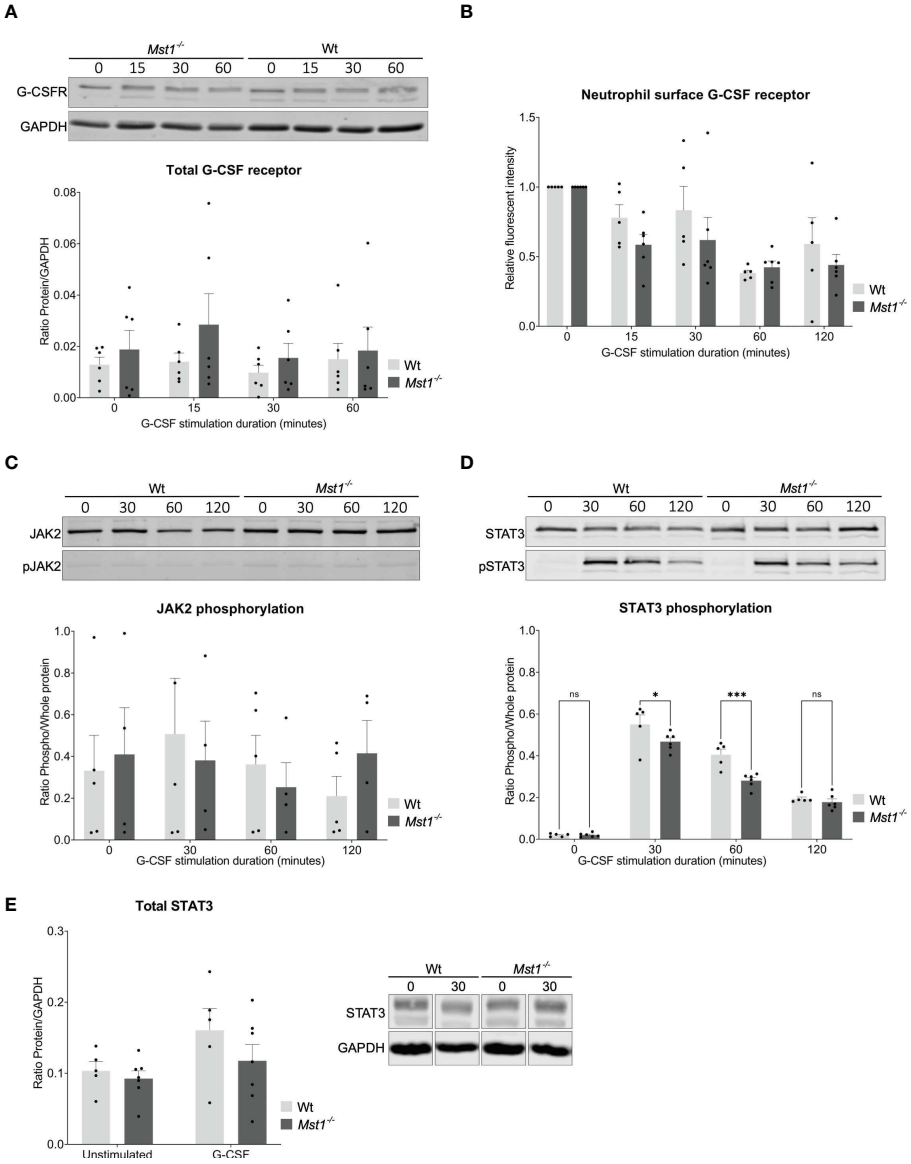

FIGURE 3
STAT3 phosphorylation reduced in *Mst1*$^{-/-}$ neutrophils after G-CSF stimulation. **(A)** Western blot analysis of total G-CSFR levels in unstimulated and G-CSF stimulated purified bone marrow neutrophils normalised to GAPDH; n=6. **(B)** Fold change of membrane levels of G-CSFR in G-CSF stimulated relative to unstimulated bone marrow neutrophils; n=5. **(C)** Neutrophil JAK2 phosphorylation normalized to total JAK2; n=5. **(D)** Neutrophil STAT3 phosphorylation normalized to total STAT3; n=5. **(E)** Total levels of STAT3 analysed by western blot in unstimulated and 30 minute G-CSF stimulated purified bone marrow neutrophils from WT and *Mst1*$^{-/-}$ mice; n=5. Two-way ANOVA; ns, non significant; *p<0.05, ***p<0.001.

any of the time points investigated (Figure 3B), excluding different G-CSFR surface expression levels between *Mst1*$^{-/-}$ and WT neutrophils to account for the impaired mobilization of bone marrow neutrophils into the circulation in the absence of MST1.

Engagement of G-CSFR activates several signaling pathways that depend on phosphorylation of respective signaling molecules. We screened for phosphorylation patterns of several proteins downstream of G-CSFR after neutrophils were stimulated with G-CSF. We did not find any differences in JAK2, JAK1, STAT5, AKT, ERK, and MAPK phosphorylation (Figure 3C, data not shown). In contrast, we observed significantly diminished phosphorylation of STAT3 in *Mst1*$^{-/-}$ compared to WT neutrophils after 30 and 60 minutes of G-CSF stimulation (Figure 3D). To elucidate whether MST1 also regulates overall STAT3 expression, we assessed the levels of total STAT3 by western blot and found similar expression levels of total STAT3 in unstimulated and G-CSF-stimulated *Mst1*$^{-/-}$ and WT neutrophils (Figure 3E) suggesting that MST1 influences STAT3 phosphorylation but not overall STAT3 expression levels.

Activated STAT3 acts as a transcription factor promoting the expression of genes enhancing neutrophil mobilization such as chemokine receptor CXCR2 (11). Therefore, we first evaluated the levels of CXCR2 and CXCR4 on the surface of circulating neutrophils under baseline conditions. Interestingly, CXCR2 expression was reduced in *Mst1*$^{-/-}$ neutrophils (Figure 4A), while CXCR4 surface levels were unaltered (Figure 4B). The expression of CXCR2 and CXCR4 on bone marrow neutrophils was similar between WT and *Mst1*$^{-/-}$ unstimulated mice (Figures 4C, D). However, 24h after G-CSF stimulation *Mst1*$^{-/-}$ bone marrow neutrophils failed to upregulate CXCR2 in contrast to WT neutrophils (Figure 4C) indicating that G-CSF-induced upregulation of CXCR2 surface expression in neutrophils is impaired in the absence of MST1.

4 Discussion

The serine/threonine kinase MST1 is a critical factor in regulating various biological processes including organ growth and morphology, cell proliferation and apoptosis through activation of the canonical Hippo signaling pathway (31). Recently, several reports have revealed that MST1 is also involved in various immune cell functions through MST1-

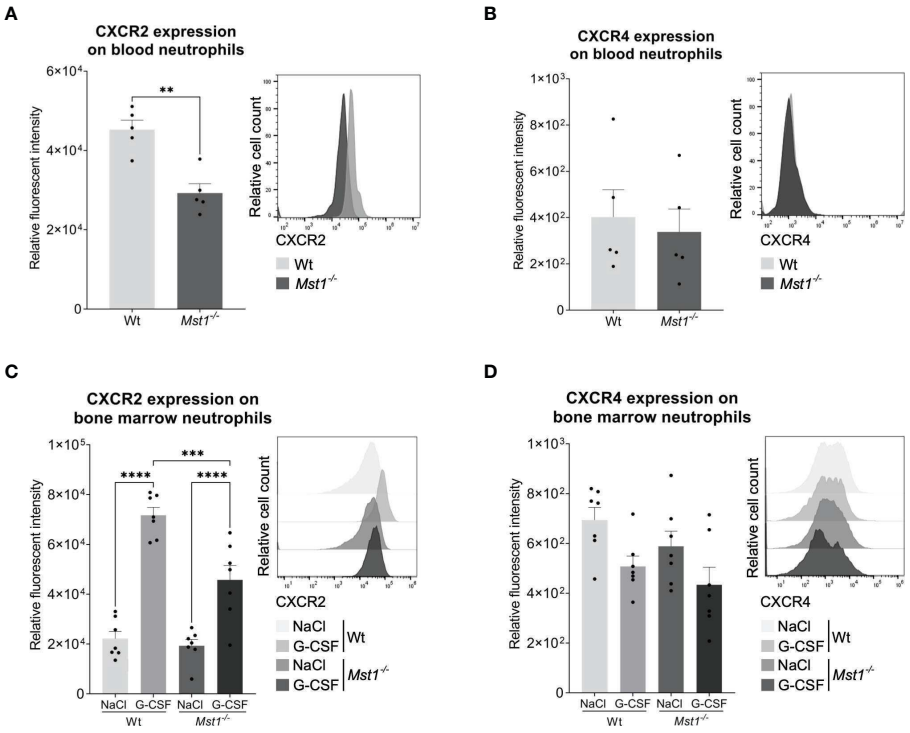

FIGURE 4
STAT3 downstream target CXCR2 is reduced in *Mst1*$^{-/-}$ neutrophils after G-CSF stimulation. **(A, B)** CXCR2 **(A)** and CXCR4 **(B)** expression in peripheral blood neutrophils of unstimulated mice; n=5. **(C, D)** CXCR2 **(C)** and CXCR4 **(D)** expression in bone marrow neutrophils 1 day after *in vivo* G-CSF stimulation; n=7. Unpaired t-test; **p<0.05 **(A, B)**. Two-way ANOVA **(C, D)**; ***p<0.001, ****p<0.0001.

dependent non-canonical signaling events (32, 33). Here, we expand this knowledge and demonstrate that MST1 regulates G-CSF receptor-dependent signaling affecting neutrophil homeostasis *in vivo*. Specifically, we show that *Mst1*$^{-/-}$ mice fail to mobilize neutrophils from the bone marrow into the blood circulation and that this impaired response is due to diminished activation of STAT3, one of the major transcription factors activated by G-CSF receptor signalling.

In humans, nonsense mutations that cause a functional deficiency of the protein MST1 provoke an immunodeficiency syndrome characterized by severe lymphopenia, transient neutropenia, and recurrent bacterial and viral infections (34, 35). Interestingly, *Mst1*$^{-/-}$ mice did not present any alterations in circulating blood neutrophil counts, but showed defective neutrophil transendothelial migration into inflamed tissue (14). Of note, loss of both MST1 and MST2 even leads to neutrophilia, as reported recently (17). This might reflect a more pronounced neutrophil trafficking defect in *Mst1/2* double knockout conditions than in *Mst1*-deficient mice leading to the inability of circulating neutrophils to extravasate into tissue. Remarkably, neutrophilia is also a hallmark of leukocyte adhesion deficiencies I-III (36). Interestingly, in contrast to the normal blood neutrophil counts observed in *Mst1*$^{-/-}$ mice, the absolute numbers of bone marrow resident neutrophils were significantly increased in *Mst1*$^{-/-}$ mice. This was associated with an enhanced generation of neutrophils in the bone marrow of *Mst1*$^{-/-}$ mice, a finding which is in agreement with an earlier study by Lee and colleagues in *Mst1/2* double deficient mice, where the authors described an increased pool of hematopoietic stem and precursor cells (HSPCs) and hypercellularity of the bone marrow (17).

Although we did not detect neutropenia in the absence of MST1, the fact that high bone marrow neutrophil numbers do not translate into higher counts in circulating neutrophils might point towards defective differentiation of myeloid precursor cells to mature neutrophils and/or an impaired release of bone marrow-derived neutrophils into the blood circulation. To investigate this, we analyzed neutrophil subset frequencies in the bone marrow, which revealed that *Mst1*$^{-/-}$ mice do not have a neutrophil differentiation defect. We then focused on the mobilization of neutrophils from the bone marrow into the circulation, which is controlled by G-CSF both under steady state and inflammatory conditions (29). The assessment of G-CSF serum levels revealed that both under resting conditions as well as following stimulation with the proinflammatory cytokine TNF-α, G-CSF levels were higher in *Mst1*$^{-/-}$ than WT mice suggesting that loss of MST1 leads to impaired G-CSF-dependent mobilization of neutrophils into the blood circulation. This could be confirmed in experiments where we injected G-CSF and assessed neutrophil counts 4h after G-CSF treatment. This led to a significant increase in blood neutrophil counts in WT but not in *Mst1*$^{-/-}$ mice. The role of G-CSF and G-CSFR in regulating blood neutrophil counts was clearly demonstrated in *Csf3*$^{-/-}$ (G-CSF deficient) and *Csf3r*$^{-/-}$ (G-CSFR deficient) mice in response to an infection (28, 37, 38).

To further explore why *Mst1*$^{-/-}$ neutrophils did not appear in the circulation upon G-CSF stimulation, we evaluated G-CSF induced neutrophil migration in *Mst1*$^{-/-}$*Lyz2*^{eEGP} and *Lyz*^{eGFP} mice using two-photon laser scanning microscopy and observed reduced neutrophil motility within the bone marrow. In addition, we found a reduced number of intravasating neutrophils. Similar results had been obtained in *Csf3r*$^{-/-}$ mice (28, 37–39). Currently, it is unclear whether reduced intravasation of neutrophils from the bone marrow into the blood circulation in *Mst1*$^{-/-}$ mice is linked to the described defect in trans-endothelial migration of *Mst1*$^{-/-}$ neutrophils into inflamed tissue. This defect is caused by impaired intracellular mobilization of VLA-3, VLA-6, and NE-containing vesicles to the neutrophil surface (14, 19), a prerequisite for vascular basement membrane penetration. Of note, bone marrow sinusoidal vessels show a discontinuous endothelial lining affecting also the vascular basement membrane (40), which might facilitate the intravasation of neutrophils into the blood circulation.

To identify molecular mechanisms, which might explain how MST1 regulates granulopoiesis and neutrophil homeostasis, we investigated G-CSF/G-CSFR dependent signaling events. G-CSFR is a transmembrane protein that upon G-CSF binding activates several signalling pathways, such as PIK3/Akt, MAPK, and JAK-STATs (41, 42). The G-CSF induced activation leads to receptor internalization, that can then follow two pathways: degradation *via* the lysosome or recycling through the endoplasmic reticulum and Golgi apparatus (29). As MST1 was reported to interact with the vesicular trafficking machinery in immune cells (14, 19), we looked for alterations in G-CSFR expression. We did not observe any changes neither in the overall G-CSFR levels nor in the G-CSFR membrane levels during G-CSF stimulation indicating that receptor degradation and recycling are not altered in *Mst1*$^{-/-}$ mice. The major signalling cascade activated downstream of G-CSFR is the JAK2-STAT3 signaling pathway. Phosphorylation patterns of JAK2 and STAT3 in *in vitro* G-CSF-stimulated neutrophils revealed no difference for JAK2 between WT and *Mst1*$^{-/-}$ neutrophils. However, STAT3 phosphorylation was significantly diminished in the absence of MST1, although total STAT3 levels in both unstimulated and G-CSF-stimulated neutrophils were not affected in the absence of MST1. Interestingly, studies in *Stat3* deficient mice showed that STAT3 is dispensable for neutrophil differentiation but affects G-CSFR dependent neutrophil mobilization (43, 44), although STAT3 can also promote the transcription of suppressor of cytokine signalling 3 (SOCS3) that negatively regulates G-CSFR signalling (45). In mature neutrophils, G-

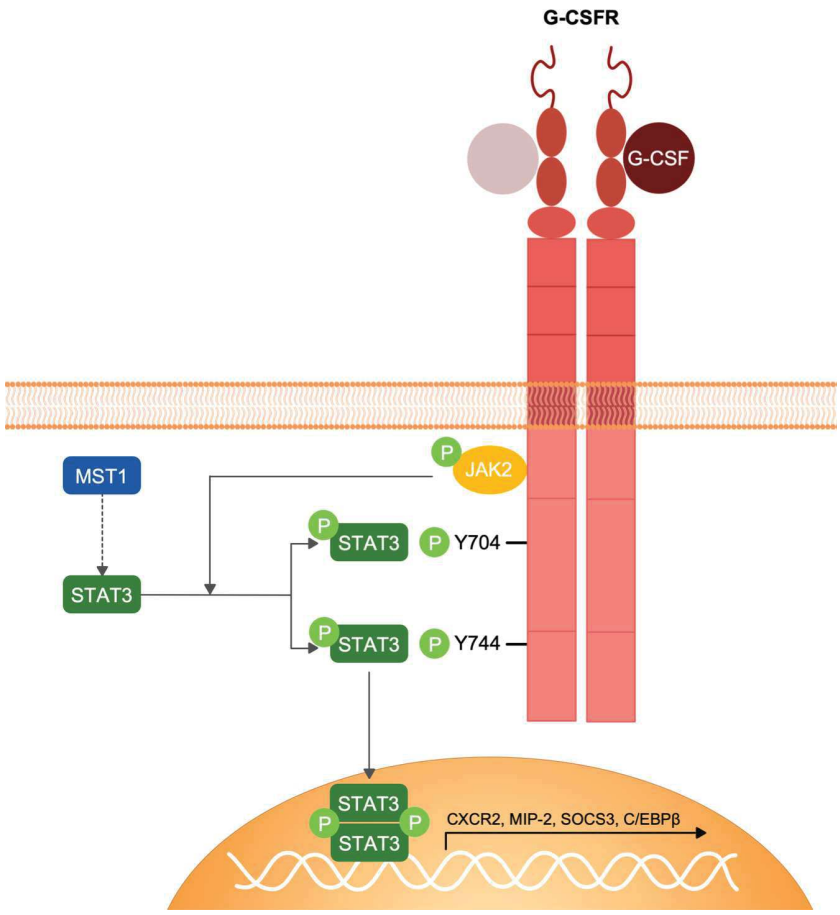

FIGURE 5
Schematic representation of G-CSFR signalling and MST1-dependent regulation of STAT3 phosphorylation. G-CSF interaction with G-CSFR induces the homo-dimerization of the receptor and the conformational change of its intracellular domain that favours the activation of JAK2 by trans-phosphorylation. JAK2 in turn phosphorylates G-CSFR and STAT3. STAT3 phosphorylation by JAK2 following G-CSFR stimulation is regulated by MST1 indicating an important role of MST1 in the G-CSF/JAK2-STAT3 signaling axis.

CSFR-activated STAT3 is key for neutrophil release from the bone marrow to the circulation (11). Accordingly, *Stat3* deficient mice show a similar phenotype after G-CSF stimulation (46) to that we observed in *Mst1*$^{-/-}$ mice. Following G-CSF binding to G-CSFR, STAT3 activation controls neutrophil mobilization by [1] downregulating CXCR4 ligands and upregulating CXCR2 ligands, [2] controlling the amplitude of CXCR2 signalling, and [3] directly promoting the transcription of CXCR2 (11). In our study we found that after *in vivo* application of G-CSF bone marrow resident *Mst1*$^{-/-}$ neutrophils had reduced expression of CXCR2 compared to WT mice which strongly indicates impaired signaling through the G-CSFR/JAK2/STAT3 axis in *Mst1*$^{-/-}$ mice.

In conclusion, we have identified MST1 as an important regulator of the G-CSFR/STAT3 signalling pathway in neutrophils (Figure 5) that orchestrates neutrophil mobilization from the bone marrow into the blood circulation and hence neutrophil homeostasis. These insights expand the ever-growing non-canonical functions of MST1 in innate immune cells illustrating the complex role of this kinase in modulating the innate immune system and opens new therapeutic perspectives for those suffering from the MST1 absence-derived immunodeficiency.

Data availability statement

The raw data supporting the conclusions of this article will be made available by the authors, without undue reservation.

Ethics statement

The animal study was reviewed and approved by Regierung von Oberbayern project number ROB-55.2-2532.Vet_02-17-102.

Author contributions

SM-A designed and conducted experiments, analyzed data and wrote the manuscript. LMW performed the neutrophil survival experiment. D-SL provided critical tools and edited the manuscript. MS set up the project, designed experiments and wrote the manuscript. All authors contributed to the article and approved the submitted version.

Funding

This work was supported by the German Research Foundation (DFG) individual grant SP621/5-1 (M.S.) and collaborative research grant SFB914, projects B01 (M.S.).

Acknowledgments

We would like to thank Dorothee Gössel and Anke Lübeck for their excellent technical help. We would also like to thank Lisa Richter from the core facility Flow Cytometry and Steffen Dietzel from the core facility Bioimaging at the Biomedical Center, LMU, Planegg-Martinsried, Germany.

Conflict of interest

The authors declare that the research was conducted in the absence of any commercial or financial relationships that could be construed as a potential conflict of interest.

Publisher's note

All claims expressed in this article are solely those of the authors and do not necessarily represent those of their affiliated organizations, or those of the publisher, the editors and the reviewers. Any product that may be evaluated in this article, or claim that may be made by its manufacturer, is not guaranteed or endorsed by the publisher.

Supplementary material

The Supplementary Material for this article can be found online at: https://www.frontiersin.org/articles/10.3389/fimmu.2022.1038936/full#supplementary-material

References

1. Pillay J, Den Braber I, Vrisekoop N, Kwast LM, De Boer RJ, Borghans JAM, et al. *In vivo* labeling with 2H2O reveals a human neutrophil lifespan of 5.4 days. *Blood* (2010) 32(8):350–7. doi: 10.1182/blood-2010-01-259028

2. Bratton DL, Henson PM. Neutrophil clearance: When the party is over, clean-up begins. *Trends Immunol* (2011) 32(8):350–7. doi: 10.1016/j.it.2011.04.009

3. Bendall LJ, Bradstock KF. G-CSF: From granulopoietic stimulant to bone marrow stem cell mobilizing agent. *Cytokine Growth Factor Rev* (2014) 25(4):355–67. doi: 10.1016/j.cytogfr.2014.07.011

4. Watari K, Asano S, Shirafuji N, Kodo H, Ozawa K, Takaku F, et al. Serum granulocyte colony-stimulating factor levels in healthy volunteers and patients with various disorders as estimated by enzyme immunoassay. *Blood* (1989) 73(1):117–22. doi: 10.1182/blood.v73.1.117.bloodjournal731117

5. Stark MA, Huo Y, Burcin TL, Morris MA, Olson TS, Ley K. Phagocytosis of apoptotic neutrophils regulates granulopoiesis *via* IL-23 and IL-17. *Immunity* (2005) 22(3):285–94. doi: 10.1016/j.immuni.2005.01.011

6. Gaffen SL, Jain R, Garg AV, Cua DJ. The IL-23-IL-17 immune axis: From mechanisms to therapeutic testing. *Nat Rev Immunol* (2014) 14(9):585–600. doi: 10.1038/nri3707

7. Tian SS, Lamb P, Seidel HM, Stein RB, Rosen J. Rapid activation of the STAT3 transcription factor by granulocyte colony- stimulating factor. *Blood* (1994) 84(6):1760–4. doi: 10.1182/blood.v84.6.1760.bloodjournal8461760

8. Hirai T, Masaki T, Kuratsune M, Yorioka N, Kohno N. PDGF receptor tyrosine kinase inhibitor suppresses mesangial cell proliferation involving STAT3 activation. *Clin Exp Immunol* (2006) 144(2):353–61. doi: 10.1111/j.1365-2249.2006.03073.x

9. Li HS, Watowich SS. Innate immune regulation by STAT-mediated transcriptional mechanisms. *Immunol Rev* (2014) 261(1):84–101. doi: 10.1111/imr.12198

10. Petit I, Ponomaryov T, Zipori D, Tsvee L. G-CSF induces stem cell mobilization by decreasing bone marrow SDF-1 and up-regulating CXCR4. *Nat Immunol* (2002) 3(7):687–94. doi: 10.1038/ni813

11. Nguyen-Jackson H, Panopoulos AD, Zhang H, Li HS, Watowich SS. STAT3 controls the neutrophil migratory response to CXCR2 ligands by direct activation of G-CSF-induced CXCR2 expression and *via* modulation of CXCR2 signal transduction. *Blood* (2010) 115(16):3354–63. doi: 10.1182/blood-2009-08-240317

12. Németh T, Sperandio M, Mócsai A. Neutrophils as emerging therapeutic targets. *Nat Rev Drug Discovery* (2020) 19(4):253–75. doi: 10.1038/s41573-019-0054-z

13. Masgrau-Alsina S, Sperandio M, Rohwedder I. Neutrophil recruitment and intracellular vesicle transport: a short overview. *Eur J Clin Invest* (2020) 50(6): e13237. doi: 10.1111/eci.13237

14. Kurz ARM, Pruenster M, Rohwedder I, Ramadass M, Schäfer K, Harrison U, et al. MST1-dependent vesicle trafficking regulates neutrophil transmigration through the vascular basement membrane. *J Clin Invest* (2016) 126(11):4125–39. doi: 10.1172/JCI87043

15. Stanger BZ. Organ size determination and the limits of regulation. *Cell Cycle* (2008) 7(3):318–24. doi: 10.4161/cc.7.3.5348

16. Wen W, Zhu F, Zhang J, Keum YS, Zykova T, Yao K, et al. MST1 promotes apoptosis through phosphorylation of histone H2AX. *J Biol Chem* (2010) 285 (50):39108–16. doi: 10.1074/jbc.M110.151753

17. Lee DH, Kim TS, Lee D, Lim DS. Mammalian sterile 20 kinase 1 and 2 are important regulators of hematopoietic stem cells in stress condition. *Sci Rep* (2018) 8(1):942. doi: 10.1038/s41598-018-19637-y

18. Li P, Chen Y, Mak KK, Wong CK, Wang CC, Yuan P. Functional role of MsT1/MsT2 in embryonic stem cell differentiation. *PloS One* (2013) 8(11):1–17. doi: 10.1371/journal.pone.0079867

19. Nishikimi A, Ishihara S, Ozawa M, Etoh K, Fukuda M, Kinashi T, et al. Rab13 acts downstream of the kinase Mst1 to deliver the integrin LFA-1 to the cell surface for lymphocyte trafficking. *Sci Signal* (2014) 7(336):1–14. doi: 10.1126/scisignal.2005199

20. Faust N, Varas F, Kelly LM, Heck S, Graf T. Insertion of enhanced green fluorescent protein into the lysozyme gene creates mice with green fluorescent granulocytes and macrophages. *Blood* (2000) 96(2):719–26. doi: 10.1182/blood.v96.2.719.014k29_719_726

21. Oh S, Lee D, Kim T, Kim T-S, Oh HJ, Hwang CY, et al. Crucial role for Mst1 and Mst2 kinases in early embryonic development of the mouse. *Mol Cell Biol* (2009) 29(23):6309–20. doi: 10.1128/mcb.00551-09

22. Bajrami B, Zhu H, Kwak HJ, Mondal S, Hou Q, Geng G, et al. G-CSF maintains controlled neutrophil mobilization during acute inflammation by negatively regulating CXCR2 signaling. *J Exp Med* (2016) 213(10):1999–2018. doi: 10.1084/jem.20160393

23. Uhl B, Vadlau Y, Zuchtriegel G, Nekolla K, Sharaf K, Gaertner F, et al. Aged neutrophils contribute to the first line of defense in the acute inflammatory response. *Blood* (2016) 128(19):2327–37. doi: 10.1182/blood-2016-05-718999

24. Evrard M, Kwok IWH, Chong SZ, Teng KWW, Becht E, Chen J, et al. Developmental analysis of bone marrow neutrophils reveals populations specialized in expansion, trafficking, and effector functions. *Immunity* (2018) 48 (2):364–79. doi: 10.1016/j.immuni.2018.02.002

25. Butcher S, Chahel H, Lord JM. Ageing and the neutrophil: No appetite for killing? *Immunology* (2000) 100(4):411–6. doi: 10.1046/j.1365-2567.2000.00079.x

26. Boivin G, Faget J, Ancey PB, Gkasti A, Mussard J, Engblom C, et al. Durable and controlled depletion of neutrophils in mice. *Nat Commun* (2020) 11(1):2762. doi: 10.1038/s41467-020-16596-9

27. Roberts AW. G-CSF: A key regulator of neutrophil production, but that's not all! *Growth Factors* (2005) 23(1):33–41. doi: 10.1080/08977190500055836

28. Liu F, Wu HY, Wesselschmidt R, Kornaga T, Link DC. Impaired production and increased apoptosis of neutrophils in granulocyte colony-stimulating factor receptor-deficient mice. *Immunity* (1996) 5(5):491–501. doi: 10.1016/s1074-7613(00)80504-x

29. Dwivedi P, Greis KD. Granulocyte colony-stimulating factor receptor signaling in severe congenital neutropenia, chronic neutrophilic leukemia, and related malignancies. *Exp Hematol* (2017) 46:9–20. doi: 10.1016/j.exphem.2016.10.008

30. Katagiri K, Imamura M, Kinashi T. Spatiotemporal regulation of the kinase Mst1 by binding protein RAPL is critical for lymphocyte polarity and adhesion. *Nat Immunol* (2006) 7(9):919–28. doi: 10.1038/ni1374

31. Ma S, Meng Z, Chen R, Guan KL. The hippo pathway: Biology and pathophysiology. *Annu Rev Biochem* (2019) 88:577–604. doi: 10.1146/annurev-biochem-013118-111829

32. Kurz ARM, Catz SD, Sperandio M. Noncanonical hippo signalling in the regulation of leukocyte function. *Trends Immunol* (2018) 39(8):656–69. doi: 10.1016/j.it.2018.05.003

33. Ueda Y, Kondo N, Kinashi T. MST1/2 balance immune activation and tolerance by orchestrating adhesion, transcription, and organelle dynamics in lymphocytes. *Front Immunol* (2020) 11:733. doi: 10.3389/fimmu.2020.00733

34. Abdollahpour H, Appaswamy G, Kotlarz D, Diestelhorst J, Beier R, Schäffer AA, et al. The phenotype of human STK4 deficiency. *Blood* (2012) 119(15):3450–7. doi: 10.1182/blood-2011-09-378158

35. Halacli SO, Ayvaz DC, Sun-Tan C, Erman B, Uz E, Yilmaz DY, et al. STK4 (MST1) deficiency in two siblings with autoimmune cytopenias: A novel mutation. *Clin Immunol* (2015) 161(2):316–23. doi: 10.1016/j.clim.2015.06.010

36. Schmidt S, Moser M, Sperandio M. The molecular basis of leukocyte recruitment and its deficiencies. *Mol Immunol* (2013) 55(1):49–58. doi: 10.1016/j.molimm.2012.11.006

37. Lieschke GJ, Grail D, Hodgson G, Metcalf D, Stanley E, Cheers C, et al. Mice lacking granulocyte colony-stimulating factor have chronic neutropenia, granulocyte and macrophage progenitor cell deficiency, and impaired neutrophil mobilization. *Blood* (1994) 84(6):1737–46. doi: 10.1182/blood.v84.6.1737.1737

38. Basu S, Hodgson G, Zhang HH, Katz M, Quilici C, Dunn AR. "Emergency" granulopoiesis in G-CSF-deficient mice in response to candida albicans infection. *Blood* (2000) 95(12):3725–33. doi: 10.1182/blood.v95.12.3725.012k06_3725_3733

39. Betsuyaku T, Liu F, Senior RM, Haug JS, Brown EJ, Jones SL, et al. A functional granulocyte colony-stimulating factor receptor is required for normal chemoattractant-induced neutrophil activation. *J Clin Invest* (1999) 103(6):825–32. doi: 10.1172/JCI5191

40. Inoue S, Osmond DG. Basement membrane of mouse bone marrow sinusoids shows distinctive structure and proteoglycan composition: A high resolution ultrastructural study. *Anat Rec* (2001) 264(3):294–304. doi: 10.1002/ar.1166

41. Souza LR, Silva E, Calloway E, Cabrera C, McLemore ML. G-CSF activation of AKT is not sufficient to prolong neutrophil survival. *J Leukoc Biol* (2013) 93 (6):883–93. doi: 10.1189/jlb.1211591

42. Marino VJ, Roguin LP. The granulocyte colony stimulating factor (G-CSF) activates Jak/STAT and MAPK pathways in a trophoblastic cell line. *J Cell Biochem* (2008) 103(5):1512–23. doi: 10.1002/jcb.21542

43. Zhang H, Nguyen-Jackson H, Panopoulos AD, Li HS, Murray PJ, Watowich SS. STAT3 controls myeloid progenitor growth during emergency granulopoiesis. *Blood* (2010) 116(14):2462–71. doi: 10.1182/blood-2009-12-259630

44. Lee CK, Raz R, Gimeno R, Gertner R, Wistinghausen B, Takeshita K, et al. STAT3 is a negative regulator of granulopoiesis but is not required for G-CSF-dependent differentiation. *Immunity* (2002) 17(1):63–72. doi: 10.1016/S1074-7613(02)00336-9

45. Kamezaki K, Shimoda K, Numata A, Haro T, Kakumitsu H, Yoshie M, et al. Roles of Stat3 and ERK in G-CSF signaling. *Stem Cells* (2005) 23(2):252–63. doi: 10.1634/stemcells.2004-0173a

46. Panopoulos AD, Zhang L, Snow JW, Jones DM, Smith AM, El Kasmi KC, et al. STAT3 governs distinct pathways in emergency granulopoiesis and mature neutrophils. *Blood* (2006) 108(12):3682–90. doi: 10.1182/blood-2006-02-003012

MST1 controls murine neutrophil homeostasis via the G-CSFR/STAT3 axis

Sergi Masgrau-Alsina[1], Lou Martha Wackerbarth[1], Dae-sik Lim[2], and Markus Sperandio[1]

[1]Institute of Cardiovascular Physiology and Pathophysiology, Walter Brendel Center of Experimental Medicine, Ludwig-Maximilians University Munich, Planegg-Martinsried, Germany

[2]Department of Biological Sciences, Korea Advanced Institute of Science and Technology (KAIST), Daejeon, South Korea

ORCIDs:
M.S.: 0000-0002-7689-3613

***Correspondence:**

Markus Sperandio, M.D.
Institute of Cardiovascular Physiology and Pathophysiology
Walter Brendel Center of Experimental Medicine
Biomedizinisches Centrum
Ludwig-Maximilians-Universität
Großhaderner Str. 9
82152 Planegg-Martinsried
GERMANY
Voice: +49 (0)89 2180 71513
Fax: +49 (0)89 2180 71511
Email: markus.sperandio@lmu.de

Key words: MST1, neutrophils, G-CSF, STAT3, granulocytes.

Running title: MST1 and neutrophil homeostasis

Supplemental content: supplemental methods, figures, references, tables, and videos.

Supplemental reference count: 2

Supplemental figures: 1

Supplemental tables: 1

Videos: 3

Supplemental Methods

Flow Cytometry

Isolated cells were stained for 30 minutes on ice in a solution of PBS-1%BSA or HBSS (250mg BSA, Capricorn Scientific; 238mg HEPES, Sigma-Aldrich,; 100mL Hank's solution, pH7.4) containing the manufacturer's recommended antibody concentration. Samples were analysed using Gallios (Beckman Coulter), CytoFlex S (Beckman Coulter), or Fortessa (BD Biosciences). Neutrophils were identified in bone marrow and spleen samples as $CD45^+$, $CD11b^+$, and $Ly6G^+$ cells and in blood samples as $CD45^+$, $CD11b^+$, $CD115^-$, and $Gr1^{high}$ cells. For identifying the neutrophil subsets in the bone marrow, the gating strategy described by Evrard and colleagues was applied (Evrard et al., 2018) (Supplemental Figure 1). For the neutrophil survival experiment, isolated neutrophils were incubated in HBSS with and without $1ug \cdot mL^{-1}$ G-CSF at 37ºC for 24 or 48h and later stained with FITC Annexin V Apoptosis Detection Kit with PI (BioLegend) following the manufacturer instructions. The complete list of the antibodies used can be found in Supplemental Table 1.

Bromodeoxyuridine (BrdU) cell proliferation assay

Bone marrow neutrophil proliferation in C57BL/6 and *Mst1*$^{-/-}$ mice was assessed using the APC BrdU Flow Kit (BD Biosciences) following the manufacturer's protocol. One hour after 2.5µg BrdU intravenous injection, 2.5µg recombinant murine G-CSF (ImmunoTools) was administrated intravenously to promote neutrophil proliferation. Mice were sacrificed and bone marrow isolated two days after the injection and further processed to be analysed by flow cytometry.

TNF-α induced peritonitis and G-CSF serum levels

C57BL/6 and *Mst1*$^{-/-}$ mice were injected with either NaCl (control) or 500ng recombinant murine TNF-α (R&D Systems) intraperitoneally to induce peritonitis, as described (Kurz et al., 2016). Serum was collected 4 hours after injection and processed as indicated by the protocol of Mouse G-CSF Quantikine® ELISA (R&D Systems) and read with the Spark™ 10M microplate reader (Tecan).

Western Blot

Purified bone marrow neutrophils were incubated in a solution of $1ug \cdot mL^{-1}$ G-CSF at 37ºC for different time points. Neutrophils were then immediately lysed and

homogenized in a lysis buffer containing Laemmli (150mM NaCl, 1% Triton X-100, AppliChem; 0.5% sodium deoxycholate Sigma-Aldrich; 50mM Tris-HCl at pH7.3, 2mM EDTA, both Merk; 0.8% protease/phosphatase inhibitor, Cell Signalling) on a concentration of $100\mu L \cdot 10^6 cells^{-1}$ and boiled for 5 minutes. SDS-PAGE of the lysates was performed on 10% or 12% self-casted acrylamide gels. Protein was transferred into PVDF membranes that were incubated with the corresponding antibody. The following antibodies were used: sheep anti-G-CSFR (R&D Systems), rabbit anti-JAK2 (Cell Signalling), rabbit anti-Phospho-JAK2 (Tyr1007/1008, Cell Signalling), mouse anti-STAT3 (Cell Signalling), rabbit anti-Phospho-STAT3 (Tyr705, Cell Signalling), and mouse anti-GAPDH (Merk). Western Blot membranes were scanned with an Odyssey scanner (LI-COR) and analysed with Image Studio Lite software (LI-COR).

Supplemental References

1. Kurz ARM, Pruenster M, Rohwedder I, et al. MST1-dependent vesicle trafficking regulates neutrophil transmigration through the vascular basement membrane. *J. Clin. Invest.* (2016) 126(11):4125–4139. doi: 10.1172/JCI87043.
2. Evrard M, Kwok IWH, Chong SZ, et al. Developmental Analysis of Bone Marrow Neutrophils Reveals Populations Specialized in Expansion, Trafficking, and Effector Functions. *Immunity*. (2018) 48(2):364-79. doi: 10.1016/j.immuni.2018.02.002.

Supplemental Figure 1

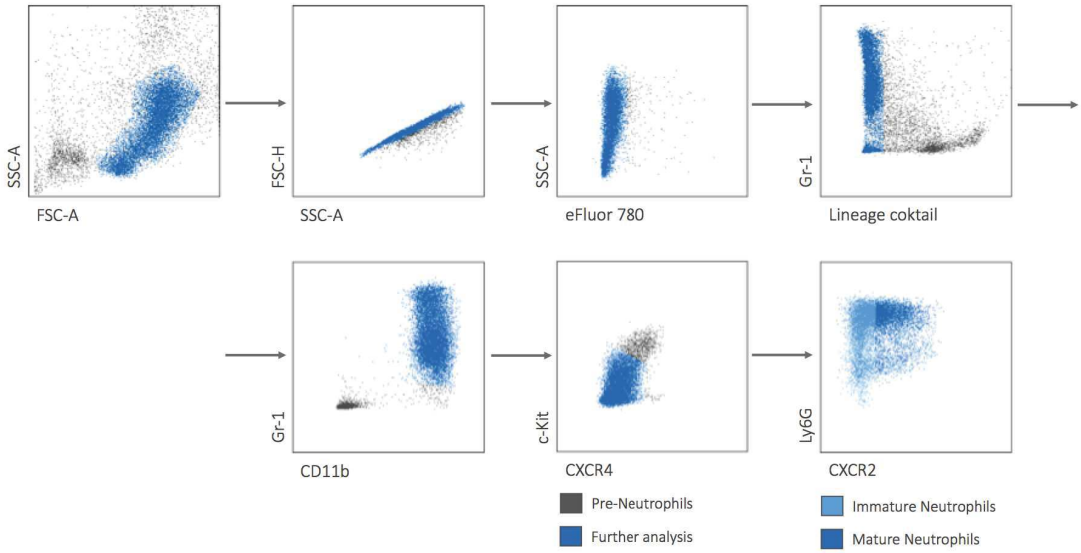

Supplemental Figure 1. Representative plots of neutrophil subsets in the bone marrow panel. Blue highlight indicates the populations selected for the following step in the gating strategy. For the last plots the populations of interest are highlighted as indicated in the legend.

Supplemental Table 1

Antibody	Conjugate	Host	Isotype	Clone	Company
CD3e	PE	Hamster	IgG	145-2C11	BioLegend
CD11b (Mac-1)	PE	Rat	IgG2b k	M1/70	BioLegend
CD11b (Mac-1)	PE-Cy7	Rat	IgG2b k	M1/70	BioLegend
CD11b (Mac-1)	AF 700	Rat	IgG2b k	M1/70	BioLegend
CD45	BV 570	Rat	IgG2b k	IM7	BioLegend
CD45	PerCP-Cy5.5	Rat	IgG2b k	30-F11	BioLegend
CD45	FITC	Rat	IgG2b k	30-F11	BioLegend
CD45	APC	Rat	IgG2b k	30-F11	BioLegend
CD45R (B220)	PE	Rat	IgG2a k	B220	BioLegend
CD90.2 (Thy-1.2)	PE	Rat	IgG2b k	30-H12	BioLegend
CD114 (G-CSFR)	AF 647	Rat	IgG2a	723806	R&D
CD115 (M-CSFR)	PE	Rat	IgG2a k	AFS98	BioLegend
CD115 (M-CSFR)	APC	Rat	IgG2a k	AFS98	BioLegend
CD117 (c-Kit)	BV 421	Rat	IgG2a k	2B8	BioLegend
CD170 (SiglecF)	PE	Rat	IgG2a	E50-2440	BD Pharm
CD182 (CXCR2)	APC	Rat	IgG2a k	SA044G4	BioLegend
CD184 (CXCR4)	FITC	Rat	IgG2b	2B11	Pharmingen
IgG1 k	PE	Mouse	Isotype	P3.6.2.8.1.	Invitrogen
IgG2a k	APC	Rat	Isotype	RTK2758	Biolegend
IgG2a k	AF 647	Rat	Isotype	RTK2758	Biolegend
IgG2b k	FITC	Rat	Isotype	RTK4530	Biolegend
Nk1.1	PE	Mouse	IgG2a k	PK136	BioLegend
Ly6A/E (Sca-1)	PE	Rat	IgG2a	D7	eBioscience
Ly6G/C (Gr-1)	PB	Rat	IgG2b	RB6-8C5	BioLegend
Ly6G/C (Gr-1)	PE-Cy7	Rat	IgG2b k	RB6-8C5	BioLegend
Ly6G	PB	Rat	IgG2a k	1A8	BioLegend
Ly6G	AF 488	Rat	IgG2a k	1A8	BioLegend
Ly6G	PE-Dazzle 594	Rat	IgG2a k	1A8	BioLegend

Supplemental Table 1. List of antibodies for flow cytometry.

Video Legend

Video 1. Time-lapse intravital multi-photon microscopy video of the skull bone marrow of an unstimulated *Lyz2*^{eEGP} mouse showing neutrophils (green) and vessels (red). Projection of 12 z-stacks. Total imaging time of 10 minutes. Scale bar 50µm.

Video 2. Time-lapse intravital multi-photon microscopy video of the skull bone marrow of a *Lyz2*^{eEGP} mouse 2 hours after G-CSF stimulation showing neutrophils (green) and vessels (red). Projection of 12 z-stacks. Total imaging time of 30 minutes. Scale bar 50µm.

Video 3. Time-lapse intravital multi-photon microscopy video of the skull bone marrow of a *Mst1*$^{-/-}$*Lyz2*^{eEGP} mouse 2 hours after G-CSF stimulation showing neutrophils (green) and vessels (red). Projection of 12 z-stacks. Total imaging time of 30 minutes. Scale bar 50µm.

References

1. Ley K, Hoffman HM, Kubes P, Cassatella MA, Zychlinsky A, Hedrick CC, et al. Neutrophils: New insights and open questions. Science immunology. 2018;3(30).

2. Shane AL, Sánchez PJ, Stoll BJ. Neonatal sepsis. Lancet (London, England). 2017;390(10104):1770-80.

3. Wynn JL. Defining neonatal sepsis. Current opinion in pediatrics. 2016;28(2):135-40.

4. Fleischmann C, Reichert F, Cassini A, Horner R, Harder T, Markwart R, et al. Global incidence and mortality of neonatal sepsis: a systematic review and meta-analysis. Archives of disease in childhood. 2021;106(8):745-52.

5. Levy O. Innate immunity of the newborn: basic mechanisms and clinical correlates. Nature reviews Immunology. 2007;7(5):379-90.

6. Borghesi A, Stronati M, Castagnoli R, Ioimo I, Achille C, Manzoni P, et al. Novel Approaches to the Study of Neonatal Infections. American journal of perinatology. 2018;35(6):570-4.

7. Kollmann TR, Kampmann B, Mazmanian SK, Marchant A, Levy O. Protecting the Newborn and Young Infant from Infectious Diseases: Lessons from Immune Ontogeny. Immunity. 2017;46(3):350-63.

8. Semmes EC, Chen JL, Goswami R, Burt TD, Permar SR, Fouda GG. Understanding Early-Life Adaptive Immunity to Guide Interventions for Pediatric Health. Frontiers in immunology. 2020;11:595297.

9. Dinarello CA. Immunological and inflammatory functions of the interleukin-1 family. Annual review of immunology. 2009;27:519-50.

10. Sharma AA, Jen R, Butler A, Lavoie PM. The developing human preterm neonatal immune system: a case for more research in this area. Clinical immunology (Orlando, Fla). 2012;145(1):61-8.

11. Wynn JL, Scumpia PO, Winfield RD, Delano MJ, Kelly-Scumpia K, Barker T, et al. Defective innate immunity predisposes murine neonates to poor sepsis outcome but is reversed by TLR agonists. Blood. 2008;112(5):1750-8.

12. Burg ND, Pillinger MH. The neutrophil: function and regulation in innate and humoral immunity. Clinical immunology (Orlando, Fla). 2001;99(1):7-17.

13. Amulic B, Cazalet C, Hayes GL, Metzler KD, Zychlinsky A. Neutrophil function: from mechanisms to disease. Annual review of immunology. 2012;30:459-89.

14. Ley K, Laudanna C, Cybulsky MI, Nourshargh S. Getting to the site of inflammation: the leukocyte adhesion cascade updated. Nature reviews Immunology. 2007;7(9):678-89.

15. Sperandio M, Smith ML, Forlow SB, Olson TS, Xia L, McEver RP, et al. P-selectin glycoprotein ligand-1 mediates L-selectin-dependent leukocyte rolling in venules. The Journal of experimental medicine. 2003;197(10):1355-63.

16. Nussbaum C, Gloning A, Pruenster M, Frommhold D, Bierschenk S, Genzel-Boroviczeny O, et al. Neutrophil and endothelial adhesive function during human fetal ontogeny. J Leukoc Biol. 2013;93(2):175-84.

17. Sperandio M, Quackenbush EJ, Sushkova N, Altstätter J, Nussbaum C, Schmid S, et al. Ontogenetic regulation of leukocyte recruitment in mouse yolk sac vessels. Blood. 2013;121(21):e118-28.

18. Shih VF, Tsui R, Caldwell A, Hoffmann A. A single NFκB system for both canonical and non-canonical signaling. Cell research. 2011;21(1):86-102.

19. Pomerantz JL, Baltimore D. Two pathways to NF-kappaB. Molecular cell. 2002;10(4):693-5.

20. Millet P, McCall C, Yoza B. RelB: an outlier in leukocyte biology. J Leukoc Biol. 2013;94(5):941-51.

21. Calmon-Hamaty F, Combe B, Hahne M, Morel J. Lymphotoxin α revisited: general features and implications in rheumatoid arthritis. Arthritis research & therapy. 2011;13(4):232.

22. Hayden MS, Ghosh S. Signaling to NF-kappaB. Genes & development. 2004;18(18):2195-224.

23. Tamassia N, Le Moigne V, Calzetti F, Donini M, Gasperini S, Ear T, et al. The MyD88-independent pathway is not mobilized in human neutrophils stimulated via TLR4. Journal of immunology (Baltimore, Md : 1950). 2007;178(11):7344-56.

24. Ciesielska A, Matyjek M, Kwiatkowska K. TLR4 and CD14 trafficking and its influence on LPS-induced pro-inflammatory signaling. Cellular and molecular life sciences : CMLS. 2021;78(4):1233-61.

25. Margraf A, Sperandio M. Leukocyte Trafficking and Hemostasis in the Mouse Fetus in vivo: A Practical Guide. Frontiers in cell and developmental biology. 2020;8:632297.

26. Pickart CM, Eddins MJ. Ubiquitin: structures, functions, mechanisms. Biochimica et biophysica acta. 2004;1695(1-3):55-72.

27. Cooper JT, Stroka DM, Brostjan C, Palmetshofer A, Bach FH, Ferran C. A20 blocks endothelial cell activation through a NF-kappaB-dependent mechanism. The Journal of biological chemistry. 1996;271(30):18068-73.

28. Ma A, Malynn BA. A20: linking a complex regulator of ubiquitylation to immunity and human disease. Nature reviews Immunology. 2012;12(11):774-85.

29. Vereecke L, Beyaert R, van Loo G. The ubiquitin-editing enzyme A20 (TNFAIP3) is a central regulator of immunopathology. Trends in immunology. 2009;30(8):383-91.

30. Lee EG, Boone DL, Chai S, Libby SL, Chien M, Lodolce JP, et al. Failure to regulate TNF-induced NF-kappaB and cell death responses in A20-deficient mice. Science (New York, NY). 2000;289(5488):2350-4.

31. Matmati M, Jacques P, Maelfait J, Verheugen E, Kool M, Sze M, et al. A20 (TNFAIP3) deficiency in myeloid cells triggers erosive polyarthritis resembling rheumatoid arthritis. Nature genetics. 2011;43(9):908-12.

32. Kunkel EJ, Ley K. Distinct phenotype of E-selectin-deficient mice. E-selectin is required for slow leukocyte rolling in vivo. Circulation research. 1996;79(6):1196-204.

33. Rohwedder I, Wackerbarth LM, Heinig K, Ballweg A, Altstätter J, Ripphahn M, et al. A20 and the noncanonical NF-κB pathway are key regulators of neutrophil recruitment during fetal ontogeny. JCI insight. 2023;8(4).

34. Pruenster M, Vogl T, Roth J, Sperandio M. S100A8/A9: From basic science to clinical application. Pharmacology & therapeutics. 2016;167:120-31.

35. Edgeworth J, Gorman M, Bennett R, Freemont P, Hogg N. Identification of p8,14 as a highly abundant heterodimeric calcium binding protein complex of myeloid cells. The Journal of biological chemistry. 1991;266(12):7706-13.

36. Morikis VA, Chase S, Wun T, Chaikof EL, Magnani JL, Simon SI. Selectin catch-bonds mechanotransduce integrin activation and neutrophil arrest on inflamed endothelium under shear flow. Blood. 2017;130(19):2101-10.

37. Pruenster M, Kurz AR, Chung KJ, Cao-Ehlker X, Bieber S, Nussbaum CF, et al. Extracellular MRP8/14 is a regulator of beta2 integrin-dependent neutrophil slow rolling and adhesion. Nat Commun. 2015;6:6915.

38. Voganatsi A, Panyutich A, Miyasaki KT, Murthy RK. Mechanism of extracellular release of human neutrophil calprotectin complex. J Leukoc Biol. 2001;70(1):130-4.

39. Urban CF, Ermert D, Schmid M, Abu-Abed U, Goosmann C, Nacken W, et al. Neutrophil extracellular traps contain calprotectin, a cytosolic protein complex involved in host defense against Candida albicans. PLoS pathogens. 2009;5(10):e1000639.

40. Broz P, Dixit VM. Inflammasomes: mechanism of assembly, regulation and signalling. Nature reviews Immunology. 2016;16(7):407-20.

41. Kelley N, Jeltema D, Duan Y, He Y. The NLRP3 Inflammasome: An Overview of Mechanisms of Activation and Regulation. International journal of molecular sciences. 2019;20(13).

42. Pillay J, den Braber I, Vrisekoop N, Kwast LM, de Boer RJ, Borghans JA, et al. In vivo labeling with 2H2O reveals a human neutrophil lifespan of 5.4 days. Blood. 2010;116(4):625-7.

43. Bratton DL, Henson PM. Neutrophil clearance: when the party is over, clean-up begins. Trends in immunology. 2011;32(8):350-7.

44. Bendall LJ, Bradstock KF. G-CSF: From granulopoietic stimulant to bone marrow stem cell mobilizing agent. Cytokine & growth factor reviews. 2014;25(4):355-67.

45. Watari K, Asano S, Shirafuji N, Kodo H, Ozawa K, Takaku F, et al. Serum granulocyte colony-stimulating factor levels in healthy volunteers and patients with various disorders as estimated by enzyme immunoassay. Blood. 1989;73(1):117-22.

46. Tian SS, Lamb P, Seidel HM, Stein RB, Rosen J. Rapid activation of the STAT3 transcription factor by granulocyte colony-stimulating factor. Blood. 1994;84(6):1760-4.

47. Masgrau-Alsina S, Sperandio M, Rohwedder I. Neutrophil recruitment and intracellular vesicle transport: A short overview. European journal of clinical investigation. 2020;50(6):e13237.

48. Stanger BZ. Organ size determination and the limits of regulation. Cell cycle (Georgetown, Tex). 2008;7(3):318-24.

49. Kurz AR, Pruenster M, Rohwedder I, Ramadass M, Schäfer K, Harrison U, et al. MST1-dependent vesicle trafficking regulates neutrophil transmigration through the vascular basement membrane. The Journal of clinical investigation. 2016;126(11):4125-39.

50. Nguyen-Jackson H, Panopoulos AD, Zhang H, Li HS, Watowich SS. STAT3 controls the neutrophil migratory response to CXCR2 ligands by direct activation of G-CSF-induced CXCR2 expression and via modulation of CXCR2 signal transduction. Blood. 2010;115(16):3354-63.

51. Masgrau-Alsina S, Wackerbarth LM, Lim DS, Sperandio M. MST1 controls murine neutrophil homeostasis via the G-CSFR/STAT3 axis. Frontiers in immunology. 2022;13:1038936.

Acknowledgements

The herein presented work was performed in the group Prof. Dr. med. Markus Sperandio at the Walter Brendel Centre of Experimental Medicine, Biomedical Center, Institute of Cardiovascular Physiology and Pathophysiology, LMU Munich. During the time of my thesis, many people supported me, and I gratefully thank the following people:

- Markus. First of all, thank you for giving me the opportunity to do my doctoral thesis in your laboratory, supervising me, providing me with excellent tools and equipment and last but not least for allowing and encouraging me to broaden not only my scientific horizon by attending numerous conferences.
- Ina. Thanks a lot for your mentorship and scientific input and most importantly for being my trustworthy partner of “Team Fetal” or sometimes better “Team Fatal”.
- Monika and Roland. Thank you for sharing your knowledge and for supporting me in every occasion, and last but not least for always guaranteed entertainment whenever needed.
- Doro. Thank you for your continuous assistance and help.
- Verena. I could not imagine any better and more organized support concerning every aspect of my time as a doctoral candidate. Thank you for your caring, your patience and for providing a solution for every problem, inside or outside the lab.
- Sonja aka the Queen of Western Blotting and pretty lunch boxes. A huge thank you for being the best, biggest and most fun support. Working with you was a real pleasure.
- Molli and Anna. Thanks for all the shared laughs as well as all the shared ups and downs during our time in the lab, but even more importantly for being part of my life outside the lab and making it so much more fun.
- A huge thank you to all members of the Institute for their continuous support and help throughout the time of my thesis. Thank you for answering all my questions and your help whenever I had a problem. I really enjoyed working with you.
- Best comes last: Matteo and Sergi. Too many lines would be needed to describe all the crazy amazing moments we shared during this PhD journey together. Let´s put it like this: I am more than grateful that from day one on, I was lucky to get not only the two best colleagues you could ever imagine, but also two best friends at the same time.
- And at the very end: My parents; Isi for being my forever-supervisor in every aspect and Hannah and Nina, because nothing works without Triangolo.